NORTHWESTERN UNIVERSITY

Cells on Microfabricated Elastic Substrates: Effects of Substrate's Mechanical Property on Cell Behavior

A DISSERTATION

SUBMITTED TO THE GRADUATE SCHOOL
IN PARTIAL FULFILLMENT OF THE REQUIREMENT

for the degree

DOCTOR OF PHILOSOPHY

Field of Mechanical Engineering

By

Abel Lianzauk Thangawng

EVANSTON, ILLINOIS

December 2007

ABSTRACT

Cells on Microfabricated Elastic Substrates: Effects of Substrate's Mechanical Property on Cell Behavior

Abel Lianzauk Thangawng

Cells are known to respond to external stimuli such as chemical, physical and mechanical cues from their microenvironments. In this work, we developed the technology to to complement the previously reported studies that deal with substrates' mechanical property by developing thin polydimethlysiloxane (PDMS) membrane microdevices using microfabrication technology. Typically, multiples substrates, each with different stiffness, are used to study the differences in cell's response to the different mechanical properties. With the PDMS membrane devices, a variation in stiffness across a single substrate was generated by strategically integrating micropatterns on a freely suspended PDMS membrane. Human epidermal keratinocytes (HEK) were seeded on the devices and cell migration and accumulation trends, laminin-332 secretion, and focal adhesion and hemidesmosome assembliy were monitored. It was observed that cells within the regions with a small gradient of stiffness were very static while their counterparts on regions with a large gradient of stiffness were extremely active and mobile. This suggests that not only the changes in the property of substrate affect the cells, but the rate at which the changes occur, gradient of stiffness, play a critical role in determining the cells' response. Preliminary data also suggest that HEK specifically secreted more laminin on the softer region of the membrane. Focal adhesion complexes are more prominent on the stiffer region while

hemidesmosomes complexes are better developed on the softer region. Concurrently, the same cellular matrix organization on compliant PDMS substrates with Young's modulus ranging from ~1.2 Pa to 744 kPa was studied. Similar to the membrane devices, more laminin protein secretion and more exptensive hemidesmosome assemblies were observed on the softer substrate while focal adhesions were more prominent, size and number, on the stiffer substrates. We speculate that assembly of hemidesmosome on a less stiff substrate by HEK is typical of normal tissue while enhanced assembly of focal adhesion on stiff substrates reflects what occur when cells interact with the matrix of diseased tissue.

ACKNOWLEDGEMENT

I would like to take this opportunity to express my gratitude to all the people who helped me get to this place in my life since I was a small child.

First of all, I want to praise God for guiding me through my life, and bestowing blessings one after another. He gave me the health, strength, and will to do what I needed to do in my life, and He always pave a way for me to thread, including my journey to pursuing this Ph.D. degree at Northwestern University. He is able, and every thing is possible with Him.

I would also like to express my utmost gratitude and appreciation to my mom and dad, Assumpta Suihlen and Robert Thangawng. They have sacrificed their own comfort by leaving our homeland Lairam (known as Chin State in Myanmar), and brought us to the US so that we, their children, may have better education and life. They are the ones who instilled the value of education in me. I still remember all of us sitting around a charcoal burning heater in the living room of our house in Falam, reading our notes by heart to mom and dad and munching on late night snack (seu faak). They still prepare some of the same snacks for me when I visit them in Maryland. Many of those nights, we used candle sticks because we did not have electric power. I also would like to thank all my brothers and sisters, Tawng[2], Thang[2], Mang[2] and Farhniang (Sui[2]), for their supports and encouragements, and helping me in ways that they don't even know.

I also would like to thank every one from our Chin communities in the US, especially from Michigan and Maryland, for their continuous encouragements and prayers. I would also like to acknowledge all my teachers from Bladensberg High School who helped me beyond their duties. Special thanks go to Mr. Ross (chemistry) and Ms. Womack (physics) for the before-and-after-school classes.

It would be a sin to not thank the special people God placed in my life, my wonderful and caring wife Noela Thi Thi and our precious son Seth Thangcinlian. Thanks Thi! I say this from the bottom of my heart for taking care of me in every way and taking this journey with me. I should also mention that I appreciate the many weekends that you come to the Evanston and Chicago labs to accompany me, even the days that you are just sleeping beside my works table. May God bless you continuously! I am looking forward to the new journey that we are about to embark together. *I AP-PRE-CI-ATE!!*

It would be incomplete if I don't thank all my former and current mentors and advisors from Northwestern University and Oak Ridge National Lab. I really appreciate my advisors Dr. Matthew R. Glucksberg and Dr. Rodney S. Ruoff for supporting me on my research. I have met and collaborated with many scientists through Matt and I really want to say a special thank for opening the doors for me. I also want to thank Melody (Dr. Melody Swartz, EPFL) for providing funding for my research. Also, I would like to thank Dr. Jonathan C. Jones for his advises, equipment, resources, and for allowing me to use his laboratory in Northwestern medical school. I am also very thankful for the financial support during Spring 2007. Without Jonathan's help

and generosity, I could never have done most of my experiments. I would also like to express my sincere appreciation to Dr. Jerry (Zhiyu) Hu and Dr. Thomas Thundat from ORNL for inviting me to work with them for a summer. I would also like to thank Dr. Krishwasnamy for serving in me thesis committee. Also, I like to thank Dr. Junghoon Lee (now at Seoul National University) for his support for the first two years of my study at NU.

Lasty, I would like to say thank you to all Ruoff's group members and former Junghoon's group members for all the conversations and discussions, and ranting sessions. Without you my study would be very dull. Thanks also to Phil from Dr. Jones lab for all the helps he provided for cell culture and imaging.

DEDICATION

In memory of my homeland Lairam

- Chin State, Myanmar-

and its people

Table of Contents

List of Figures

List of Tables

Chapter 1 : INTRODUCTION

1.1. Background

With the advance of micro and nanofabrication techniques, there have been unique opportunities to apply them in many different fields. In this study, the technology was employed to study how the cellular microenvironment affects cells. Since cells are the bases of all living organisms, it is critical to understand basic mechanisms by which they interact with their environment. Cells are extremely sensitive to their environment, detecting mechanical (substrate stiffness) [1-16], chemical [15, 17, 18], ligands (adhesive molecules) [8, 15, 20-30], and topographical [31-45] signals among many other environmental cues. Among these stimuli, the effects of chemical and topography are the most widely studied. This thesis deals with the development of micrfabricated tools/devices to study cell-substrate interaction. In this introduction, I will discuss what is currently known about the effects of some of these microenvironmental stimuli on cells.

1.1.1. Mechanotaxis (Durotaxis)

Recently, the effects of substrate's mechanical properties on a cell's behavior have become a hot topic since the discovery that there are changes in morphologies and motility of both normal rat kidney epithelial and 3T3 fibroblastic cells on substrates with different stiffness [1]. The cells were well spread on stiffer substrate with Young's modulus, E, ~ 65 Pa where as they were irregularly shaped on softer substrate with E ~ 16 Pa. 3T3 cells were also observed to migrate

faster on more compliant substrate, 0.06 μm/min for E ~ 65 Pa and 0.55 μm/min for E ~ 16 Pa. Lo, et al. [2] further demonstrated the preferential migration of 3T3 cells (individual) toward substrate with increasing stiffness. In this study two different polyacrylamide substrates with different stiffness (E=14 and 30 kPa) were placed side by side. The individual cells (no contact with other cells) were observed to migrate toward the stiffer side but no cell accumulation was observed [Figure 1-1]. The traction force of the cells was also found to be stronger on the more rigid substrate.

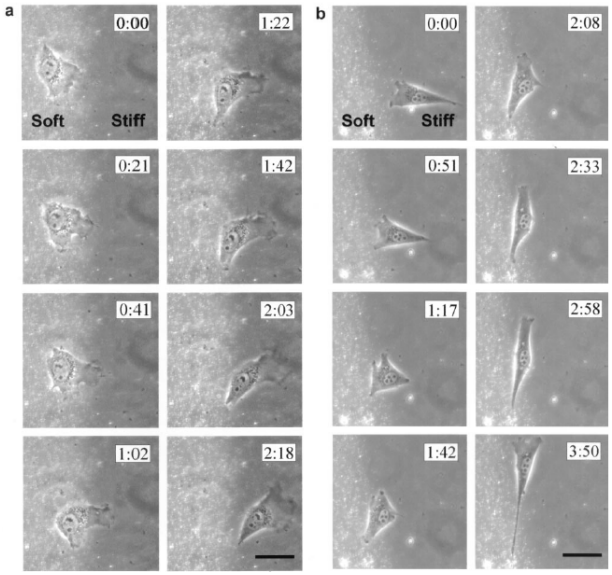

Figure 1-1: NIH 3T3 cells on a substrate with two different stiffness: (*a*) A cell moved from the soft side to the stiff side of the substrate, and (*b*) A cell moved from the stiff side of the substrate toward the gradient and moved along the boundary (Reproduced from [2]).

Using micromolding technique, Gray et al. [6] fabricated polyacrylamide and polydimethylsiloxane (PDMS) substrates with well defined regions of soft and stiff areas. NIH/3T3 cells were observed to migrate toward the stiff regions in both substrates [Figure 1-2]. Unlike the study done by Lo, et al. [2], cells accumulated in the stiffer region of both substrates.

Interestingly, cell accumulation was more pronounced on PDMS compared to the polyacrylamide. The authors speculated that the accumulation in PDMS substrate was due to the patterns being more precise compare to that on the polyacrylamide. It should also be noted that the Young's modulus of the soft and the stiff region were 1.3 kPa and 34 kPa for the polyacrylamide and 12 kPa and 2.5 MPa for PDMS respectively. Wong, et al. [5] fabricated a substrate with a stiffness gradient varying gradually by exposing the polymer to a UV source. The intensity of the UV light was controlled by a mask that has a gradient of transparency, which in turn created the gradient in polymerization, resulting in the variation of stiffness. Vascular smooth muscle cells were observed to migrate toward the stiffer region and accumulated there. It has also been reported that the stiffness of the substrate regulates cells growth and apoptosis [3], motility [4, 9], and differentiation [7].

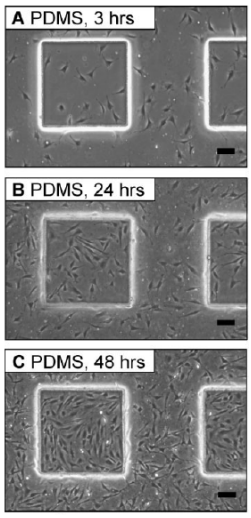

Figure 1-2: NIH 3T3 cell preferentially accumulated on stiff region (square) of the substrates (Reproduced from [6])

Interestingly, there are some inconsistencies in the experimental results reported. For example, Saez, et al. [10] reported that the traction force of epithelial cells is proportional to the rigidity of the substrate. The deformation of the substrate (polymeric pillars) was found to be constant regardless of the substrate stiffness. On the other hand, Freynman et al. [11] reported that the contractile force of fibroblasts is independent of the substrate stiffness.

1.1.2. Haptotaxis

Similar to both chemical and mechanical cues, the density of ligands on a substrate has a major influence on the behavior of the cells [8, 15, 21]. Cells tend to attach more strongly to a region of the substrate that has a more densely packed ligand compare to a region where the ligands are less dense. In order to properly understand the effects of ligands density on the cells, one needs to carefully design the surface. Different research groups have studied these effects by growing cells on individual substrates that have been treated with different density of the same ligand [8]. These experiments can be time consuming, and are quite problematic because more variables need to be controlled at the same time. In order to overcome these problems, some workers have developed techniques that would allow the formation of a continuous ligand on the surface with gradually changing concentration. By exposing cells to surfaces coated with ligands that have varying density gradient, one combines multiple experiments in one, allowing the observation of cell behavior on such a substrate and it potentially can also be used to identify the optimal ligand density for adhesion and motility of a cell type of interest. Several techniques have been reported for creating surfaces with gradient ligand signals [20-30]. The techniques may be categorized into four general groups, (1) timed dip-coating, (2) microfluidic network based mixing and depositing, (3) mechanical induced stretch-surface activation and (4) photoactivation of surfaces.

The timed-coating methods may be done by directly dipping the substrate in the solution and varying the emersion time of the substrate by slowly pulling out to vary the amount of ligand attached on the surface. The longer the substrate is exposed to the protein the more protein is attached to the surface. On the other hand, the concentration of the ligand solution can be pre-calculated so that the portion of the surface that comes in contact with the solution absorbs the protein and depletes the amount of ligand that remain in the solution. As the substrate is dipped deeper in to the solution, less and less ligand attach to the substrate due to the reduced concentration. This eventually creates a surface that has a gradient of protein.

Recently, Dertinger, et al. [18] demonstrated the generation of gradient solution using microfluidic networks. Jeon, et al. [19] used the device to create linear and complex gradients of interleukin-8 and observed that neutrophils migrated preferentially toward the increasing concentration of the chemoattractant. In the microfluidic network technique, solutions with ligands at different concentration are injected in the fluidic channels. They are then mixed and split continuously until the solutions reach the final branch at which point they are recombined into one large channel. The laminar flow in the channels allows the proteins solutions to travel straight onto the surface without further mixing to their adjacent stream of solution. This technique was demonstrated to be capable of creating not only gradient patterns but also intricate gradients within the final channel by simply varying the position of the solution in the initial injection. For example, if solutions with three different ligand densities were injected adjacent to each other in order of their density, the final surface will have ligand with gradually changing

density. On the other hand, if the solution with the highest density is injected in the middle, the final surface will have a peak density of ligand in the middle, and the surface will have a bell curve density gradient. In all cases these gradients are formed in perpendicular to the channel flow. Alternative to this novel and intricate method of mixing and branching the ligand solution, one can simply device a simple fluidic system for a gradually gradient surface. A fluidic channel may be placed on top of the desired surface to form reversible bonding. The solution with pre-calculated density and volume may then be placed on the inlet of the channel, allowing the solution to diffuse into the channel. As the solution starts flowing, the ligand will form non-specific binding to all the exposed surfaces, which will deplete the ligand in the solution. Consequently, less and less ligand will be deposited in the channel as the solution flows, resulting in a gradually changing gradient of ligand density.

Mechanically induced stress for varying the ligand density was demonstrated by Genzer, et al. [46, 47]. In this technique, the surface of the elastic substrate is treated with UVO while it is stretched. By doing so, more of the functional groups on the surface are exposed and treated, allowing more ligands to be attached. For simple shape substrate, the strain is uniform and thus creates a surface that has uniform density of ligand. The density itself, however, is higher than one that would be seen on an un-stretched membrane. By cutting the membrane in a dog bone shape the strain distribution no longer is uniform and thus it allows the creation of gradient protein.

1.1.3. Topographic effects

Topological features of the substrate also play critical roles in cell's behavior. The topologies reported in literatures are usually uniform in size throughout the substrate and most of them are in the form of lines (ridges and groves) [31-45]. With the advance of nano/microfabrication, investigators have started to probe the effects of well-defined nano/micrometer length scale topography on the cells. Typically, cells align themselves along the ridges and elongated. The focal adhesions of the cells are reported to be mature on patterns with micrometer length scale and they tend to be less developed on nanometer scale ridges [34, 35].

1.2. Research Purpose

In this thesis, a fabrication technology was developed for preparing suspended PDMS mebmbranes that can be used to study cellular mechanics. As an example, the effect of a substrate's mechanical properties, specifically the gradient of stiffness on the substrate, on cells was studied. Human epidermal keratinocytes (HEK) was used as a model for all studies. It should be noted that a cell's interaction with its environment is cell type specific. Most researchers have studied the effect of varying stimuli, whether that be concentration of the absorbed ligands, or the rigidity (mechanical property) of the substrates and multiple substrates with varying properties were used. For example, Semler, et al. [8] devised an experiment where the effects of the gradient of substrate rigidity and ligand concentration were studied in a systematic way. However, their experimental setup used a 96-well dish, varying the substrate rigidity in one direction and ligand concentration in the perpendicular direction. Studies with gradient of stiffness are typically done by simply placing two substrates with very different

mechanical properties side by side, which generate a very sharp gradient [2, 6] and perhaps not an ideal situation in some cases since the change in the material property is abrupt where it is more likely to be more gradual in vivo.

In this current work, two substrate systems were utilized. First, multiple compliant polydimethylsiloxane (PDMS) substrates with varying Young's modulus were prepared on coverslips. For a second set of system, a PDMS micromembrane-based substrate that has multiple gradients of stiffness was fabricated in one device. Using these devices/substrates, HEK cells' response to the mechanical properties of the substrates was studied.

The rest of the thesis is organized as followed. In Chapter 2, the development of unconventional micro/nanofabrication techniques based on nanospheres lithography, and thin PDMS membrane are described. Chapter 3 discussed the preparation of compliant PDMS substrates and fabrication of PDMS micromembrane devices in detail. The organization of focal adhesion, hemidesmosomes complexes, and laminin-332 secretion, and by HEK on compliant PDMS substrates and membrane device with multiple gradients of stiffness are discussed in Chapter 4. Chapter 4 also discussed the migration and accumulation behavior of HEK. A brief conclusion remark is presented in Chapter 5 and some future works are discussed in Chapter 6.

Chapter 2 : Development of Unconventional Micro-Nanofabrication Techniques

2.1. Introduction

As more and more research utilizing nano-microfabrication technologies are interdisciplinary, the devices that one fabricate may not be possible using existing technology. An example of this is the fabrication of microdevices used for biological experiments. In general, biological experiments need to be carried out in liquid. As such, there are cases where one needs to combine the traditional fabrication processes with nontraditional ones, either changes in processes, or addition of one or more new materials. Beyond the technical issues, there is the issue that since much of the equipment used in nano-microfabrication technology is either extremely expensive, or needs to be operated in a cleanroom environment, and it is not always easy for researchers to have access. More and more devices are being developed at nanometer length scales, or nanofeatures are being integrated with microfeatures to make the device more sensitive or effective. Many mainstream systems such as electron beam lithography, or nanoimprint lithography [1] are either too expensive or unsuitable for mass production due to the serial processing nature of the technology. As such, there is a great interest in developing new non-traditional fabrication technologies that can be combined with traditional techniques.

In this chapter, two non-traditional nano-microfabrication techniques developed during the course of this thesis work are described. The first technique used a self-assembled monolayer of polystyrene micro/nanospheres as a mask to transfer nano and micropatterns to the substrates. The second technique, called bond-detach lithography (BDL), used a polydimethylsilosane

(PDMS) stamp to transfer patterns from the stamp to PDMS film coated substrate by selectively removing materials from surfaces that are in contact with features on the stamp.

2.2. Fabrication of Nano/Micropatterns using Nanosphere Lithography

2.2.1. Introduction

There is great interest in the capabilities to fabricate large arrays of nanofeatures. Simple features such as circles and lines meet the required functions of many devices. Currently, the most popular technique to make these features is to employ electron beam (e-beam) lithography. However, e-beam lithography used in most educational institution has limitations at the moment, since it can only write a limited number of features, and there is also a limit on how far the sample stage can move. The latter limitation physically limits how big an area of the substrate can be populated with the desired nanofeatures in one single run. On top of this, e-beam lithography is a serial process, making the process tedious. To overcome some of these limitations, many unconventional lithographic techniques, including nanoimprint lithography [1], dip pen nanolithography (DPN) [71], and nanosphere lithography (NSL) [72, 73] have been developed. NSL is an attractive alternate system for creating some nanostructures as it is fairly simple, and very cheap compared to the others. One of the goals of this thesis research is to establish methods to prepare substrates that are biocompatible and use nano-microfabrication technology for probing cell mechanics at the nano-micro length scale. In the following sections, a general fabrication process using microspheres as both the etching mask and the patterns to create submicron/nano features is described.

2.2.2. Preparing microspheres coated substrate

In this work, 1.1μm diameter latex polystyrene microspheres are used. The microspheres, suspended in water, were purchased from Duke Scientific Corporation. The microspheres can be replaced by nanospheres if smaller features are desired. To use these microspheres for nano/microfabricttion, they must be assembled on a substrate. First, the substrate was cleaned by submerging it in piranha (3 to 1 ratio mixture of H_2SO_4 and 30% H_2O_2) for 15 minutes followed by a thorough rinsing with DI water. For the polystyrene spheres to spread and adhere to the substrate's surface, the surface must be hydrophilic. Thus, silicon substrates were used. To further enhance the hydrophilicity of the surface, the piranha-cleaned substrate was further treated by a 5:1:1 mixture of H_2O, NH_4OH and H_2O_2 (30%) for 5 minutes, to enhance the hydrophilicity [73]. Once the substrate was rinsed in DI water, it was kept fresh by keeping it under DI water until it was needed. The sphere solution was then diluted with an equal volume of ethanol and dispensed on a silicon substrate. Prior to dispensing the microsphere suspension, the excess liquid from the substrate was removed by touching the edge of the substrate with a lint-free paper. A drop of the diluted microsphere suspension is then dispensed on the substrates. 10-15 μl of suspension was dispensed for each 1x1 cm^2 of substrate area. The substrate was air-dried. The substrate can be used at this stage or the spheres may be transferred to another substrate. At this stage, multiple tightly packed islands of spheres along with many empty sites (voids) were formed as shown in Figure 2-1.

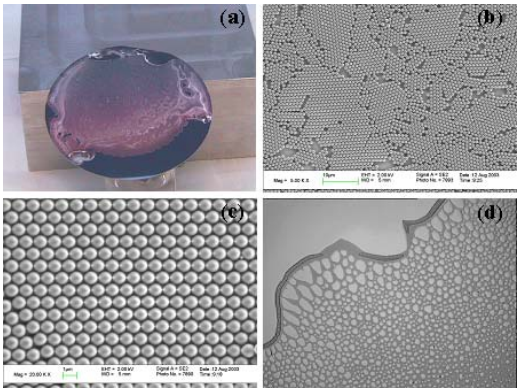

Figure 2-1: Nanospheres packing for NSL: (a) photograph of 1.1μm diameter spheres packed on a 3 inch silicon wafer, (b)-(c) SEM images of the substrate, and (d) a microscope image of the islands and voids (light areas) on an edge of a transfer substrate

To transfer the spheres to another substrate, the monolayer was slowly immersed in a beaker of deionized water. As the spheres touched the water, they separated from the substrate and floated on the surface of the water, aggregating together to form a larger area of microspheres monolayer. A new substrate was then dipped slowly into the beaker, attracting the film of spheres due to surface tension. The substrate was then slowly pulled up along with the spheres. The spheres were thus lifted off the water and air-dried on the final substrate. The substrate at this stage had multiple tightly packed islands separated by grain-boundary like defects [Figure 2-1 (b)]. The final substrate could be plain silicon, silicon nitride coated substrate or others such as silicon on insulator (SOI) or glass.

2.2.3. Transferring nano/micropatterns using the microspheres layer as a physical mask

A monolayer of polystyrene microspheres assembled on a substrate can be exploited in two different ways. Firstly, the monolayer can be used directly as a mask for reactive ion etching [74]. Secondly, the spheres can be used as tightly assembled circular patterns, more specifically as shadow mask. In both cases, the interstitial gaps are crucial as they allow the ions or metal particles to travel through to the substrate for the desired patterns to be transferred.

2.2.3.1. Microspheres as reacting ion etching mask

To use the spheres as an etching mask for reactive ion etching (STS 340, Surface Technology System), the substrates with assembled spheres were etched without any further processing after the monolayer had dried on the substrate. Many different nanofeatures can be obtained by this technique. By exposing the substrate to $SF_6 + O_2$ plasma, nano-triangles shown in Figure 2.2 (a) were obtained. Each nanotriangle is defined by the interstitial gap defined by three neighboring spheres. If desired, smaller triangles could be obtained by using smaller spheres.

By changing the gas and or other parameters such as the etch time, cylindrical nano-pillars, Figure 2.2(b), and nano-cones/pillars, Figure 2.2(c), could be obtained. The cones have six sides since each sphere has six neighboring spheres. While anisotropic etching during the RIE process results in cylindrical nano-pillars, coned structures rely on isotropic etching [75]. The cone structures result from the top of the substrate being exposed to lateral etching for a longer time than the base. Typically, $CF_4 + O_2$ plasma was used for cylindrical pillar fabrication and $SF_6 + O_2$

plasma for conical pillars. It was possible to fabricate cones with very sharp tips (a few nanometers in radius of curvature). By using a silicon nitride coated substrate, other structures, such as conical structures with circular nitride caps could be obtained as shown in Figure 2.2(d). This was possible due to different etching rates between the two materials in the RIE [76], and also because of the difference in exposed surface area. In this case, the nitride layer was protected from direct ion bombardment from the RIE machine and the undercutting was done to the base silicon surface. In all of these cases, the spheres act as stencil mask. The spheres were removed from the surface of the substrate by sonicating the substrate in ethanol.

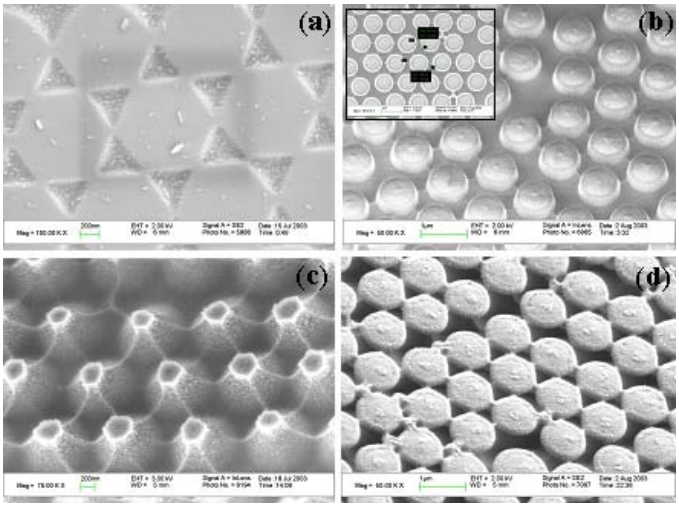

Figure 2-2: SEM images of nanofeatures obtained by using the microspheres as etching mask: (a) Nano-triangle (b) Nano-pillars (c) Coned silicon nano-pillars and (d) Coned silicon nano-pillars with silicon nitride caps.

2.2.3.2. Microspheres as a shadow mask

To generate the circular patterns projected by the spheres, a metallic mask was first deposited on a spheres-masked substrate using an electron beam evaporation system (NCR 3117, Varian). Others have used this as a way to fabricate nanofeatures [72, 73, 77, 78] using directional deposition of the metal. In the current technique, the samples were rotated during the metal

deposition to obtain a conformal coating. This way, the metal particles were able to travel under the spheres, leaving only a small area that was unmasked under each sphere. The spheres in this process, act as a shadow mask [79]. The final features, exposed silicon of circular patterns, were smaller than the initial diameter of the spheres. For the 1.1μm diameter spheres, 200-300 *nm* diameter circular features were achieved. It should be possible to further reduce this size by depositing a thicker metallic mask. After the metallic mask deposition, the spheres were removed by sonication in an ethanol. The patterns could then be transferred to the substrate by RIE. If a chromium or gold mask was used, wet etching with KOH for a short time can also be performed on the substrate.

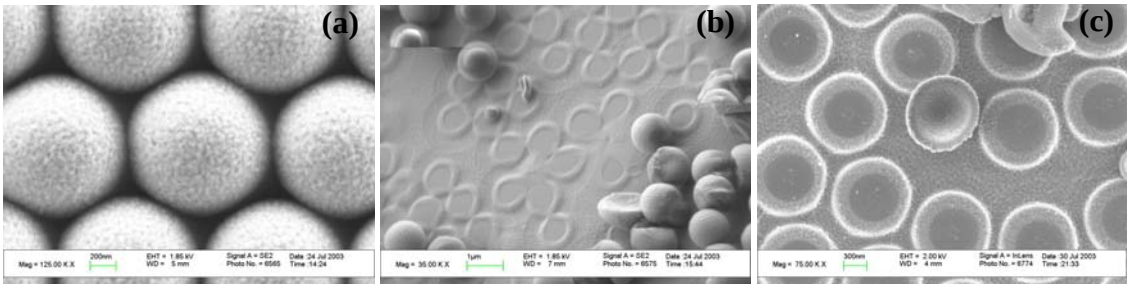

Figure 2-3: SEM images of (a) Microspheres coated with aluminum (b) Note the rings formed under the spheres by the metal deposition. The patterns inside the rings are the exposed silicon substrate (c) a pre-trenched substrate after metal deposition. The darker area in each circular pattern is the bare silicon. Also note the reduced diameter of the sphere, half of which is covered by the metal.

By combining the two uses of microspheres mentioned above, some interesting mechanical structures can be realized, as shown in Figure 2-3(c). In this case, the spheres-masked substrate was first etched for a short time with $CF_4 + O_2$ plasma to obtain a network of shallow trenches. At the same time these trenches are created, the oxygen plasma reduced the size of the spheres,

making each sphere an isolated feature. Once the metallic mask was deposited as described above, the substrate shown in Figure 2-3(c) was obtained. Since the size of the spheres was already reduced, the final resulting pattern, the uncoated silicon, became smaller than it would be if there were no pre-etching.

One feature that can be obtained using the micro/nanosphere mask, is an array of sub-micron wells, described in detail in the following section. Other features fabricated using this method include sharp silicon tips in a hexagonal array (Figure 2-4a) and a suspended porous metallic membrane (Figure 2-4b). The silicon tips were obtained by etching the exposed silicon with an isotropic recipe, $SF_6 + O_2$, using RIE. Initially, an array of sub-micron size wells was obtained. Upon over-etching, the lateral etching thins the separation between the adjacent wells, eventually causing the walls to be completely etched away. Since the separations between the microwells were greatest at the initial interstitial gaps in this processes, the high aspect ratio silicon pillars/tips remained on those sites. By etching the substrate longer until the sharp tips are gone, the metallic mask could be suspended, shown in Figure 2-4b, making a porous metallic membrane. The porous metallic membrane could be flat (Figure 2-4b), or with raised patterns (Figure 2-5) by using a pre-trenched substrate. The porous membrane can also be fabricated using silicon nitride, silicon dioxide, or silicon. As seen in Figure 2-4b, there are tips still present at the interstitial sites, under the metallic membrane. The tips are shaped by three curve surfaces since three neighboring spheres define them. These tips can be completely removed if desired.

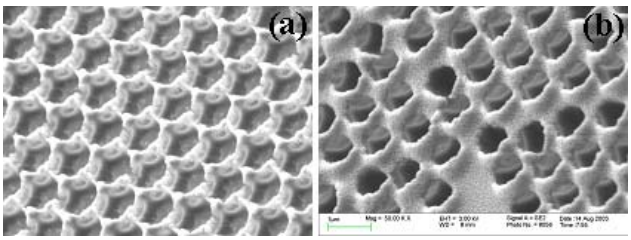

Figure 2-4: SEM images of (a) Nano pillars (metal mask not yet removed) in hexagonal array obtained by etching circular patterns obtained by the metallic mask deposition using micro/nanosphere shadow mask, (b) Suspended metallic membrane with submicron pores.

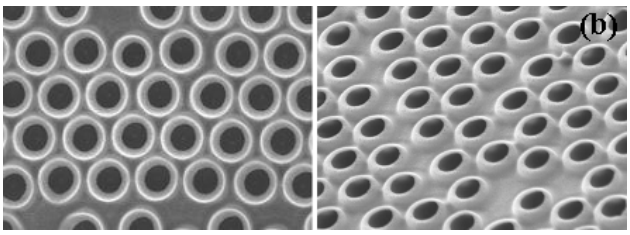

Figure 2-5: SEM images of (a) Top and (b) slanted view of RIE etching of the exposed silicon on a pre-trenched substrate masked with aluminum. The walls between the patterns are starting to open up in the image shown.

2.2.4. Preparing micro/nanospheres with integrated nanofeatures

It is possible to convert the smooth micro/nanospheres into those that are covered with even smaller nanofeatures by exposing them in Ar + O_2 plasma in a RIE chamber. The surfaces of the spheres were modified as shown. Instead of a smooth surface, the exposed spheres surfaces were covered by 50-80 nm diameter nanoparticles (Figure 2-6).

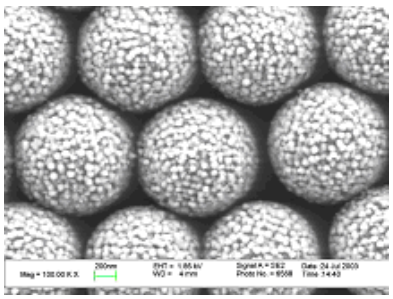

Figure 2-6: SEM image of nanoparticles on microspheres obtained by etching the spheres with Ar + O_2 plasma.

2.2.5. Application of NSL in fabricating a membrane-based superhydrophobic surface

Nano-micron patterns obtained by NSL have been used in many different applications including Raman spectral based biosensors [80, 81]. Here, a fabrication of submicron wells using the spheres as shadow mask was explored. The submicron wells were then used in preparing superhydrophobic PDMS substrates. The super-hydrophobic surfaces may be used in surface tension based on-chip liquid manipulation [82-91]. A schematic of the process flow along with some SEM images depicting some of these steps are shown in Figure 2-7.

First, the microspheres assembly on a silicon substrate was carried out as described above, and the monolayer was allowed to dry in air (step 1). The spheres' diameter was shrunken and a network of shallow trenches was etched (step 2) in the same process with CF_4 +O_2 plasma using RIE. It should be noted that high power RF can also contribute to sphere shrinkage. After the initial RIE process, an aluminum mask was deposited (step 3) conformally using an e-beam metal deposition system. The conformal coating was attained by rotating the substrate holder

during deposition. The spheres were then removed (step 4) by sonicating the substrates in ethanol, rinsed with DI water and dried. The patterns were then transferred to the substrate (step 5) using RIE. The metallic mask was then removed by wet etching (Step 7). A thin layer of adhesion reduction agent, 10% dodecyl sodium sulfate, was spun and dried on the substrate (Step 8). The substrate could be coated with silicon nitride or silicon oxide prior to depositing the adhesion reduction layer to reduce the size of the wells.

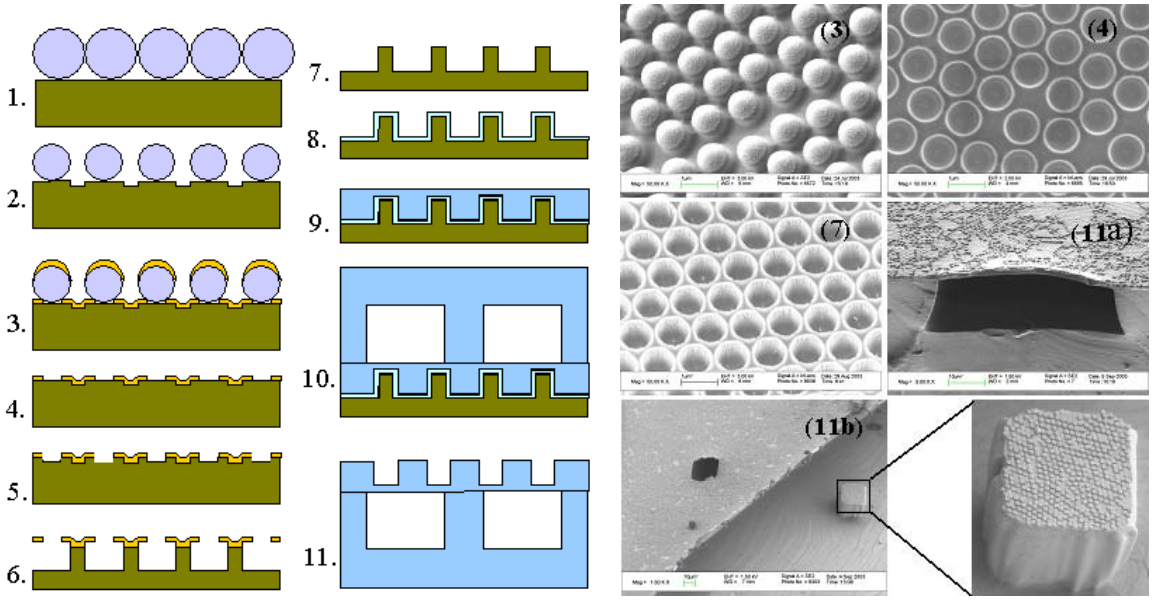

Figure 2-7: Schematic of fabrication steps for double roughened PDMS structure using NSL and SEM images representing some of the fabrication steps (corresponding fabrication step number is shown on each image).

To form a roughened superhydropobic surface, a thin PDMS membrane was spin-coated and cured on the substrate that was coated with an adhesion reduction layer (Step 9). A prefabricated PDMS structure having the primary roughness (micron size pillars) and the membrane were treated with oxygen plasma and bonded together (Step 10). The permanent bonding was formed

between the two PDMS parts, creating a structure that had both the micron roughness and the nano roughness (membrane). The device was then carefully peeled from the silicon mold (Step 11). The bottom left (with inset) and bottom right of Figure 2-7 show a roughened membrane suspended on pillars and over a groove, respectively. As apparent from the images, the membrane suspension was not very successful due to the inadequacy of the adhesion reduction layer. The improved fabrication technique is discussed in detail in Chapter 3.

To test the hydrophobicity of the replicated PDMS membrane surfaces obtained with the above fabrication technique, a droplet of water was placed on the membrane that had the integrated submicron patterns. A goniometer (AST Products Inc., VCA Optima XE, Boston, MA) was used to take the contact angle measurement. The contact angle of water on a roughened PDMS membrane replica was measured to be 140.3°, see Figure 2-8. It should be noted that the pillars on the membrane were not well defined, yet the contact angle was increased by 27° on this roughened surface compare to a flat PDMS (Figure 2-8) on which the contact angle of water was 113°.

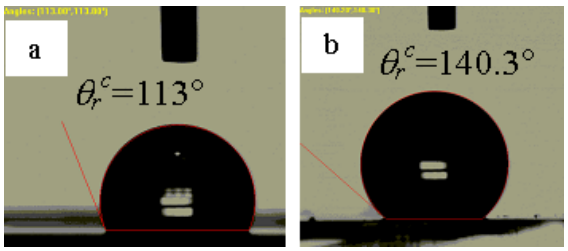

Figure 2-8: Contact angle of water on (a) flat PDMS and (b) thin membrane with submicron pillars (~850nm diameter)

For membranes with proper roughness prepared by NSL, and assuming perfect packing of the spheres (see Figure 2-9) for theoretical calculation, the wetted (Wenzel's theory) [83, 85] and

composite (Cassie's theory) [84, 85] contact angles for cylindrical pillars can be written in terms of the geometry of the surface [88] as:

$$\cos\theta_r^w = \left(1 + \frac{2\pi dH}{\sqrt{3}D^2}\right)\cos\theta_e \qquad \text{Equation 2.1}$$

and

$$\cos\theta_r^c = \frac{\pi d^2}{2\sqrt{3}D^2}(\cos\theta_e + 1) - 1 \qquad \text{Equation 2.2}$$

respectively, where D is the initial spheres diameter, d is the diameter of the PDMS pillar replica, and H is the height of the pillars. Conservatively assuming the pillar height to be 0.6 μm, which should be attainable with most RIE systems using 1.1μm diameter spheres as masks, the critical point for a robust super-hydrophobic surface [88] will be attained if the pillar diameter is around 0.6μm. At this critical point, the wetted and composite contact angles are equal to each other. For the above parameters, the critical point contact angle is ~147.50°. The contact angle of 140.3° with the imperfect sample shown above was already very close to achieving this.

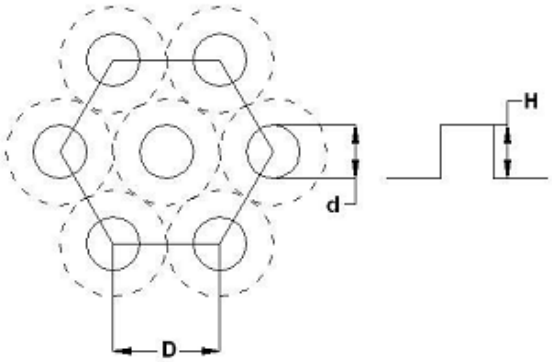

Figure 2-9: Schematic showing the geometry of roughened PDMS structure fabricated by NSL

2.2.6. Conclusion

In this section, the usefulness of a monolayer of polystyrene nano/microspheres in generating nano/micropatterns was demonstrated. Many of the fabricated structures have diverse applications. The porous membranes can be optimized and used for nanofiltration systems or cellular substrates to study the interaction of two different cell types where each type is cultured on opposite sides of the membrane to limit the interaction to occur through the nanopores. The submicron/nanowells may also be used as a master to replicate an elastic master. The master may then be may be manipulated mechanically, similar to Genzer, et al. [47], to change the spatial location in one direction so as to generate with a gradient of stiffness (See Chapter 3). The hexagonally arranged nanopillars array may also be used as the sites for nanotube growth, or as a mold to fabricate dissolvable polymeric nanoneedles for transdermal drug delivery [75]. Fabrication processes for micro/nano integrated roughened superhydrophobic PDMS surfaces were described in detailed as an example application, and in the process, the usefulness of NSL in overcoming the shortcomings of other lithography systems was demonstrated. Much improvement has been achieved in preparing the silicon mold fabrication (see step 7 in Figure 2-7) since the PDMS replicas were made. By actuating the membrane on the primary pillar structures, there by creating a double roughened surface, it is expected that a contact angle exceeding that of a lotus leaf [82, 85] can be achieved. The fabricated superhydrophobic roughened surface further improves the possibility of realizing roughness induced droplet transportation [63, 91].

2.3. Bond-Detach Lithography (BDL) for nano/microfabrication

2.3.1. Introduction

As the name suggests, the technique is based on bonding of two parts, followed by detaching to selectively create the patterns. It is based on bonding a PDMS stamp that has predefined nano/microfeatures to a PDMS film formed on a substrate. Once the master mold is obtained, the technique can be used in fabricating nano/microfeatures without needing the use of lithography equipment. Lithography is only used during the preparation of the master mold. One can then replicate the features of a master mold many times before needing to replace the mold. In fact, the stamp itself can be used to fabricate a master mold by making the negative of the stamp first. The stamps can be used multiple times, depending on the feature size. As the features get smaller the stamp needs to be changed more frequently as PDMS membrane will be building up on the stamp. The technique provides a very inexpensive way of nano/micropatterning where access to the traditional lithography equipments, is unavailable.

It is very time consuming to build devices that integrate both the nano and micro length scale features. Typically, one would fabricate the different length scale features separately, which requires a difficult alignment. Many times, the process is too difficult as repeated resist spinning, baking, patterning, and removing needs to be done for each set of features. If one resorts to e-beam lithography and optical lithography, which are the most common combination in academic setting, to do such a task, the devices have to be processed one at a time due to the serial processing in the e-beam lithography system. Similar to nanoimprint lithography [70], BDL requires only one master mold, from which multiple samples can be processed very quickly. The

master may be fabricated using a combination of multiple lithography equipments and multiple length scale. Once the master is fabricated it can last a very long time.

Not only is the technique cheap, it can also be used to fabricate critical features such as selective protection/exposure of a device. The technique is an extension of the "dry-removal soft lithography" technique [118] where patterned PDMS stamps are used to selectively remove part of the anodically etched porous silicon to generate the patterns. In "dry-removal soft lithography", the surface of the pattern is very rough since the material patterned is porous. With BDL technique PDMS film is used as the "resist." Since PDMS is widely used in research for many different applications including micro/nanofluidics [92], insulation or micro/nanoelectromechanical (MEMS/NEMS) devices [93], and soft lithography [94-109]. PDMS is also biocompatible [110]. The ability to pattern PDMS reliably in the form of both thick substrates and thin membranes/films is expected to lead to expanding the scope of its applications.

Other methods of PDMS patterning have been reported in the literature. The simplest form of patterned PDMS is a perforated membrane which was accomplished by spin-coating PDMS on a substrate with predefined photoresist posts [111]. Ryu, et al. [112] reported patterning PDMS by pouring it on a substrate with predefined patterns and removing the excess PDMS by traversing it with a blade. The process produced PDMS structures with concave profiles. Moreover, the operation of the blade traversing the photoresist can destroy the patterns. Pawlowski, et al. [113] used a similar method to create a PDMS mask that was used to fabricate glass structures by

powder blasting. Garra, et al. [114] also attempted to pattern PDMS by both wet chemical etching and dry (plasma) etching, but the patterned PDMS had a very high surface roughness that is likely to prevent its use for some applications. Childs, et al. [115] developed "decal transfer microlithography (DTM)" where patterned PDMS is added to a substrate (an additive method). The *cohesive mechanical failure* patterning process in DTM is achieved by bonding a patterned PDMS mold to the substrate and peeling it until the mold is torn and the patterns are left behind. This technique is reliable only for smaller features and the torn surface is very rough. In *selective pattern release*, an alternate procedure to DTM, the PDMS is spin-coated on a master, followed by a surface treatment to create a nonstick surface. The support PDMS layer is then cast on the pattern and cured. The pattern is removed from the master and bonded to a substrate. The handle PDMS is then peeled off, leaving behind the patterned PDMS. In the DTM technique, the PDMS patterning is achieved by a molding process and has to be done each time the pattern is transferred. Decal transfer lithography has been used for patterning non-planar substrates [116] and for large area patterning of coinage thin metal films [117].

2.3.2. Forming ultra thin PDMS film

Sylgard 184, a two-part elastomer from Dow Corning Corporation, was used in all the processes reported in this thesis. The first step of BDL requires the formation of a PDMS membrane with the desired thickness. To make a thin PDMS film, the PDMS (10:1 ratio of elastomer to curing agent) was first diluted by weight in hexane. Dilution ratio is given by the content of hexane in the solution, e.g. 10:1 dilution indicates 10 g hexane and 1 g mixed PDMS. The dilution level was varied according to the desired membrane thickness. The diluted PDMS solution was spin-

coated on the substrates using a spin coater (PMW101, Headway Research), and cured on a hot plate (TP781, Sigma Systems) for 15 minutes at 95ºC. The spin-coating parameters (6000 RPM, duration of 150 seconds) were kept constant for all samples. The thickness of the membrane was determined by removing a portion of the membrane using BDL, and then measuring the thickness with an AFM (MultiMode SPM; Digital Instruments) in contact mode.

Table 2-1: PDMS film thickness on 3 different types of substrates

Dilution ratio	Silicon [nm]	Photoresist [nm]	Teflon [nm]
5:1	NA	1250 [91	NA
10:1	NA	800 [91]	NA
15:1	NA	500 [91]	800
20:1	375	NA	451
50:1	158	180	160
75:1	123	129	96
100:1	71	56	75

The film thickness on different substrates with multiple dilution ratios is shown in Table 2-1 and Figure 2-10. The three types of substrates (diced to 1x1 cm^2) used for the data presented in Figure 2-10 were (a) (100)- P-Type silicon, (b) silicon wafer coated with Shipley 1818 photoresist, and (c) silicon wafer coated with Teflon® AF diluted with FC-77 Fluorinert (3M). In all three cases, the membrane thickness decreases dramatically as the dilution ratio increases

until it approached 20, after which the decrease in membrane thickness becomes gradual and eventually leveled off at around 70 nm.

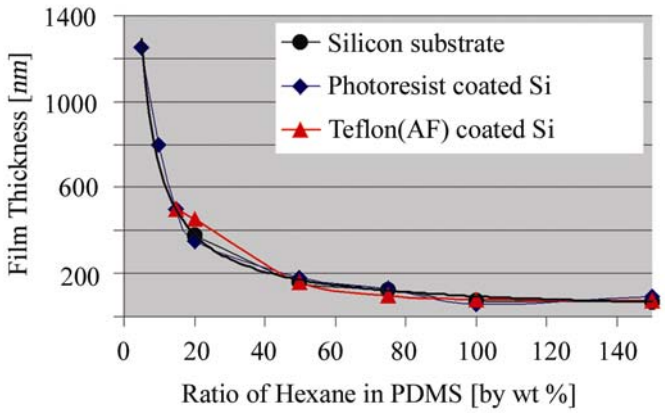

Figure 2-10: PDMS film thickness on 3 different types of substrates for different dilution ratios with hexane.

2.3.3. Patterning PDMS film

The BDL fabrication process is shown in Figure 2-11. A thin PDMS film, ~50-100 *nm* thick, was first spin-coated on a substrate (Step 1A). For the PDMS stamp, the master mold was fabricated by patterning the desired features with photoresist (SU8, MicroChem Corp) on a silicon substrate (Steps 1B-2B). Undiluted PDMS was poured on the substrate and spun at low speed (~500 RPM) for a few seconds to obtain a ~300-500 μm thick structure (Step 3B). After curing the PDMS film and stamp on a hot plate for 15-60 minutes at 95°C, the stamp that had the desired final PDMS film pattern was peeled from the substrate. The surfaces of the PDMS film and the stamp were then treated with air plasma to make the surface more hydrophilic (Steps 2A, 4B). Typically, the surfaces were treated with plasma for about 15 seconds at an RF power of ~70W. The two parts were then bonded by placing an edge of the patterned side of the stamp on the film and slowly lowering the stamp until the two surfaces formed contact (Step 5). The bonding

process was found to be easier with a more flexible substrate, and thus the stamps were made relatively thin. Placing a drop of ethanol on the membrane or structure was found to be an affective means of ensuring good contact between the patterned structure and the film [111]. The ethanol allowed the stamp to spread out due to the surface tension, and delayed bonding. The two parts were bonded after the ethanol evaporated from the surface. This is especially useful for nanoscale features in low density to ensure that (a) the patterns contact the film, and (b) the mechanical force that tends to "press" the stamp is eliminated. Applying pressure on the stamp usually causes the undesirable formation of larger contact areas and results in larger features than are present on the designed patterns (Figure 2-13).

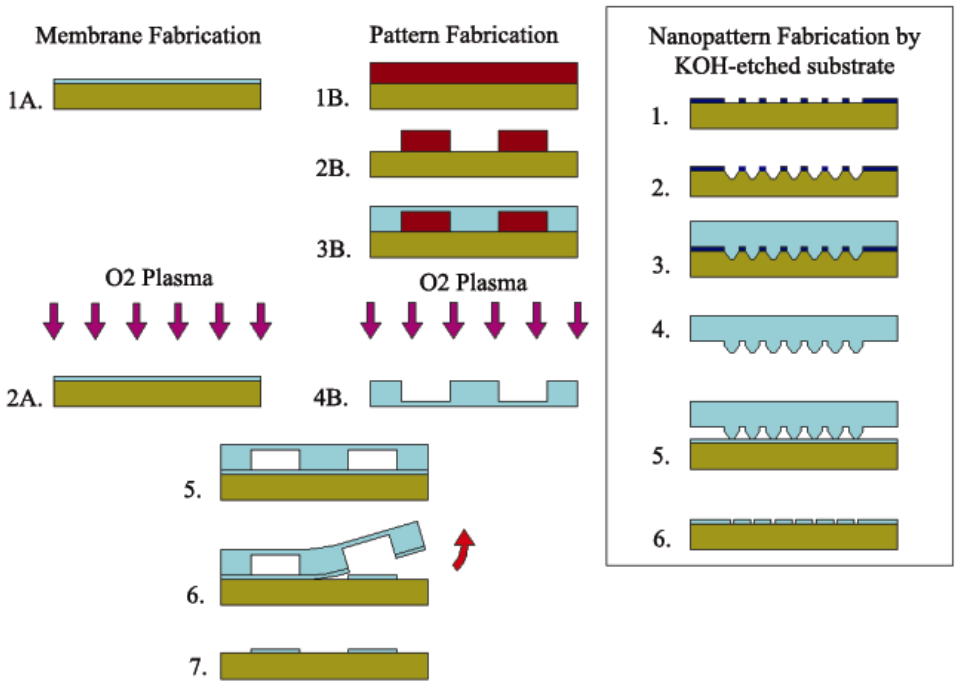

Figure 2-11: Process flow for the Bond-Detach Lithography technique. (The process flow for nanofeature patterning using a KOH-etched substrate is also shown.)

After a few minutes of bonding the two PDMS parts, the stamp was carefully peeled from the substrate that had the PDMS film (Steps 6 and 7). If good adhesion between the PDMS film and the stamp was achieved, the two parts became one solid piece. When the stamp was peeled, the film was fractured and torn along the edges where there was no contact with the structure (Step 7). It is therefore easier to tear a thinner film and thus carry out patterning. However, it should be noted that if the patterning is done directly on substrates that can form permanent bonding with PDMS, such as silicon and silicon dioxide, and film is too thin, the bonding tends to become permanent or so strong that the stamp cannot be peeled from the substrate without destroying both the pattern and the structure. The detaching step should be done within a few minutes of the bonding to prevent such permanent bonding.

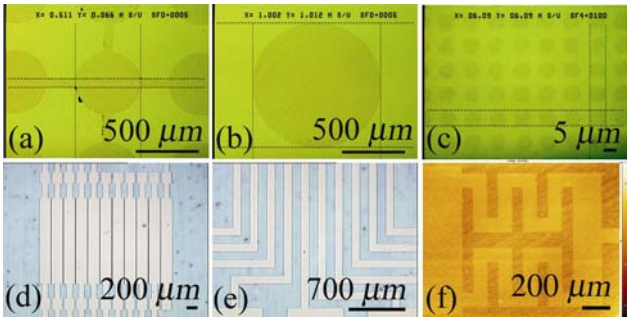

Figure 2-12: Optical images of several micropatterns of PDMS film achieved with BDL: (a) array of 511 μm diameter circles connected by 66 μm wide lines, (b) array of 1 mm diameter circles (one shown here), (c) array of 5.56 μm diameter circles, (d) array of (pattern for) electrodes with 10 μm gap between adjacent electrodes, (e) lines leading to contact pads for the electrode pattern shown in d, and (f) serpentine-shaped electrode pattern. The patterns are defined by the PDMS film left behind for (a-c) while the patterns are defined by the removed PDMS film for (d-f).

Features were fabricated to demonstrate the BDL technique (See Figure 2-12 - Figure 2-16). Optical lithography was used to prepare the molds for the micro patterns shown. The master for

nanoscale features can be fabricated using other nanolithographic techniques such as e-beam lithography. Initially, a simple KOH etch of a (100) silicon substrate and patterns generated by nanosphere lithography [72, 73, 77] was used. A wafer with a prefabricated array of circular nanoscale features was also employed. A silicon nanoimprint mold with an array of line features having widths ranging from 80 nm to 3 μm was also purchased from NTT Advanced Technology Corporation, Japan.

For the KOH-etched substrate samples, the patterns were first generated using standard optical lithography on a silicon nitride (using LPCVD) coated 3" p-type Si (100) wafer. After removing the silicon nitride pattern by reactive ion etching, the substrates were etched in KOH, which created inverted nanofeatures (pits, some were elongated lines) defined by the <111> surfaces with the <100> surface as the floor. PDMS was then poured and cured (See Figure 2-11). For the NSL molds used to replicate the circular nano patterns, the fabrication process is detailed in section 2.2. Polystyrene microspheres with a 1.1 μm diameter were used in this process to obtain features on the order of a few hundred nanometers.

For the PDMS stamp replicated with a KOH-etched substrate, the nanoscale features were much more flexible than the support structure since the aspect ratio (tapered) of the nanofeatures was very large and the features were too far apart. The patterns on the PDMS stamps were approximately 250 nm (acquired SEM images, not shown). The initial mask had 10 μm wide lines and circular patterns with 6 μm diameter. Because the structures were tall and far apart, they collapsed during the bonding process, increasing the contact area between the film and

substrate. This resulted in the final patterns being larger than the designed patterns (Figure 2-13). In general, the high-density features should have low aspect ratios to ensure mechanical integrity of the structure, so that the film is torn rather than the features on the patterned structure, and to avoid collapse of the features. Low-density features, on the other hand, should have high aspect ratio to avoid the "snap-down" due to the surface tension force [122, 123].

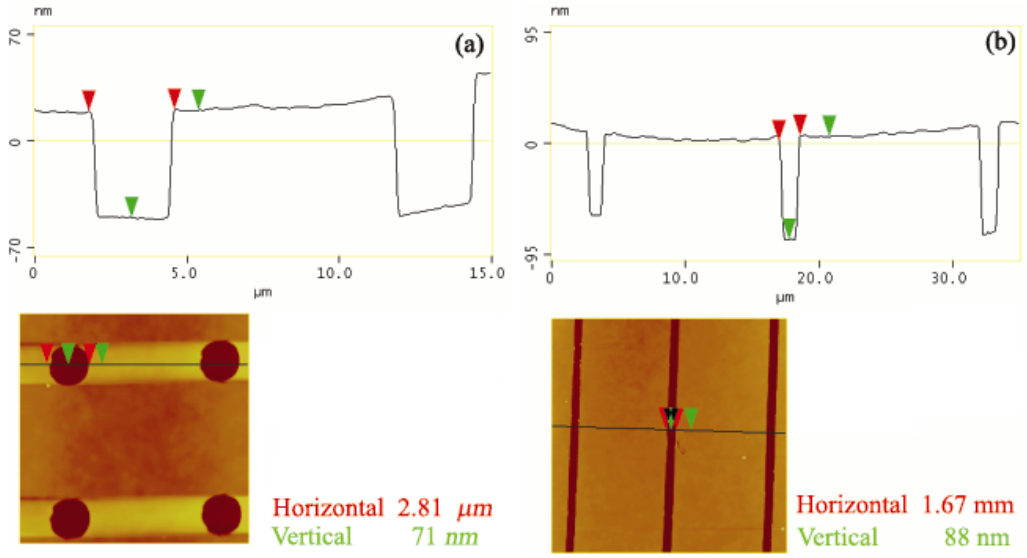

Figure 2-13: AFM scans of patterned PDMS film obtained using PDMS replicas from KOH-etched substrate. The transferred patterns shown on the films are larger than those on the master mold due to the increase of contact area resulting from the lateral collapse of the features during the bonding process. The feature size on the master PDMS structures for the diameter of the circles (left image) and width of the lines (right image) were approximately 250 *nm*.

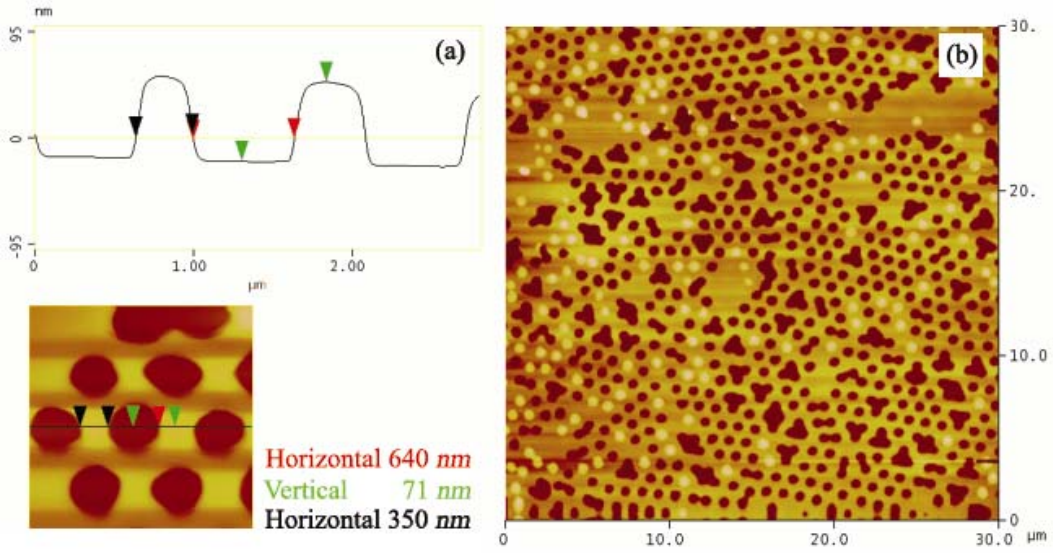

Figure 2-14: AFM scan of nanofeatures obtained by patterning the film with a PDMS replica of a substrate prepared by nanosphere lithography.[35] (a) A magnified view from (b) with the corresponding profile. White spots in (b) are patterns that were not detached successfully due to the roughness of the surface of the structural mold/stamp (AFM, picture not shown).

Since BDL relies on bonding between the PDMS film and the patterned stamp, it is critical for the mold surface to be smooth. The individual features should have smooth, continuous surfaces, and all features should be in the same plane if they are to be transferred to one surface. When the surfaces of the features are flat and have good contact with the film, the patterns can be transferred successfully as shown in Figure 2-14 and Figure 2-15. Figure 2-14a shows a magnified view with the profile of an area from Figure 2-14b. The smallest feature in Figure 2-14 is ~350 nm. As apparent from the image, only features that had good contact with the membrane transferred the patterns. The irregular features on the films are due to defects present on the stamp, which are formed by a cluster of three or four features. Figure 2-15 shows a 100 nm thick PDMS film patterned using a replica of a silicon nanoimprint mold (NTT Corp.) with

line features ranging from 80 nm to 3 μm. Features down to 80 nm were successfully transferred using this mold as shown in Figure 5. These feature sizes are comparable with that of many nontraditional lithographic techniques [94-109]. The larger features, 1μm and 3μm lines, failed during experiments because the PDMS stamp collapsed ("roof collapse") on the film. Some smaller patterns, 80-500 nm lines, also failed due to lateral collapse. If a mold is designed so that the stamp does not collapse, BDL should be a reliable, wafer-level nanopattern transfer technique. A so-called "hard PDMS" has already been developed to improve the resolution of features on the PDMS stamp, and it was also shown to eliminate roof and lateral collapses in soft lithographic processes [97, 123]. With the "hard PDMS" stamp, one can expect to eliminate the patterning failures and also minimize defects since the features will be defined with higher resolution.

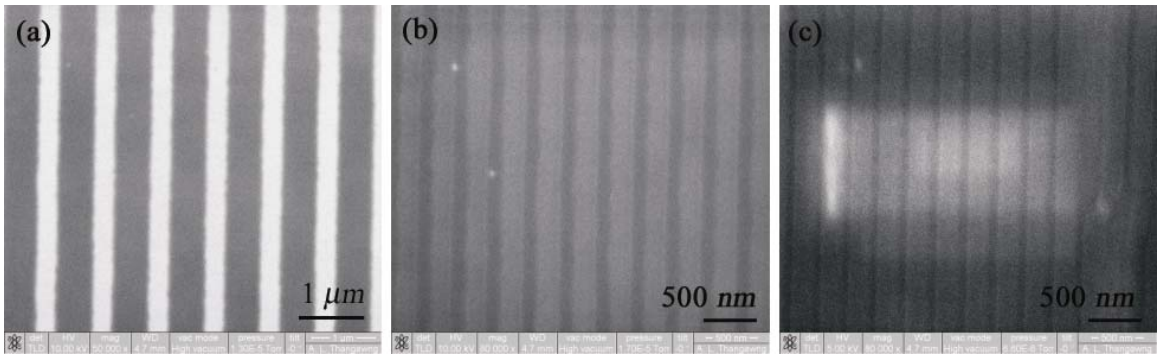

Figure 2-15: SEM images of nanofeatures patterned on silicon substrate with replica of commercially obtained mold: (a) 300 nm (b) 100 nm and (c) 80 nm lines

2.3.4. Nanofeatures generated by adhesion failure between PDMS stamp and membrane

When the surface on the stamp is not flat and good contact with the film is not achieved, the film cannot be successfully patterned. Instead of obtaining the intended features, raised patterns (nanobumps) were obtained as shown in the SEM images in Figure 2-16. The white spots from Figure 2-14b are also nanobumps. The height of the nanobumps is usually around 130 *nm* (AFM data, not shown). SEM images are shown in Figure 2-17 of the PDMS stamps used to obtain the patterns in Figure 2-16. It seems likely that the nanobumps were created when the film was stretched and started to delaminate from the substrate but adhesion between the film and structure failed before the film was torn. This patterning "failure," however, can be thought of as a different patterning mechanism to achieve nanoscale features. It is in fact related to the soft molding technique [99, 100]. In the soft molding process, part of the wet film that patterned structure contacts are removed, whereas in our method the contacted parts have raised features. By tailoring parameters such as RF power, exposure time, gas flow rate during the plasma treatment, and time before the PDMS film and stamp are brought into contact, one can likely ensure failure of the adhesion rather than the tearing of the film as occurs in BDL.

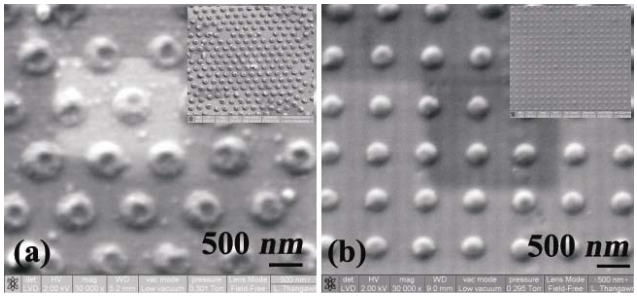

Figure 2-16: SEM images of nanobumps obtained due to the weak bonding of the PDMS stamps to the PDMS film. (a) Pattern from an NSL mold replica and (b) pattern from a replica of prefabricated substrate. (Both samples were tilted during imaging.)

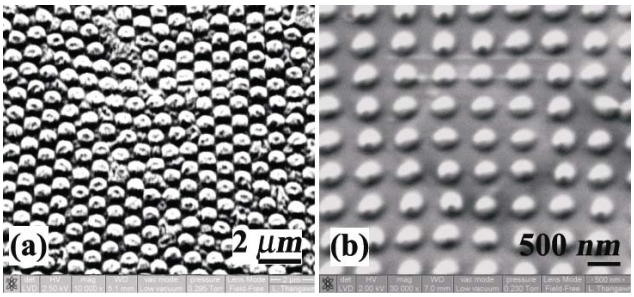

Figure 2-17: SEM images of PDMS replica from (a) substrate prepared by NSL (with Au coating), and (b) prefabricated substrate used to make nanobumps. (Both samples were tilted during imaging.)

2.3.5. Pattern transfer by microfabrication processes

2.3.5.1. Pattern transfer by reactive ion etching (dry etching)

If BDL is to become a viable lithography technique, it should allow the transfer of patterns onto the base substrate. This was tested by first etching the silicon substrate, already patterned with PDMS features, with RIE. CF_4+O_2 plasma was used for the patterns shown in Figure 2-18. The PDMS patterns acted as the etching masks in this case. The PDMS membrane is also etched by CF_4+O_2 plasma but at a much slower rate compare to the silicon. Just as in traditional lithography, the remaining resist needs to be removed. Depending on what kind of patterns were

transferred, the remaining PDMS film may be removed by polishing, BDL with a new featureless stamp, or by using commercially available solvents such as Dynasolve 220 (Dynaloy Inc) [124] for removing PDMS and other silicones. The light spots on the protected portion of the pattern in Figure 2-18a were due to the particles present on the film during the spin-coating. By carefully measuring the thickness of the PDMS film and the etch rate of the film by the RIE, a range of allowable etch times can be defined. The nanobumps obtained from the failed adhesion were also transferred to the base substrate by RIE etching. The pattern of bumps obtained by etching in CF_4+O_2 plasma is shown in Figure 2-18c. A more controlled (timed) etching will improve (preserve) the shapes of these features. More importantly, the fact that the nanobumps can be transferred suggests that the PDMS film is thicker where the bumps are, or that the etch rate is slower above the bumps. This allows one to transfer the projected surface features (circles for example) if the patterning is done on a metal-coated substrate. Chromium and aluminum, for example, may be used as the etch stop for CF_4+O_2 plasma. The exposed Cr or Al film could then be removed by their respective etching solutions. (See section 2.3.5.)

2.3.5.2. Pattern transfer by wet chemical etching

For the second pattern transfer process, the PDMS film was formed on a Cr/Au (15/30 nm)-coated silicon substrate. The metallic layers were deposited using an electron beam evaporator. After generating microfeatures using BDL, the exposed metal layers were removed by appropriate etching solutions. The adhesion of the film edge to the surface was visually checked under a light microscope after removing each metal layer . Only a very slight under-etching occurs after 1 minute of etching for each metal (Figure 2-19). This process seems to be an ideal

way to transfer the patterns since the metal layer can act as electrodes and also as an etch mask for RIE. To obtain features with well-defined edges, the film should be very thin since it is easier to tear compared to the thicker film.

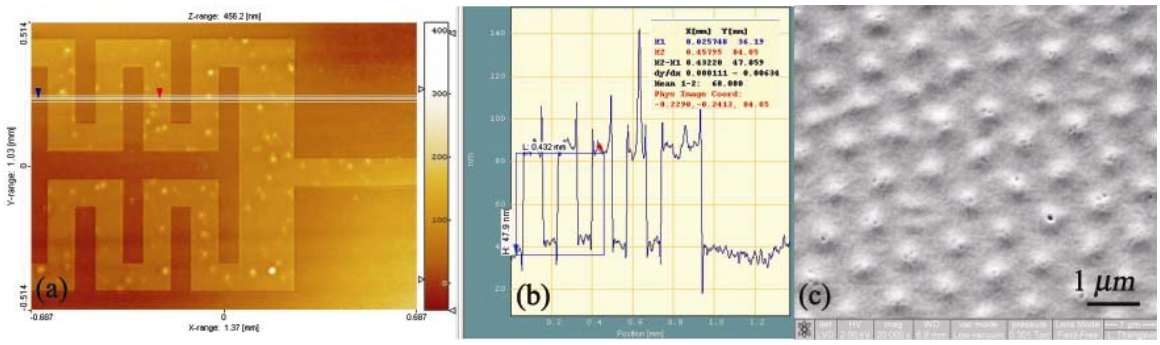

Figure 2-18: Pattern transfer to silicon substrate by RIE process: (a) optical profile image of electrode pattern and (b) step height profile of a. (c) SEM image of nanobumps in hexagonal array obtained from mold fabricated by nanosphere lithography.

Figure 2-19: BDL pattern transfer by etching metal: Optical profile images of (a) after the PDMS is patterned (b) after the Cr layer is etched, and (c) after removing the PDMS by light mechanical polishing.

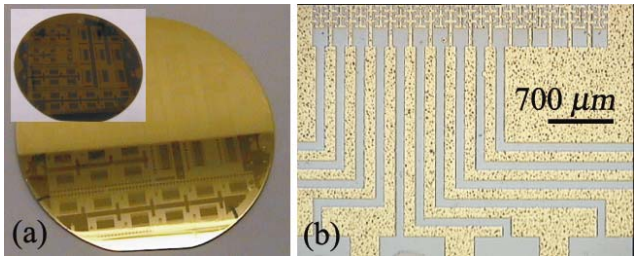

Figure 2-20: Wafer level pattern transfer on Cr/Au coated substrate: (a) photograph of before, and after etching (inset) of Au layer on a 3" wafer and (b) light microscope image of a magnified view from the same substrate (PDMS not yet removed).

2.3.6. Conclusion

This new "Bond-Detach Lithography" method based on bonding and detaching PDMS can be used to generate both micro and nano scale features. It can be a cheap and quick alternative to other lithographic techniques. Each patterning cycle takes only a few minutes and the stamp may be used multiple times, depending on feature size. Unlike many nontraditional lithography techniques, the BDL technique does not require external forces such as electrostatic force, heat, pressure or complicated surface treatment, and one does not have to worry about smudging the "ink". BDL is a parallel process, and wafer level pattern transfer can be achieved as demonstrated in Figure 2-20. Since the patterned stamp is flexible, pattern transfer on curved surfaces or uneven surfaces may be possible, as was demonstrated for microcontact lithography [101, 102]. Beside the lithographic technique, BDL has many other potential applications such as the fabrication of spacers or adhesives, electrical insulation for devices that are designed for use in liquid or moist environments, and adhesion or cells growth sites for biological studies. O-rings, seals and other such micro mechanical components can also be easily formed with BDL for other applications.

Chapter 3 : Compliant PDMS substrates and freely suspend PDMS micromembrane devices

3.1. Introduction

Historically, studies on cells have been carried out on hard substrates such as glass coverslips or polycarbonate petri dishes. However, in most cases such environments are not reflective of the natural conditions in which cells function. With the development of polymeric materials such as PDMS and acrylamide, more physiologically relevant studies on cells can be done. Most of the recent cell-substrate interaction and cell mechanics studies reported used PDMS or acrylamide gel set on a solid substrate [1-16] for two-dimensional studies of cells. The Young's modulus of the acrylamide gel substrate can range from a few (~1) kPa to a few hundreds (300) kPa where PDMS can be processed to have a Young's modulus anywhere from ~1 kPa –2.5 MPa [69, 41, 69, 128, 141]. The Young's modulus of many cells ranged from 470 Pa -15 kPa [49-55] (See Table 3-1). Many human tissues have Young's modulus in the range of 1 MPa – 5 MPa [16, 56-61] (See Table 3-2). Based on these mechanical properties of the materials, PDMS seems to have properties that can mimic a biological in vivo environment. Moreover, PDMS devices can be easily fabricated using nano/microfabrication techniques. It has been widely adopted in performing multiple experiments in many different fields of science. Most importantly for the purpose of this thesis project, PDMS is biocompatible [110]. Thus, PDMS was chosen for this cell-substrate interaction study.

Table 3-1: Elastic Young's modulus of cells

Cell Type	Young's Modulus		Ref:
HUVEC	3.4 - 15.3	KPa	49
Human tenocyte (HTIF)	87- 43	Pa	50
Cerebral endothelial cells (CEC)	0.9 – 8	kPa	51
Erythrocytes (Red blood cells)	27 – 90	kPa	52
Alveolar epithelial cells	470 – 910	Pa	53
Human foreskin epithelial cells (Young)	14 – 33	KPa	54
Human foreskin epithelial cell (Old)	37 – 110	kPa	54
Bladder epithelium cell (Normal)	7.5 – 9.5	kPa	55
Bladder epithelium cell (Cancerous)	0.3 – 1.0	kPa	55

3.2. Compliant PDMS substrates

The simplest soft substrate used to study the influence of a substrate's mechanical properties on cells is a PDMS substrate on a coverslip or culture dish. PDMS is prepared by mixing two different parts, the primary prepolymer and the curing agent. For most applications, the manufacturer recommends a 10:1 prepolymer to curing agent. It has been established that changing the ratio of prepolymer to curing agent affects the elasticity of the substrate formed upon curing [69]. On top of this, it is reported that the curing temperature of the mixed polymer caused variations in the mechanical properties [141]. Thus there are two different important

parameters that need to be tuned in order to get substrates that are comparable for all experiments performed.

Table 3-2: Elastic Young's modulus of various human tissues

Tissue	Young's Modulus		Ref:
Human Skin	3.48 – 15.3	Mpa	56
Cancerous Skin	52	kPa	57
Breast (Fibrograndular)	1.8	kPa	58
Breast (ductile carcinoma)	12	kPa	58
Airway wall (Circumferential)	3	kPa	59
Airway wall (Axial)	9.3	kPa	59
Carotid artery (Normal)	0.28	kPa	60
Carotid artery*	0.44	kPa	60
* Spontaneous cervical artery dissection			
Human gray matter	50	Pa	61
Bovine spinal cord	200	Pa	61
Thoratic aorta	1.0	MPa	16
Abdominal aorta	1.0	MPa	16
Iliac artery	3.0	MPa	16
Anterior cerebral artery	5.5	MPa	16

For this work, the PDMS mixing ratio of 10:1, 50:1, and 75:1 were chosen to cover a range of Young's modulus values. Typically, the two parts of the PDMS were weighed in a disposable

plastic beaker (Fisher Scientific) and thoroughly mixed. All the processing steps were done in a laminar flow cabinet (ESCO Technologies, Inc.). The mixed PDMS was then allowed to sit for about 10- 15 minutes to eliminate the bubbles. Once the bubbles disappeared, the PDMS was picked using a mixing spatula and a drop was placed on a previously cleaned coverslip (No.1, 130 – 170 μm thick) or in a 35 mm cell culture dish. In some cases glass bottom culture dishes were used. The PDMS drop was then allowed to spread until it covered the whole surface on which it was placed. Once that was accomplished, the substrates were transferred to an oven that was preheated to 90°C. Typically, the lids of the culture dishes were taken off so that all samples experienced the same heating condition. The samples were heated for 15 minutes after which they were taken out and left at room temperature for overnight.

3.2.1. Cleaning coverslips for PDMS substrate preparation

The coveslips were meticulously cleaned prior to placing the PDMS droplet on it. First, the coverslips were sonicated in ethanol for 30 minutes. They were then rinsed with fresh ethanol and blow-dried with a stream of compressed N_2 gas. After the coverslips were dried, they were exposed to O_2 plasma for 5 minutes on each side. The coverslips were then stored in a sterile dish for later use.

3.2.2. Mechanical properties of PDMS substrates

As mentioned above, PDMS can have different Young's modulus depending on the mixing ratio and the processing temperature. As such, it is important that the mechanical properties of the substrates are well characterized. Many research groups have characterized the Young's modulus

of PDMS and results from two groups are shown in Figure 3-1. The first set of data represents PDMS cured at 90°C for 15 minutes [69] and the second set represents those cured at 60°C for 18-20 hours [41]. Using these experimental data, exponential fits were generated. Subsequently, the Young's modulus values of the PDMS substrates used in this work were estimated from the exponential curve generated using PDMS cured at 90°C for 15 minutes, shown in Table 3-3.

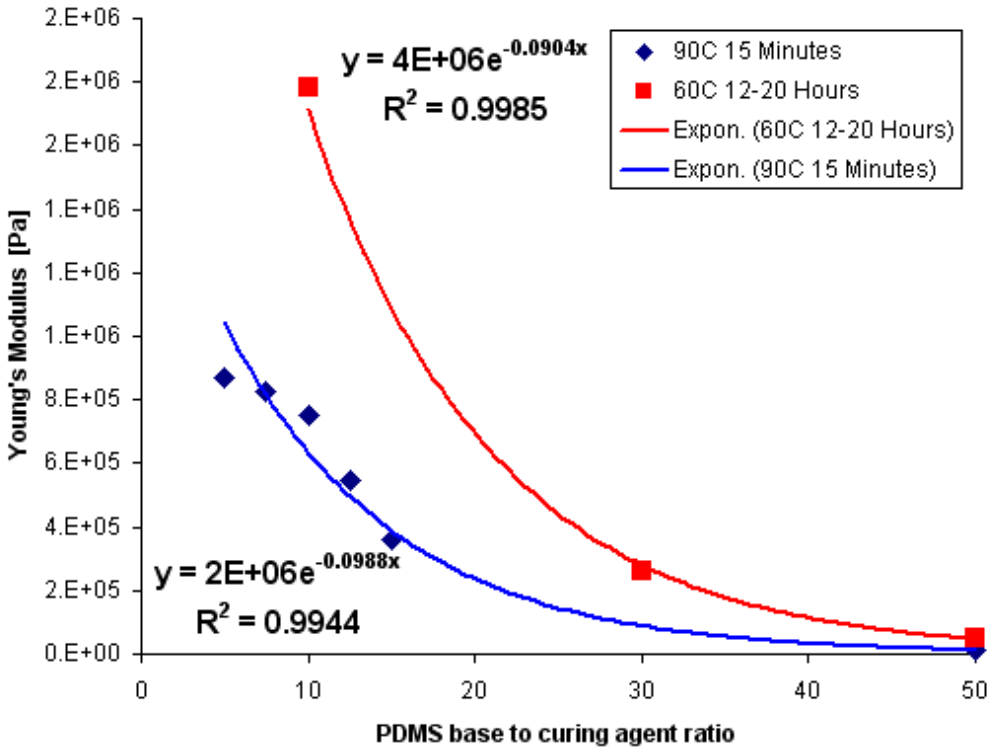

Figure 3-1: Young's modulus of PDMS based on the mixing ratio of the base prepolymer to the curing agent

Table 3-3: Young's modulus of PDMS for selected base to curing mixing ratio

(Cured at 90°C 15 minutes)

Prepolymer to Curing ratio	Young's Modulus [kPa]
10:1	744
50:1	14.3
75:1	1.2

3.3. Freely suspended ultra-thin PDMS micromembrane devices

In the following, a fabrication process of PDMS membrane device is described. The membrane device has multiple applications, including as substrates for cellular studies (See Chapter 4), micropumps, microvalves, and as scaffold for integration of other mechanical components to fabricate hybrid PDMS devices. Fabrication of the PDMS membrane devices involves processing of multiple parts that are assembled together. The processes may be divided into two groups based on the dimension of the membrane: devices with membrane thickness larger than ~500 nm with a diameter ranging from a few hundred micrometers to 2 mm, and membranes with a thickness between 70 and 500 nm for smaller diameter membranes (of a few micrometers), shown in Figure 3-2.

For the larger and thicker membrane devices, the steps related to making a perforated membrane are unnecessary. In that case, the membrane can be directly bonded to the patterned PDMS structure. Nano/micropatterns can also be incorporated onto either side of the PDMS membrane by introducing the patterns on the mold (before curing – current work), or by directly imprinting the patterns (during the curing of the flat membrane) [99, 133]. This is a case in which the NSL

based nanopattern fabrication described in Chapter 2 can be used effectively. Both the top and bottom surfaces of the large membranes are designed to be accessible for interaction with the systems studied using these devices, and also for integrating other components or devices with the system in future applications.

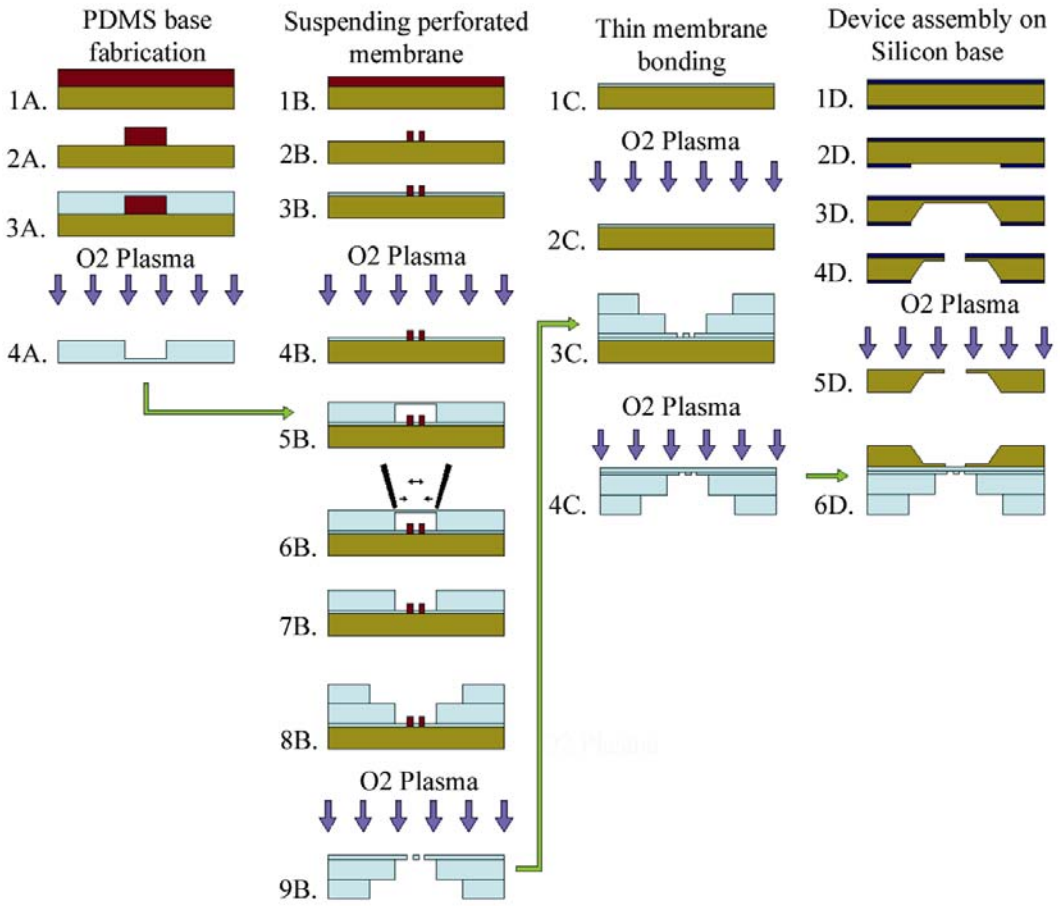

Figure 3-2: Fabrication process for ultra-thin PDMS membrane

There are two techniques to make the membrane extremely flexible. First, the mixing ratio of the polymer parts can be tuned to modulate the Young's modulus. The thickness of the membrane, however, can only be reduced down to ~3 μm [134] in the case of a pure PDMS solution. Moreover, if the Young's modulus is too low, it will be impossible to suspend the membrane.

The second option is to dilute PDMS with a solvent so that the solution becomes less viscous, allowing a thinner membrane. In this study, PDMS was diluted with hexane. This allowed the formation of membranes as thin as ~70 nm. Unless stated otherwise, a PDMS pre-polymer to curing agent ratio of 10:1 was used in all sample preparations in this project. The membrane thickness as a function of the ratio of dilution of PDMS is shown in Figure 2.10. An AFM (MultiMode SPM; Digital Instruments) or optical profilometer (MicroXam, Phase Shift Technology) was used to measure the film thickness. In the following, the details of the fabrication process are described.

3.3.1. PDMS base fabrication

The PDMS base is a substrate on which the membrane is suspended. It has a circular or rectangular through hole, that is the shape of the desired membrane. For membranes with a lateral dimension of 100 μm or larger, a ~500 μm thick SU8-2100 photoresist was first patterned to the desired size and shape of the membrane on a silicon substrate (Step 1A-2A). The patterned SU8 was hard baked at 130°C for 60 minutes. Undiluted PDMS was then spin-coated (PMW101, Headway Research) at around 500 RPM to barely cover the SU8 pillars (Step 3A). After curing the PDMS on a hotplate at 90°C for 15 minutes, the patterned PDMS film was peeled from the master and cut into individual pieces. Due to the hydrophobicity of the SU8, the PDMS meniscus was formed around the edge of the pillar, resulting a curved membrane was formed over the SU8 structure. The membranes formed over the SU8 structures were removed by peeling them off with tweezers under a microscope (Step 6B, this can also be done after bonding as well but needs to be done more carefully). The patterned PDMS surface that was formed against the silicon surface, was used for suspending the membrane.

3.3.2. Thin membrane bonding and surface treatment

To suspend a thin PDMS membrane without breaking it, the silicon substrate was first coated with diluted Teflon® solution as an adhesion reduction layer. Teflon® AF, amorphous fluoropolymer resin in solution was purchased from Dupont, Inc. Fluorinert electronic liquid (FC-77) from 3M company was used to dilute the Teflon®. A dilution of 2:1 FC-77 to Teflon® was used. After curing the Teflon® coating at 120°C for 60 minutes, diluted PDMS solution was spin-coated (Step 1C); hexane to PDMS dilution ratios (by weight) of 15:1 and 75:1 were used for ~490 nm and 100 nm thick membranes respectively. The membrane was then cured on a hotplate at 90°C for 15 minutes, and then treated with air plasma (Step 2C). At the same time the structure from the previous step (base PDMS with an opening or the perforated membrane) was also treated with air plasma to make the surfaces hydrophilic for the bonding process. The RF power of the plasma was kept approximately 70 W and the pieces were exposed to the plasma for 10 seconds. The two treated surfaces were then bonded (Step 3C). After peeling the bonded PDMS part from the silicon substrate, a freely suspended membrane over all the holes on the base PDMS structure was obtained (Step 4C). Optical images of suspended PDMS membranes are shown in Figure 3-3.

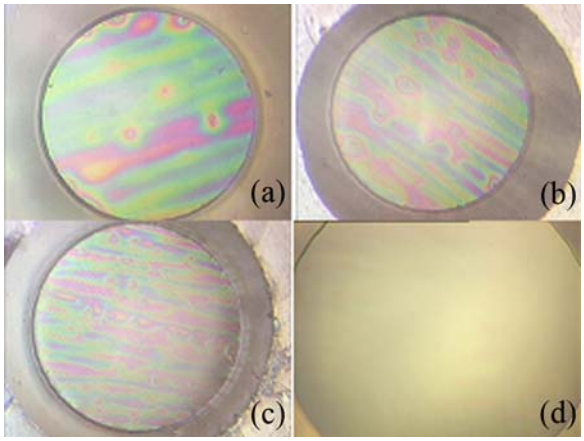

Figure 3-3: Optical images of membrane devices with different diameters (a) 315 μm (b) 488 μm (c) 723 μm (d) 491 μm. Membranes (a-c) are 492 nm thick while (d) is 3 μm* thick. (* Undiluted PDMS)

3.3.3. Fabrication of silicon base and device assembly

In most applications, the PDMS devices will interface with other components, likely, made of silicon or glass. Here, silicon was used due to the need to have a through hole to supply air or other media during testing. The silicon base for this device served two purposes: (a) it prevented the deflection of the PDMS base, and (b) it allowed the membrane to be handled more easily. To fabricate a silicon base with a circular through hole, first, a silicon nitride layer was grown (Step 1D) on a (100) silicon substrate using a low pressure chemical vapor deposition (LPCVD) furnace (BLUE, Process Technology Ltd.). The backside of the substrate was lithographically patterned to open large windows for KOH etching (Step 2D). These backside openings were designed to be much larger than the through-holes so as to not block light during characterization with an optical profilometer. The exposed silicon was etched in a KOH bath at 95°C until only a membrane with a thickness of approximately 50 μm remains (Step 3D). Circular patterns, a little larger than the PDMS membranes, were then opened from the front side using reactive ion

etching (STS 340; Surface Technology Systems) after lithographically defining them (Step 4D). A hard baked Shipley 1818 photoresist was used as the etch mask the silicon nitride layer and a 200 nm thick chromium mask (deposited using e-beam evaporator) was used for the silicon membrane. After the silicon was etched through, the nitride layer was removed by dipping the substrate in concentrated hydrofluoric acid (Step 5D). The PDMS device was then bonded to the base silicon substrate (Step 6D). Since the membrane has to be aligned to the opening of the base silicon substrate, a drop of ethanol was placed on the silicon before the two parts were brought together. The PDMS device was then manipulated under an optical microscope to align the membrane with the opening of the silicon base. Once the ethanol evaporated, a strong bond formed between the two parts. If a permanent bond was desired, the two surfaces were treated with air plasma before bonding. A thick PDMS structure with a ~5 mm diameter through-hole was then placed on the PDMS side of the device, aligning the structure hole with the membrane. This thick PDMS structure served as a seal for the liquid chamber during experiments.

3.3.4. Membrane with integrated patterns

3.3.4.1. Integration of patterns on top of the membrane

Pattern integration on the PDMS membrane is important since it provides a means to customize the membrane device. The patterns may be used, for example, as adhesion or growth sites for cells [135, 136] or as a membrane deflection readout system [137]. To integrate micro/nanopatterns on topside of the membrane, photoresist patterns were first created on a silicon substrate. The substrate was coated with diluted Teflon® AF solution, (tridecafluoro-1,1,2,2-tetrahydrooctyl) trichlorosilane (TFOTS, Gelest), or a very thin layer of parylene

(Parylene-C using PDS 2010 coater; Specialty Coating Systems) as an adhesion reduction layer. Diluted PDMS solution was then spin-coated to form a membrane on the substrate. When the patterned area of the membrane was suspended on another PDMS structure with an opening, a membrane with integrated micro/nano patterns was obtained (see Figure 3-4).

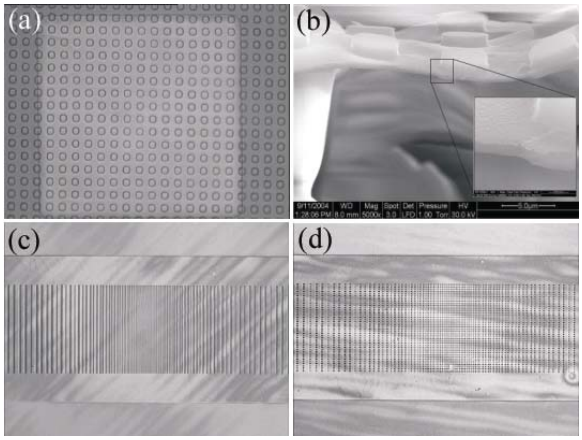

Figure 3-4. PDMS membrane with integrated patterns. (a, b) Patterns on top of suspended PDMS membrane (after suspension) and (c) Line patterns and (d) Dot patterns on the backside of the membrane (before suspension).

3.3.4.2. Integration of patterns on the backside of the membrane by Soft molding

It is possible to flip over the membrane with the patterns described above so that the patterns were on the back of the membrane. It is, however, often necessary to directly suspend the patterns on the desired (e.g., back) side. Figure 3-5 shows the process of pattern integration on a flat membrane. First, the PDMS membrane was spin-coated to the desired thickness on a substrate coated with an adhesion reduction layer. A prefabricated mold (hard or soft) was then placed on the PDMS membrane and pressure was applied, causing the mold to displace and penetrate the uncured PDMS. The membrane, with the mold and the load intact, was then heated to fully cure it. This imprinting pattern transfer technique is referred to as soft molding [99, 133].

Excessive pressure can cause penetration through the film, so an appropriate pressure must be selected. Alternatively, a height difference between the patterns and the base substrate (as represented in Figure 3-5) can be introduced to ensure that the membrane is not penetrated through. Figure 3-4 (c and d) shows 3 μm lines and dots patterns created using this technique.

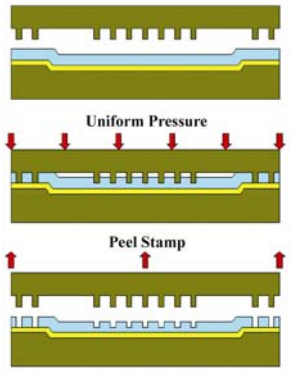

Figure 3-5. Pattern integration on PDMS membrane by soft-molding or imprinting.

3.3.5. Membrane Patterning by Micro-Die Cutting Technique

Patterning the PDMS membrane has many potential applications. In this subsection, PDMS membrane patterning by a die cutting technique is described. The fabrication process is almost exactly the same as the pattern integration shown in Figure 3-5. The only difference is in the cutting process, the stamp is pressed through the membrane. The process is similar to the microcutting process used by Stutzmann, et al. [105] to cut metal films, and is a scaled down version of the traditional die-cutting process. To cut a membrane, a cutter with sharp edges defining the desired patterns is placed on top of the membrane and pressure is applied. In general, it is difficult to completely cut a thin PDMS film with this method if the underlying substrate is hard (such as silicon). The cut may be completed with reactive ion etching. Alternatively, the membrane can be cut on a substrate that has a soft intermediate layer that will

allow the die to penetrate past the membrane. The soft intermediate layer can be a thicker PDMS film with a non-stick layer or parylene film, which can be deposited at room temperature, and can easily be removed by RIE.

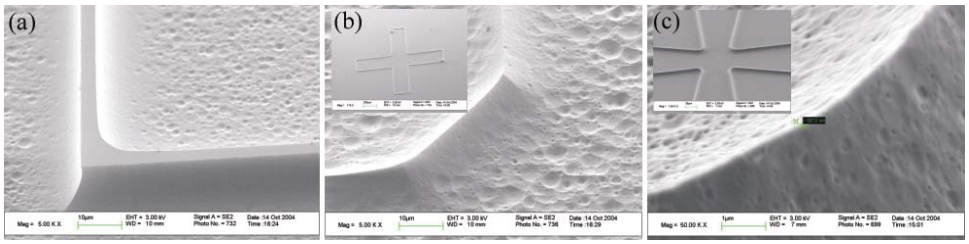

Figure 3-6. SEM images of silicon molds with different corners: (a) sharp 90° angle, (b) less sharp 45° angle and (c) rounded

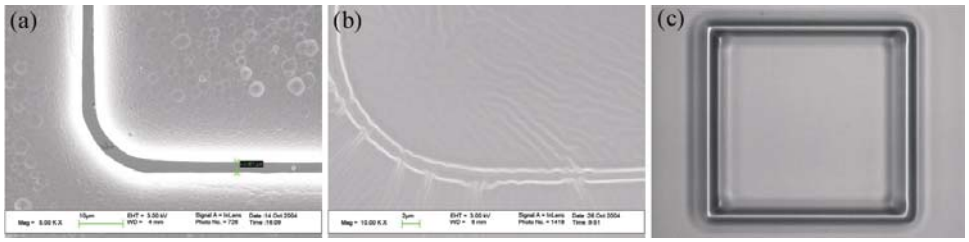

Figure 3-7. SEM images of (a) Silicon mold prepared by RIE and (b) the press-molded PDMS membrane, and (c) optical image of the same PDMS membrane

Sample dies were fabricated with silicon substrate using RIE. The desired die pattern that defines the shape of the membrane was first patterned with photolithography. The isotropic etching behavior of RIE was exploited in this process. Lateral etching in RIE causes the top of the patterned features to be narrower than the base. With appropriate parameters, this lateral etching can be exploited to fabricate patterns with a sharp edge. Since isotropic etching is desired, the corners of the features have to be rounded to eliminate the non-uniformity and discontinuity in the edge defining the patterns, shown in Figure 3-6. CF_4+O_2 plasma was used to fabricate the dies shown. An example of a cut PDMS membrane along with the die used is shown in Figure

3-7. The membranes may then be selectively suspended to make unique devices. If desired, wet etching of silicon with chemicals such as HNA (a mixture of hydrofluoric acid, nitric acid and acetic acid) may also be employed to fabricate the die. HNA, in particular, is a good candidate since it etches equally in all direction on a silicon substrate.

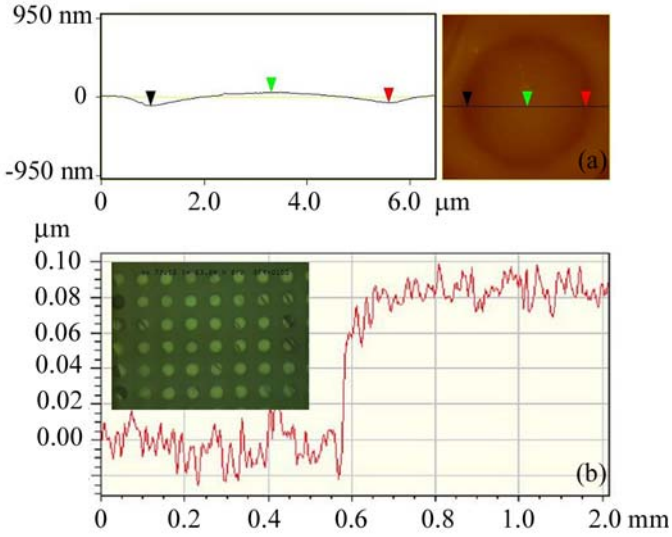

Figure 3-8: Ultra-thin PDMS membrane: (a) AFM scan of the membrane, and (b) an optical profile showing the thickness of the membrane. Inset in (b) show optical image of array of ultra-thin membrane (some are broken)

3.3.6. Suspension of ultra-thin membranes on an array of micro features

Thickness limits the size of the membrane that can be suspended without breaking. With the current fabrication protocol, membranes that are thinner than 150 nm can only be suspended over features smaller than 10 µm. If only one side of the membrane needs to be accessible, the membrane can be suspended over arrays of micro pillars or micro wells as demonstrated in Figure 3-8. The membrane shown is 80 nm thick. On the other hand, if both sides of the

membrane need to be accessible, the process shown in Figure 3-2 (with the suspension of a perforated membrane being the critical process) can be followed.

3.3.7. PDMS membrane formation on hydrophobic surfaces

PDMS bonds very well, reversibly or irreversibly, to many smooth surfaces. It was noted earlier that forming the PDMS membrane on a hydrophobic surface such as photoresist allows the membrane to be peeled without breaking it. The more hydrophobic the surface, the easier it is to peel the PDMS membrane. In the current project, Photoresist (Shipley 1818) and then separately parylene coating had been used as the adhesion reduction coating for membranes thicker than 1 μm. Though the photoresist and parylene work well for membranes thicker than 1 μm, they do not work well for membranes that are submicron thick. Thus, Teflon® AF diluted with FC-77 flourinert solution was investigated.

Diluted PDMS solution can be readily spin-coated on relatively hydrophilic surfaces such as silicon and glass substrates. However, when a highly diluted PDMS solution is dispensed on a hydrophobic surface such as a Teflon®-coated silicon substrate, the solution tends to roll off the surface, as the one property of Teflon is its ability to prevent the wetting by most liquids. Due to low surface tension between the solution and the substrate, the solution forms a sphere instead of spreading on the surface as it would on a hydrophilic surface such as a glass. Because of this, when spinning was initiated, the solution that might have remained on the substrate simply rolled off and the membrane could not be formed. To prevent the diluted PDMS solution from rolling off, the outer edge of the hydrophobic surface was patterned to expose bare silicon surface. The

exposed silicon surface is much more hydrophilic compare to the Teflon® surface and acted as a retainer for the solution during spin-coating. This allowed formation of submicron thick PDMS membranes on the Teflon® coated silicon substrate.

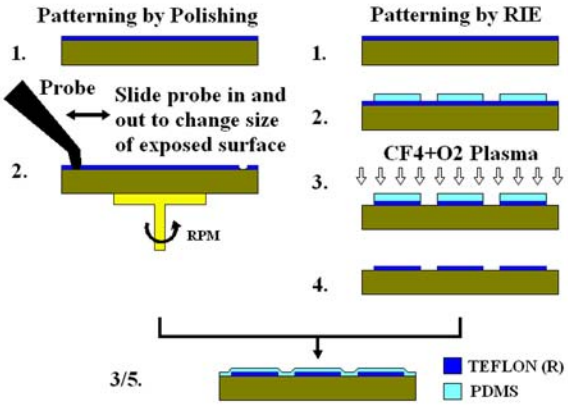

Figure 3-9: Two strategies for Patterning Teflon® coating to form hydrophilic ring for fluid retention

Two different methods of patterning Teflon® were developed, see Figure 3-9. The first uses mechanical polishing to remove the coating, while RIE is used in the second. For mechanical polishing, the Teflon®-coated substrate was spun at 2000 RPM. A polishing probe, blade or tweezers, was brought lightly into contact with the substrate at the desired location. As the substrate spins, the Teflon® is removed from wherever the probe is touching the substrate. When a direct contact of the probe and the substrate is not desired, a clean room wipe, wetted with acetone or isopropyl alcohol can be used to remove the Teflon coating. For the second patterning technique, a circular PDMS mask was placed on top of the Teflon® coating and the exposed Teflon® was etched in CF_4+O_2 plasma using RIE. The PDMS mask was peeled from the substrate after etching was completed.

3.3.8. Analytical equation for circular membrane loaded with a uniform pressure

For simplicity, a circular membrane was chosen for characterizing the PDMS membrane. The geometry defining the membrane is depicted in Figure 3-10. For larger membranes (a diameter of 300 μm and larger), the bulge test was chosen for characterization. Assuming that the membrane deflection is hemispherical, a small deflection of the membrane is given by [67, 138]

$$P = \frac{C_1 t}{a^2}\sigma_0 w_0 + \frac{C_2 f(\nu) t}{a^4}\frac{E}{1-\nu} w_0^3 \qquad \textbf{Equation 3-1}$$

where P is the pressure applied to the membrane, w_0 is the maximum deflection measured at the center of the membrane, a is the membrane radius, t its thickness, σ_0 its residual stress, E its Young's modulus, and ν its Poisson's ratio. The geometrical coefficients C_1, C_2, and $f(\nu)$ for circular membranes are 4, 2.67 and 1 respectively [67].

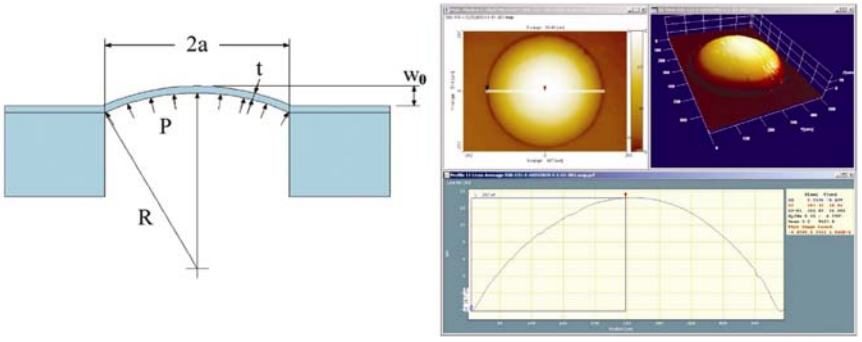

Figure 3-10. (a) A schematic showing membrane geometry and loading condition, and (b) A typical screen shot from MicroXAM profiler output for data collection.

Equation 3-1 can be further simplified to calculate the residual stress on the membrane and the Young's modulus of the material. Dividing both sides of equation 3-1 by the deflection w_0 yields:

$$\frac{P}{w_0}=\frac{C_1 t}{a^2}\sigma_0+\frac{C_2 f(\nu)t}{a^4}\frac{E}{1-\nu}w_0^2 \qquad \textbf{Equation 3-2}$$

which has the form $Y=A+Bx^2$. A plot of $\frac{P}{w_0}$ versus $w_0^{\,2}$ gives a straight line and the slope can be used to calculate the Young's modulus while the intercept is used to calculate the residual stress.

3.3.9. Characterization of PDMS substrates by bulge test

3.3.9.1. Fluidic cell design for bio/chemical experiments

Since physiological conditions will be critical for future experiments, a fluidic cell capable of delivering cell culture media to one side of the membrane was fabricated. The system also allows inflating the membrane (see Figure 3-11). The fluidic cell has three different ports, inlet, outlet, and device port, each positioned at different heights. The membrane device was placed on the lowest port and the media was supplied from the highest port, which was critical for ensuring that full contact was maintained between the membrane and the media at all times. This also eliminated the formation of bubbles inside the fluidic chamber.

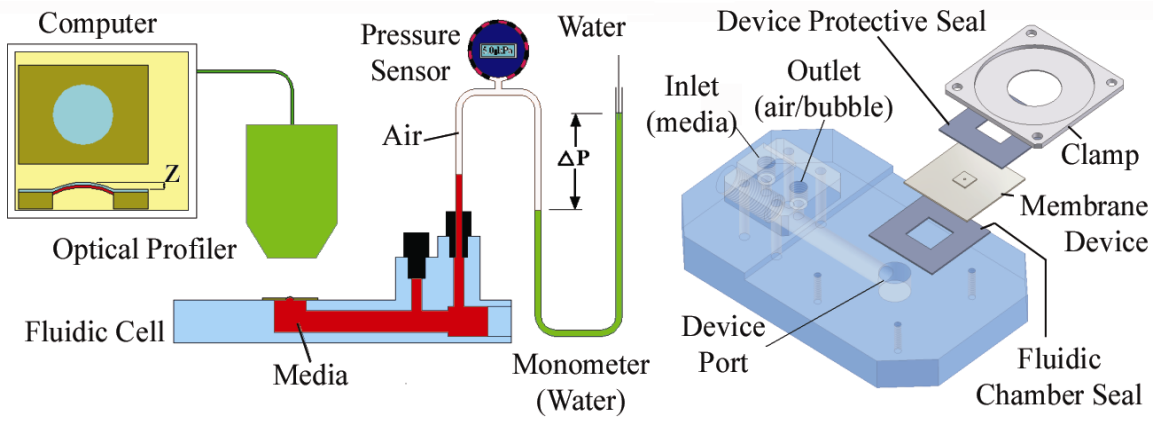

Figure 3-11: Experimental setup for PDMS membrane characterization.

The membrane device was placed over the device port that had a PDMS seal on top. The device was then clamped from the top to ensure the chamber was leak tight. Another PDMS spacer was placed between the device and the clamp, to prevent the silicon base from breaking. The culture media (water for all characterization experiments when liquid media was used) was supplied from the inlet port. The air-outlet port was maintained in the open position during the addition of the media to allow bubbles to float away. The chamber was filled with media until it completely filled the outlet port. The air outlet port (mid level) was then plugged. The highest port of the fluidic cell was then connected to a U-tube manometer that could be pressurized up to 10 kPa using water. The water column height could be read to within 1 mm, which corresponds to ~10 Pa. The initial membrane deflection was measured by scanning the membrane with an optical profilometer. The membrane was then pressurized incrementally, by adding water in the manometer tube. The corresponding membrane deflection for each pressure increment was scanned with the optical profiler. The change in water column height was also recorded for each measurement. The manometer acted as both the pressure sensor and the pressure transducer. A typical screen shot of the optical profilometer output for load-deflection data collection is shown in Figure 3-10.

One feature of the experiment setup was that the top of the membrane was dry, which was necessary for conducting measurements with the optical profilometer. Furthermore, it provided a good configuration for integrating sensors for future development. A computer-controlled pump could be easily attached to the manometer to carry out a dynamic experiment. For a small

deflection study, the manometer can be eliminated and the media inlet port can be used as a direct loading port for both static and dynamic loading.

3.3.9.2. Result and Discussion

Representative load-deflection experimental data are plotted in Figure 3-12 for two groups of devices (493 nm and 3000 nm thick). For each group of devices, three different diameters, approximately 300 μm, 500 μm and 750 μm, were tested. For clarity, data for only a single loading-unloading cycle is shown in the plots for each membrane. Up to four cycles of loading-unloading data from each membrane were used to calculate the residual stresses and effective biaxial modulus presented in Table 3.4. The membrane thickness of 492 nm is obtained by spin-coating a 1:15 diluted PDMS (in hexane), and the 3000 nm thick membrane by spin-coating undiluted PDMS. Note the difference in the deflection amplitudes in Figure 3-12 for membranes of similar diameters but with different thicknesses.

As apparent from the plots, the membranes' deflections fit extremely well with the analytical model as given by equation 3-1. Within the range of deflections tested, the membrane response was elastic, virtually without any hysteresis. The membranes are extremely flexible due to the low Young's modulus and the thickness of the PDMS. As a comparison, a 492 nm thick PDMS membrane with a diameter of 287 μm has similar load-deflection curves with a 55 nm thick 600 μm *(diameter)* Au-polymer nanocomposite membrane reported by Jiang, et al [140].

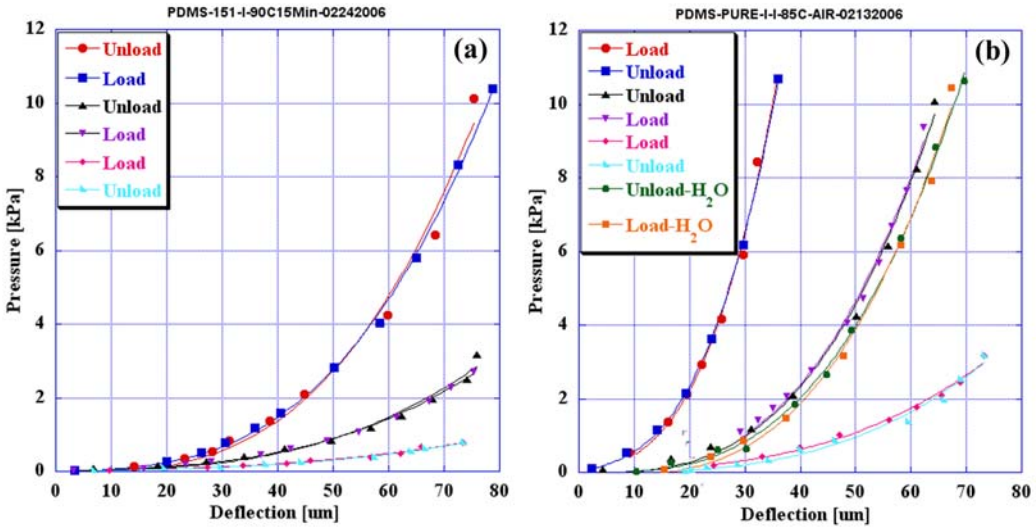

Figure 3-12: Load-deflection curves for membranes with different sizes and thicknesses: (a) 492 nm thick with a diameter of [●, ■] 315.1 μm, [▲, ▼] 488.63 μm, [◆, ◣] 731.2 μm, and (b) 3000 nm thick with a diameter of [●, ■] 287.3 μm, [▲, ▼, ●, ■] 491.32 μm, [◆, ◣] 722.7 μm.

The biaxial modulus, $\frac{E}{(1-\nu)}$, are presented in Table 3-4. Assuming $\nu = 0.5$ for PDMS [69], the average values of Young's modulus obtained from the experiments are 6.61MPa and 7.76 MPa for undiluted and diluted PDMS films respectively. These values are much higher than the normally reported values of 2.5 MPa. The Young's modulus values of bulk PDMS usually fall within 12 kPa - 2.50 MPa [6, 9, 41, 69, 128, 141], depending on the processing conditions. Since similar values of Young's modulus were obtained for membranes fabricated with diluted and undiluted PDMS, the dilution of PDMS does not seems to be the primary cause of the much larger Young's modulus obtained. Rather, it is likely due to the fact that the membranes were formed by spin-coating the PDMS solution at a high speed (6000 RPM) for a relatively long time (up to 150 seconds). The Young's modulus values reported in the literature are based on

relatively thick (a few tens of microns to two millimeters) substrates obtained by pouring the PDMS on a flat base. We speculated that the polymer chains are pre-stretched during spin-coating, while they relaxed for the ones prepared by pouring without rotation. The fact that there is a 2.51 MPa difference in the experimentally obtained biaxial modulus between the undiluted and diluted PDMS also supports this. Undiluted PDMS is extremely viscous compare to the diluted PDMS and it would require much more centripetal force to untangle the polymer chains. The processing temperature can also have a major effect on the Young's modulus of the materials [141].

Other conditions that might have contributed to the larger Young's modulus obtained are the flatness of the membrane, and the uniformity of the membrane thickness. When the membranes were peeled from the substrate, ridges were formed if the membrane got folded (small, step-wise folding), and multiple folding may occur. These ridges could become permanent if the membrane is exposed to O_2 plasma. The ridge formation was more pronounced in thinner membranes, and also when the membrane was exposed to the O_2 plasma for a longer period. Optical images showing four different membrane devices are shown in Figure 3-3. A close inspection of these images revealed that number of ridges increases as the membrane became more flexible. The colors of the membranes in the images also suggest that the membranes were not completely flat. This may be attributed to the non-uniform coating of the Teflon® layer and also the dirt particles that were introduced during the preparation of the solution.

Table 3-4: Calculated Residual stress and Young's modulus values for PDMS membranes

Sample ID	Membrane Diameter [μm]	Membrane Thickness [nm]	Process Temperature [ºC]	Residual Stress [MPa]	E/(1-v) [MPa]
300-I	287.3	3000 (Pure)	85 (15 min.)	0.072	10.40
500-I	491.3	3000 (Pure)	85 (15 min.)	0.050	15.60
500-I-H_2O	491.3	3000 (Pure)	85 (15 min.)	-0.005	14.72
750-I	722.7	3000 (Pure)	85 (15 min.)	0.048	15.06
1000-I	986.1	3000 (Pure)	85 (15 min.)	0.047	10.19
			Average	0.042	13.22
			Standard Deviation	0.028	2.64
300-I-15:1	315.1	492 (Diluted)	90 (15 min.)	0.040	9.59
500-I-15:1	488.6	492 (Diluted)	90 (15 min.)	0.162	13.87
500-II-15:1	488.0	492 (Diluted)	90 (15 min.)	0.138	19.64
750-I-15:1	731.2	492 (Diluted)	90 (15 min.)	0.177	15.66
750-II-15:1	722.9	492 (Diluted)	90 (15 min.)	0.176	18.80
			Average	0.129	15.51
			Standard Deviation	0.057	4.05

For future membrane fabrication, the non-uniformity in the adhesion reduction layer may be reduced by using a vapor-deposited adhesion reduction layer. The calculated effective Young's modulus varied between devices due to handling during fabrication and membrane geometry, but

each individual device exhibited reproducibility during experiments. They can therefore be used with proper calibration, like many other mechanical devices used for precision measurements.

The majority of data presented here was from experiments where the pressurizing media was air. Although PDMS is reported to be one of the most gas permeable polymers [142], we did not observe any pressure change inside the fluidic chamber for the duration of our experiments, which suggested that the gas permeation through the membrane can be neglected for such lengths of time. The membrane response was found to be the same when the chamber was filled with water. Data for both air and water as a function of pressure for the same membrane, with a diameter of 491.3 μm are plotted in Figure 3-12b. The difference in the membrane deflections of the two experiments was due to the initial deflection of the membrane in the water filled experiment. This initial deflection resulted from the built-up hydrostatic pressure as the membrane sat lower than the highest level of water in the fluidic cell. This hydrostatic pressure was approximately 0.30 kPa and it closely corresponded to the shift shown in Figure 3-12b. The slopes of the plot $\frac{p}{w}$ vs. w^2 (not shown), which were used to calculate the Young's modulus of the material, are essentially the same for the membrane tested with air or water as the pressure media inside the fluidic chamber.

3.4. Fabrication of PDMS membranes with precisely controlled spatially varying stiffness

Using above process, a suspended PDMS membrane with precisely controlled spatially varying stiffness was fabricated. These membrane devices were used to study cell-substrate interactions described in Chapter 4. The fabrication of these particular membranes and the assembly for cell experiment, Figure 3-13, are briefly described for clarity.

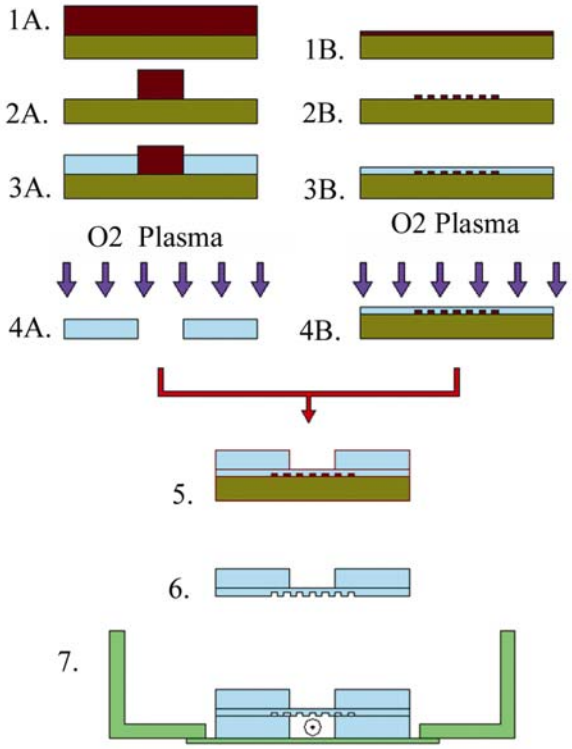

Figure 3-13. Fabrication process of PDMS membrane device and assembly in culture dish for cellular experiment

SU-8 2100 photoresist was spin-coated on a 4" silicon wafer [Step 1A] and patterned to form large rectangular islands to define the overall membrane geometry [Step 2A]. These SU-8 structures were approximately 500 μm tall with lateral dimensions of 750 μm X 4 mm. The

micropatterns, 3 μm dots or lines with a vertical dimension of 500 nm, to be integrated to the membrane were also patterned on a silicon wafer using Shipley 1805 resist [Step 1B-2B]. Both patterns were hard baked at 130°C for 60 minutes. The substrates with patterns were then coated with diluted Teflon® and cured at 120˚C for 1 hour. The thick PDMS base structure and the PDMS membrane were then formed by spin-coating as described earlier [Step 3]. 1:15 diluted PDMS (in hexane) was spin-coated at 6000 RPM for 90 seconds to form 492 nm thick membranes.

The PDMS parts were then cured on a hot plate at 90°C for 15 minutes. The thick PDMS structure was peeled from the SU8 mold and the membranes that formed on top of the SU8 structure were removed. The PDMS structure was then cut into pieces and sonicated in ethanol. After drying, the PDMS structures and the membrane were exposed to air plasma for bonding [Step 4]. Since the micropatterns needed to be located in the middle of the rectangular opening of the PDMS structure, a drop of ethanol was placed on the structure and it was brought into contact with the membrane. The base structure was manipulated to align the micropatterns [Step 5]. The two parts formed a permanent bond and were peeled from the substrate [Step 6]. The whole membrane device was then placed in a glass-bottom dish with two strips of PDMS as spacers [Step 7]. The two spacers, approximately 500 μm thick, formed a channel under the membrane, which is critical for imaging purposes. If a donut shape spacer was used, bubbles formed on the glass coverslip and interfered with imaging. By having a channel under the membrane and filling the channel with culture media, a continuous path for the light transmission is formed and images can be obtained normally. The height of the spacers is also critical. If it is too thin, the membrane

collapses on the glass due to the surface tension and if it is too thick good focus cannot be obtained for imaging.

3.4.1. Stiffness Gradient Generation

The lines or dots micropatterns were used to generate the stiffness gradient in this system. The stiffness gradient was achieved by varying the spacing between the micropatterns along the length of the membrane. The line micropatterns spanned across the width of the membrane, and the spacing between any two adjacent dot micropatterns across the width was kept constant. This ensured that the stiffness variation occurred only in one direction: along the length of the membrane. The density of the micropatterns gradually decreased from one end to the other of the active region. In general, the stiffness of the membrane increases spatially as the density of the micropatterns increases. A schematic showing the geometry of the membrane is shown in Figure 3-14. Generating a stiffness gradient on the membrane using this technique is simple, yet effective. Multiple gradients of stiffness can be incorporated on a single membrane as shown in the computational model in the next section. A detailed drawing showing the spacing of the micropatterns is shown in Appendix.

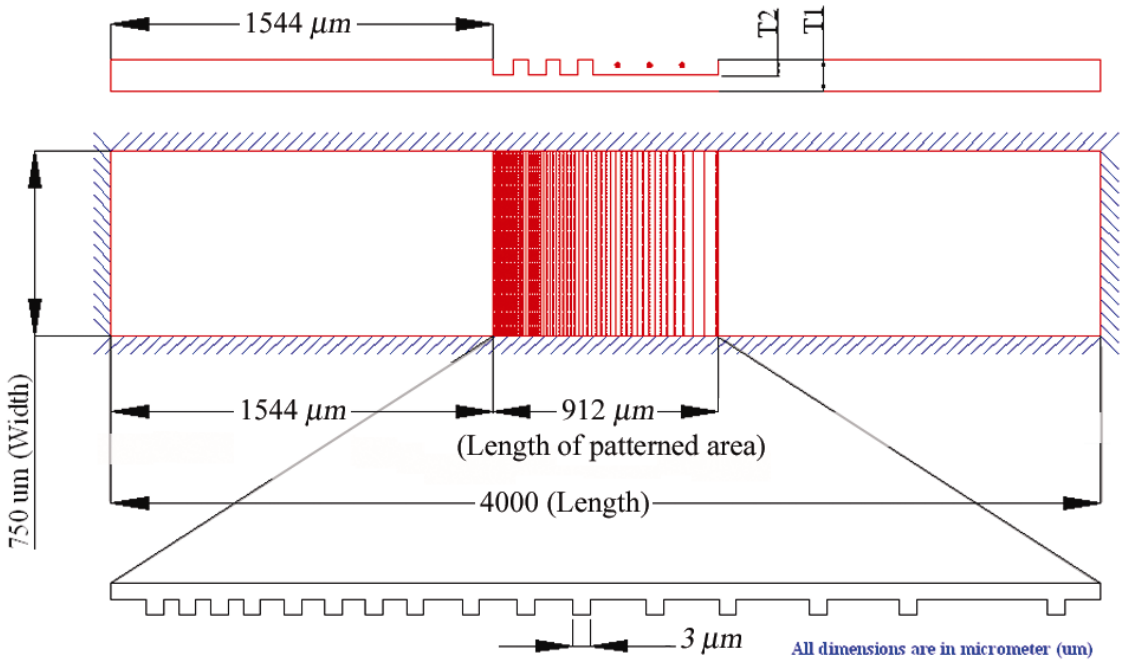

Figure 3-14. Schematic showing geometry of PDMS membrane with integrated micropatterns for spatially varying stiffness

3.4.2. Spatially varying stiffness curve by computational model

The membrane device was modeled with ANSYS® finite element software to determined the effective stiffness at different locations. These provided the relative spring constants for different positions. A 10 nN shear load was applied, at the midpoint along the width, to the membrane in the direction along the length of the membrane. The load was applied on top of the microfeatures and between two adjacent patterns. A Matlab® program was also written to estimate the stiffness in 1D. The resulting stiffness curve showed that there are three distinct slopes within the patterned region of the membrane. The first segment of the membrane, where the micropattern density is highest, has the highest rate of change in stiffness. In the middle of the patterned region, there is very little change in stiffness. The last segment of the patterned membrane area

has slightly higher rate of stiffness change relative to the middle portion but less than the stiffest part of the membrane. See Figure 3-15. The lower and upper curves are results of the Matlab® and ANSYS® programs respectively. The difference in the magnitude of the stiffness was due to the fact that the Matlab® program only considered a 1-D model where as the ANSYS® program computed for a 3-D model. The computational model used a Young's modulus of 750 kPa and a membrane thickness of 500 nm with the micropatterns having a vertical dimension of 500 nm.

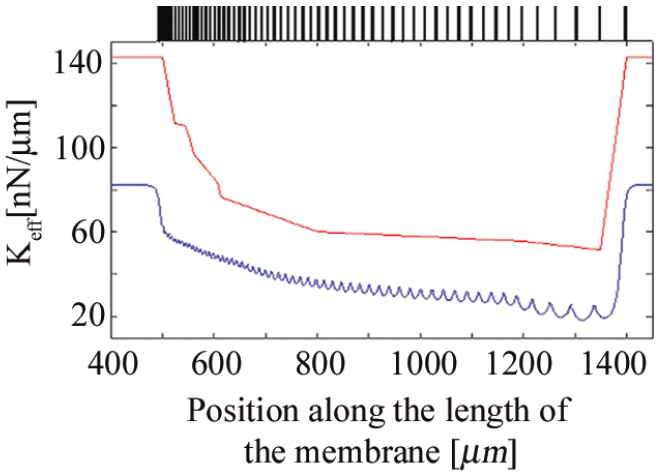

Figure 3-15: Membrane stiffness profile with lines indicating the positions of the micropatterns. The blue curve shows 1D Matlab calculation and the red curve was obtained using 3D ANSYS model (Credit: Xavier Diego and Wing Kam Liu)

Local peaks can be observed on the stiffness curve generated by Matlab program (Blue). These represent the local peak in stiffness computed right on top of the microfeatures. It should also be noted that the stiffness curves jumped to the high limit at either side of the active region. This high limit represents the stiffness on the thicker membrane that bounded the active region on

either side. Another interesting result obtained from this computational model was the fact that there were vertical components in the displacement calculation even tough there was no vertical component in the load. This vertical displacement in fact can be sometimes larger than the in-plane displacement as shown in Figure 3-16, and Figure 3-17. It should be noted from these plots that the vertical component of the membrane deflection increases as the thickness of the membrane decreases.

Table 3-5: Summary of substrate deflection for a 10 nN point load parallel to the suface

Sample Type	Thickness [nm]	Deflection X- Dir [nm]	Deflection Z- Dir [nm]	Deflection Total [nm]
Membrane (suspend)	500	3.8	10.7	11.2
Membrane (suspend)	1000	2.5	5.2	5.2
Plain (on coverslip)	100000	4.6	0.4	4.6

To compare the effective stiffness of these suspended PDMS membrane with that of plain PDMS substrates, the two systems were modeled with a multiphysics modeling software (COMSOL). The systems were subjected to similar loading condition (10nN point load parallel to the surface). For these models, Young's modulus of 7.75 MPa was used for the PDMS membrane while 750 kPa was used for plain PDMS substrate. The deflections of the three different substrates are summarized in Table 3-5. As the seen from these results, although the Young's modulus of the PDMS membrane is an order of magnitude larger than the plain PDMS substrates, the effective stiffness of the two systems are comparable.

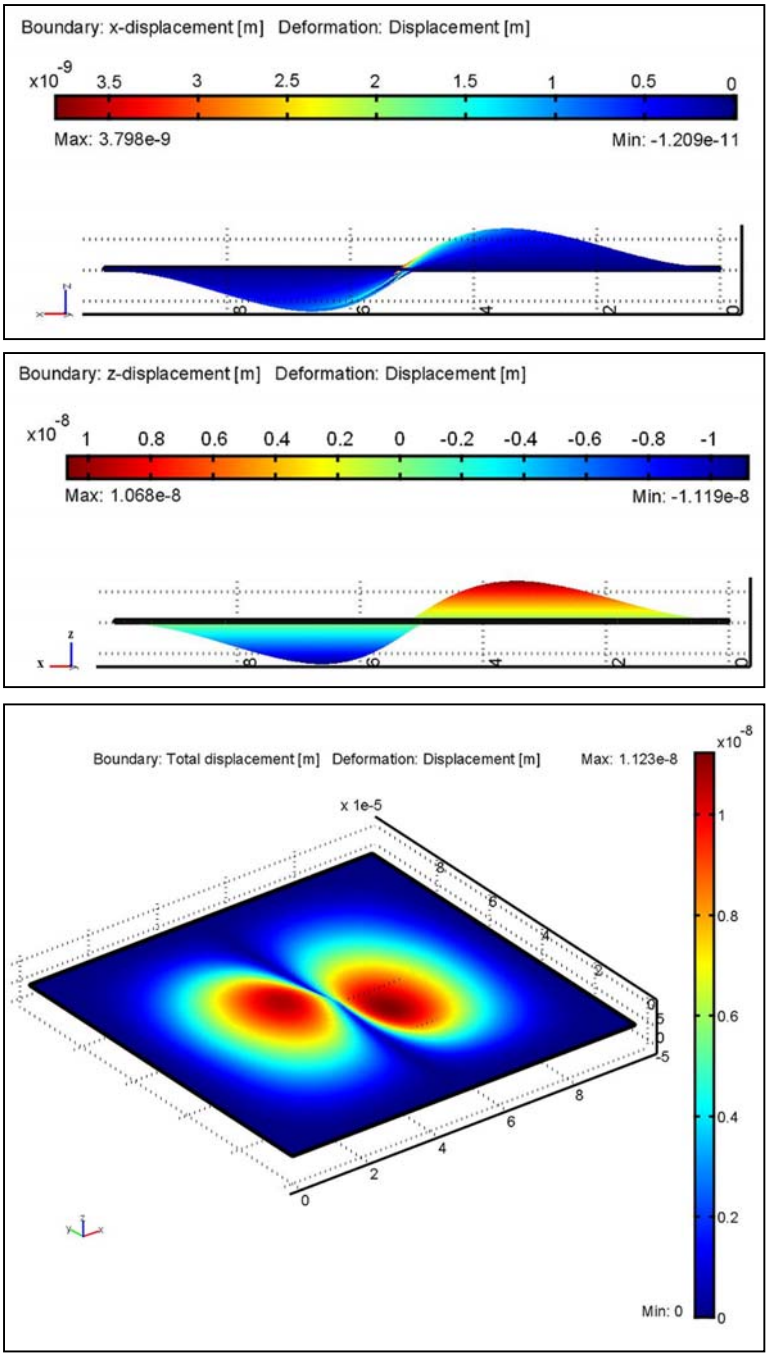

Figure 3-16. Deflection of suspended PDMS membrane (500 nm thick) (FEM modeled by COMSOL): 10 nN point load applied parallel to the surface

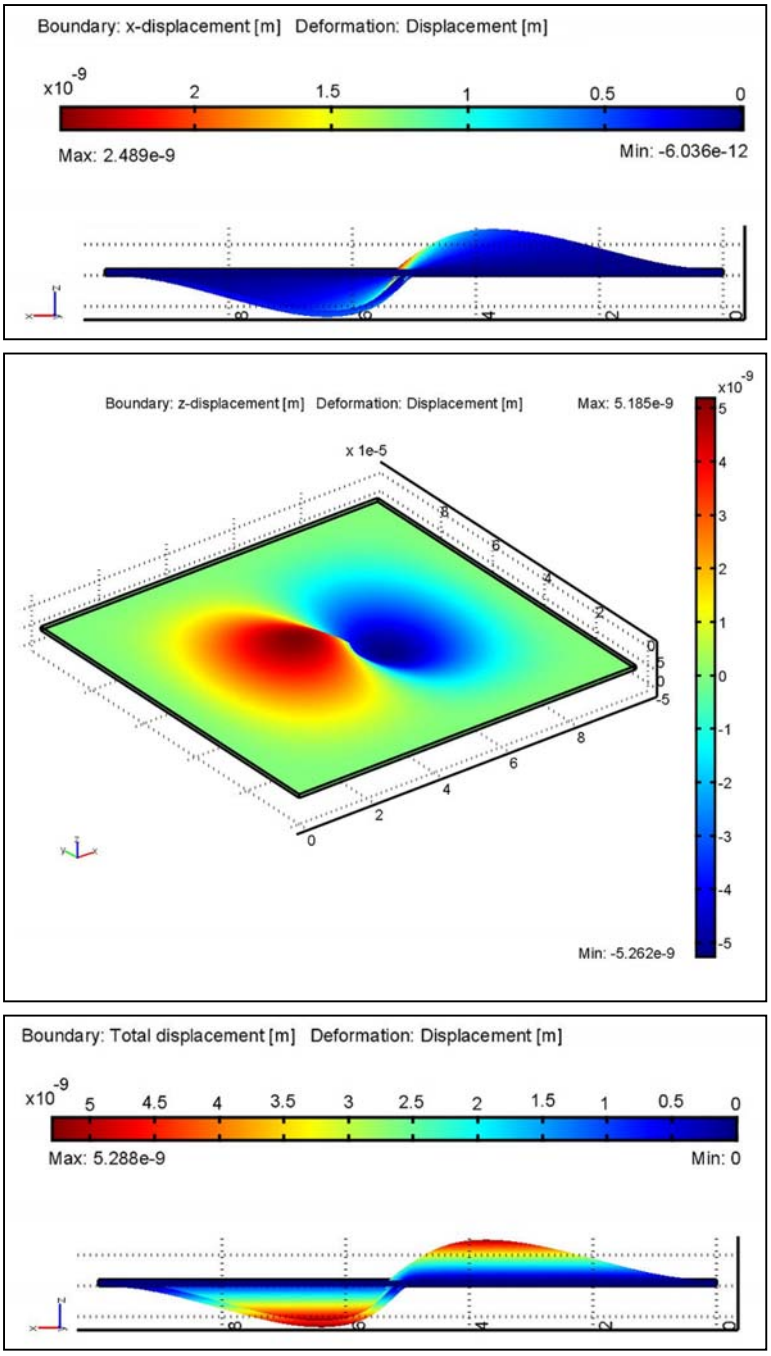

Figure 3-17: Deflection of PDMS membrane (1000 nm thick) (FEM modeled by COMSOL): 10 nN point load applied parallel to the surface

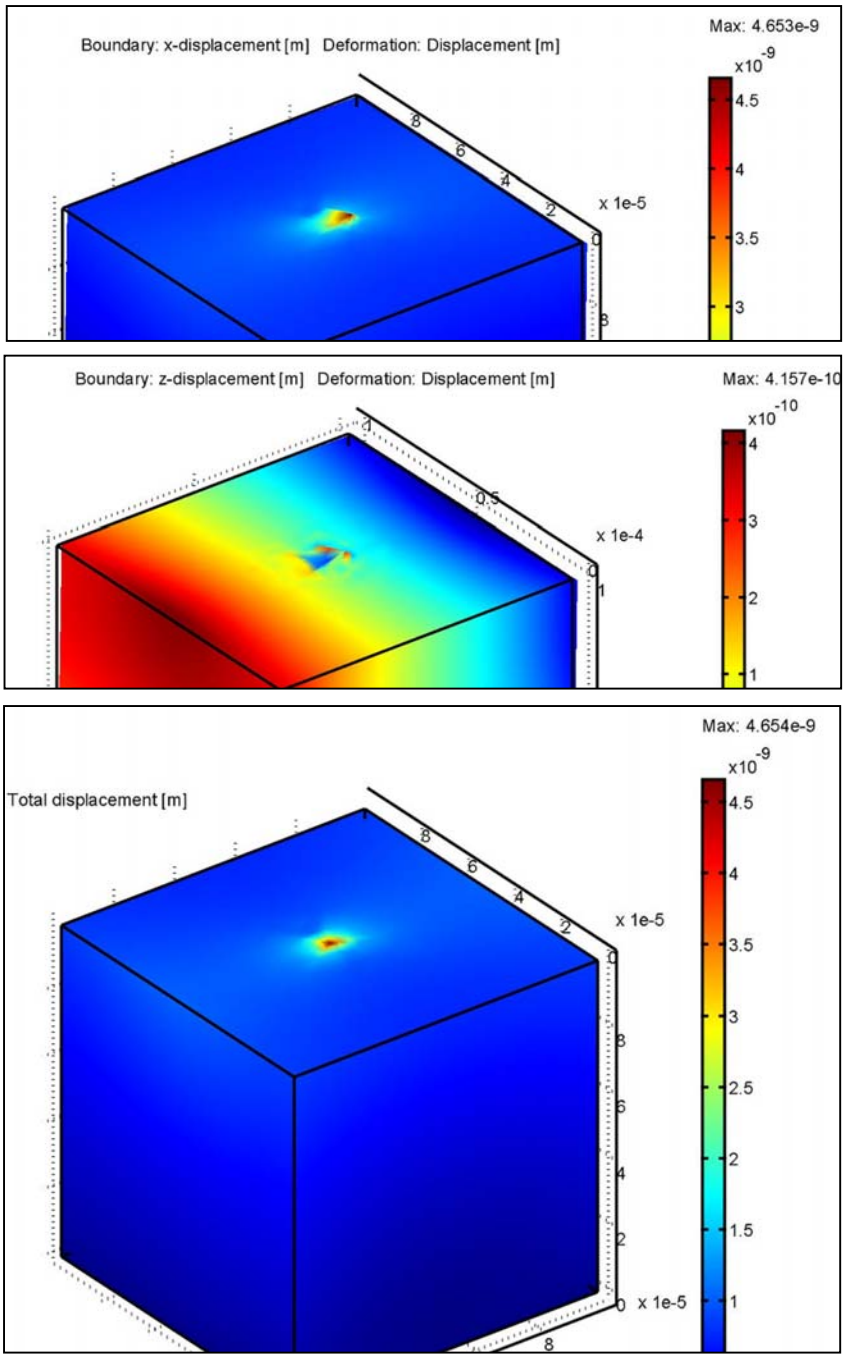

Figure 3-18: Deflection of plain PDMS substrate (FEM modeled by COMSOL): 10 nN point load applied parallel to the surface

3.5. Conclusion

In this chapter, a detailed fabrication process for ultra-thin PDMS membrane device was described. The bulge test showed the extreme flexibility of the PDMS membranes. The ease of fabrication of both plain membranes and those having integrated micro/nanopatterns, and PDMS's biocompatibility and biologically relevant mechanical properties make the system a good candidate to study cellular mechanics. By strategically integrating micropatterns, a membrane that has spatially varying stiffness was fabricated. Effects of substrate's mechanical properties on cell behavior that was studied on these devices are described in the following chapter. The membrane devices may also be further developed as bio/chemical sensors or a scaffold for integrating and assembling other micro devices.

Chapter 4 : Effect of substrate's stiffness on cellular matrix organization

4.1. Introduction

In this chapter, some preliminary results of the influence of substrate's mechanical property on cell behaviors will be discussed. As a mean to qualitatively quantify the effects of the mechanical property, laminin-332 (Laminin-5 with subunit $\alpha 3\beta 3\gamma 2$) secretion and organization, and also the assembly of focal adhesion complexes and hemidesmosomes by human epidermal keratinocytes (HEK) were monitored.

Two different types of substrates were used in these experiments. The first set consists of PDMS substrates with a mixing ratio of 10:1, 50:1, and 75:1 with Young's modulus of 744 kPa, 14.3 kPa, and 1.2 kPa respectively (See Chapter 3). These substrates were formed on glass coverslips. The second type of substrates are the freely suspend PDMS membrane with spatially varying stiffness, and the fabrication process was described in detail in the previous chapter. All the substrates were exposed to O_2 plasma and treated with aminosilane before seeding cells. No extra cellular matrix was coated on any of the substrates so that the direct effects of the mechanical property of the substrate only on the cells could be assayed. The three different cellular matrices monitored are briefly described in the following.

4.1.1. Laminin-332

Laminins are extracellular glycoproteins that are involved in important biological processes such as tissue development, wound healing, and tumorigenesis [154]. There are at least sixteen isoforms of laminin. Laminin-332, one of the isoforms in particular, is involved in maintaining tissues integrity and it has been reported that skin blistering disease, such as junctional epidermolysis bullosa (JEB), results when laminin is absent [155-157]. The laminin-332 is also a major adhesive protein that links between the basement membrane and the hemidesmosome in HEK [144, 145]. As it is generally deposited everywhere the cell migrates, laminin-332 can be used to determine the migration behavior of the cells. Moreover, the level of laminin-332 expression was shown to change for tumor cells when compared to normal tissues. In general, the laminin expression increases for tissues derived from those that normally express laminin-332, but in a few cases they actually decreases, such as in basal cells carcinomas, advanced breast and prostate cancers [154]. It should also be pointed out that laminin-332 promote the formation of focal adhesion and hemidesmosomes in epithelial cells.

4.1.2. Focal Adhesion

Focal adhesions are adhesion sites where the extracellular matrix connects to the cell's cytoskeleton [126, 159]. Unlike hemidesmosomes which interact with intermediate filaments, FAs interacts with the actin microfilaments of the cytoskeleton structure. In both cases, the interactions are not direct, but through intermediate proteins and signaling molecules. A simplified schematic showing the major filaments in a cell is shown in Figure 4-1. FA plays at least two very significant function, one of which is force transmission for adhesions to the

substrates for attachment [126, 159]. Most cells apply traction forces at these FA sites for migration on the substrate [126]. Measuring these traction force is also of important research topic as evident in the literature [125-132]. The second significant function of FA is as a signaling center through which they are involved in regulating/influence the cell. FAs are very dynamic structures; attaching and detaching frequently as the cell continuously remodel its cytoskeletal structures upon migration. In migrating cells, FAs formed at the leading edge of the cell will remain stationary until the rest of the cell structure move past/over them at which point they become the trailing edge. At that point, FA disassembled and the cycle continues [159 and references there in].

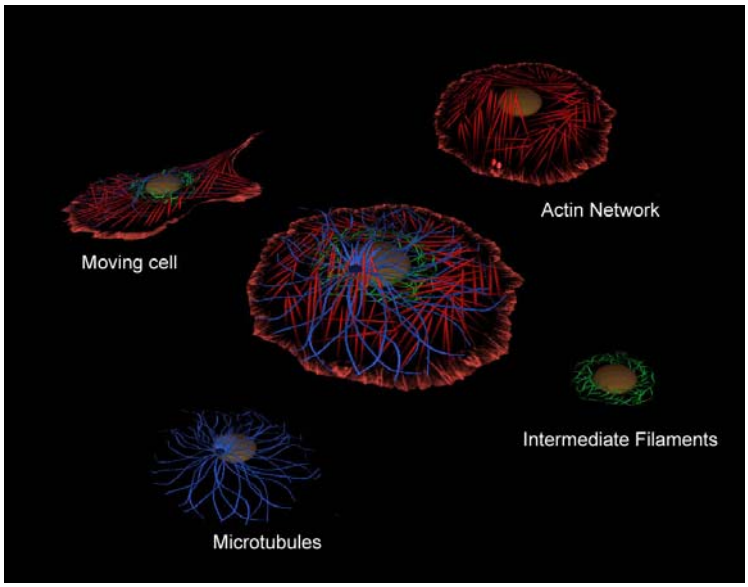

Figure 4-1: Schematic of the cytoskeleton of a cell: actin filament arrays (red), the microtubules (blue), and the intermediate filaments (green). (Reproduced from [160])

4.1.3. Hemidesmosome

Hemidesmosomes (HD) are integrin-containing multiprotein complexes that mediate the adhesion of epithelial cells to basement membrane [148, 149, 150, 162]. HD provides continuous, similar to focal adhesions, linkage between the cell (but though intermediate filament cytoskeleton) and the underlying basement membrane. In particular, $\alpha_6\beta_4$, integrin heterodimer in HD functions as receptor for various laminins, and binds with the highest affinity to laminin-221 and laminin-332 [163]. Lack of hemidesmodomes or mutation in α_6 or β_4 gene have been linked to certain skin diseases [162]. HD is expressed by cells from a host of tissues including skin, cornea, mammary gland, and bladder [150]. Similar to FA, HD was shown to be dynamic protein complexes [162], assembling and disassembling as necessary. On top of the linkage that it provides, HD has been suggested to be involved in cell signaling through the $\alpha_6\beta_4$ integrin [149, 163].

4.2. PDMS surface treatment

Cells cannot readily attach to polymers, including PDMS. Surface modification is needed to ensure cells attachment to the substrate. Most papers [1-17] have reported using the absorption or covalent bonding of integrin, fibronectin, and collagen as the adhesive layer on the substrate for cell attachment. To lengthen the adhesion time of these ligand coatings on PDMS, Genzer and Efimenko [46] developed a technique in which they stretched the PDMS mechanically and expose it to UV+O_3 at the same time. Layer-by-layer assembly of alternating positively charged and negatively charged polymers was also recently reported to treat PDMS surface [62]. For all experiments carried out in this work, the PDMS substrates were treated with aminosilane

(Adapted from C. Waters, et al. [48]) and if briefly described here. After the PDMS substrates were cured at 90°C for 15 minutes in an oven, they are typically set in room temperature for overnight. The substrates are then treated with oxygen plasma [Plasma Preen II, Plasmatic Systems] for 60 seconds at an RF power of ~70W. The oxygen plasma treatment makes the PDMS surface temporarily hydrophilic by activating the carboxyl group on the surface. An aminosilane [3-aminopropyl trimethoxysilane, Sigma-Aldrich] was coupled to the oxidized membrane according to a method described by Waters et al. [48]. A solution of 1% aminosiliane and 94% anhydrous methanol with 5% ultra pure water was prepared in a flow chamber. The substrates are then filled with the aminosilane solution for 5 minutes, followed by rinsing them three times in methanol for 1 minute. The substrates are then kept in culture dishes until they are used.

4.3. Cell culture

Human epidermal (WT) keratinocytes were a gift from Dr. Lou Laimins of Northwestern University. The cells were immortalized using human papilloma virus E6 and E7 genes (Kaur et al., 1989). They were maintained at 37°C in defined keratinocyte serum-free medium [plus growth supplements; Invitrogen Corp., Carlsbad, CA] and penicillin/streptomycin [100 IU/mL; Invitrogen Corp.]. The substrates were washed with phosphate buffered silane (PBS) and incubated for 15 minutes with the media prior to seeding the cells. The culture media is changed every two days.

More specifically, newly thawed HEKs were seeded in 100 mm cell culture dish. Two or three days after the cells are seeded, the media was aspirated and the cells are quickly rinsed with

phosphate buffered silane (PBS). After the PBS rinse, the cells were trypsinized to detach them from the culture dish. After keeping the cells with trypsin in an incubator for 2-3 minutes to promote the detachment, trypsin was quickly neutralized using serum-containing media. Typically, 3 ml of trypsin and equal amount of neutralizing media were used for 100 mm culture dish. After thoroughly mixing the cell suspension with pipette, the suspension was spun for 5 minutes in a centrifuge at approximately 1200 RPM. The media was then aspirated from the tube and the cells were resuspended with the HEK media. The volume of culture media, before and after centrifuging, was kept the same. The suspended cells were then plated onto the desired culture substrates.

To maximize adhesion of the cells to the PDMS substrates effectively, the substrates were incubated with the media for approximately 15 minutes prior to the seeding. Typically, just enough media to cover the individual PDMS substrate was dispensed. After the incubation, the cells suspension is added to the substrate, typically 22-44x10^3 cells/cm^2 culture dish for the regular PDMS substrate and 1000-2000 cells/cm^2 for the membrane devices. More media is added only after incubating the cells without adding culture media for a few minutes to have the cells attached to the substrate. If the substrate is buried in the culture media prior to adding the cell suspension the cells randomly attach to allover the surface. Our current process allows the modification of the density of cells on the device by aspirating the cell suspension after the desired number of cells have adhered to the device. New media then can be added to support the culture.

4.4. Immunofluorescence microscopy

After cells are cultured for the desired length of time, they were fixed in 3.7% formaldehyde for 5 min and extracted in 0.5% Triton X-100 (4°C) for 7 min. Antibodies and/or rhodamine-conjugated phalloidin (Molecular Probes, Eugene, OR) were overlaid onto the cells and the preparations were incubated at 37°C for 60 min. The substrates were washed in three changes of PBS, overlaid with appropriate fluorochrome-conjugated secondary antibodies, placed at 37°C for 47 min, washed extensively, and mounted on slides. All preparations were viewed with a Zeiss laser-scanning microscope (LSM) 510 confocal microscope using a 1.4 numerical aperture, x63 objective [Zeiss Inc., Thornwood, NY]. Images were exported as TIFF files, and figures were generated using Adobe Photoshop software. The primary antibody J18 (rabbit antiserum against rat laminin-332) was prepared based on a published protocol (Langhofer et al, 1993 [154]), and the secondary antibodies conjugated with various fluorochromes or horseradish peroxidase were purchased from Jackson ImmunoResearch Labs Inc. [West Grove, PA]. In all experiments normal goat serum (diluted 1:20 in PBS) was added to the primary antibody solutions. The primary and secondary antibodies combination used in the experiments are shown in Table 4-1.

Table 4-1: Antibodies and fluorescent reagents used in these studies

	Primary	Dilution	Secondary	Dilution
Focal Adhesion	Paxilin	1:40	GARb-Rh	1:20
Hemidesmosomes	β4	1:40	GAM-F	1:20
Laminin	J18	1:50	GARb-F	1:20
Actin	Phalloidin	1:40	-	-
Nuclei	DAPI	1:40	-	-

4.5. Cell-substrate interaction: HEK on compliant PDMS substrates with various stiffness

4.5.1. Laminin-332 secretion by HEK increases as substrate stiffness decreases

Typically, cells were fixed approximately 24 hours or 48 hours after they were seeded on the substrates and stained for immunofluorescence microscopy as described above. Figure 4-2 shows the liminin-332 secreted by a single cell on standard No.1 coversalips. As apparent from the intensity of the fluorescent in the images, more laminin was secreted as the culture time increased (Figure 4-2a vs. Figure 4-2b). Also apparent from the image is the increase in laminin deposition on coverslip treated with aminosilane compared to one that was not (Figure 4-2b vs. Figure 4-2c). The surface treatment with aminosilane allows protein absorption and thus promotes cell adhesion [48]. This will have effects on how quickly the cells attach to the surface, which in turn will determine how much laminin is secreted. This effect is clearly evident from Figure 4-2.

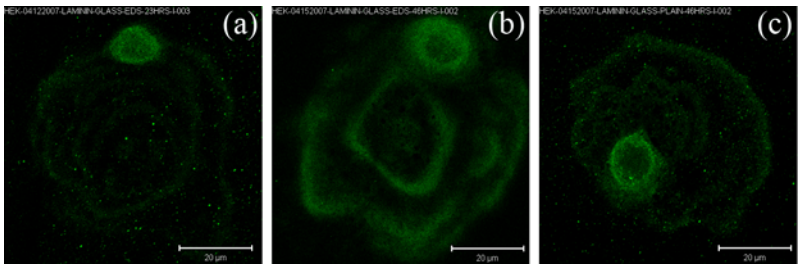

Figure 4-2: Laminin-332 secretion by HEK on glass coverslips: (a) 24 hours (b) 46 hours and (c) 46 hours after seeding. (a, b) coversips treated with aminosilane and (c) plain coverslip. More laminin are deposited as culture time increases. More laminin was secreted on silane treated coverslip than on a plain coverslip. Scale bar = 20 μm

Similar to the coverslips, more laminin-332 secretion by HEK was observed on PDMS substrate as the culture time increases. See Figure 4.2. More importantly, it was observed that HEK secreted more laminin as the stiffness of the base substrates decreases. See Figure 4.2. It should be pointed out that the cells took longer to attach to softer substrate. Although this would give cells on the less stiff substrate less time to secrete the laminin, cells on the softer substrate still secrete more laminin, even when cultured only for 24 hours (Figure 4.2 a-d). This indicates that the stiffness of the substrate is of critical importance to the ability of the cells to elaborate a laminin-332 matrix. The difference in the laminin secretion level is more evident from the ones that were cultured for 46 hours (Figure 4.2 e-d).

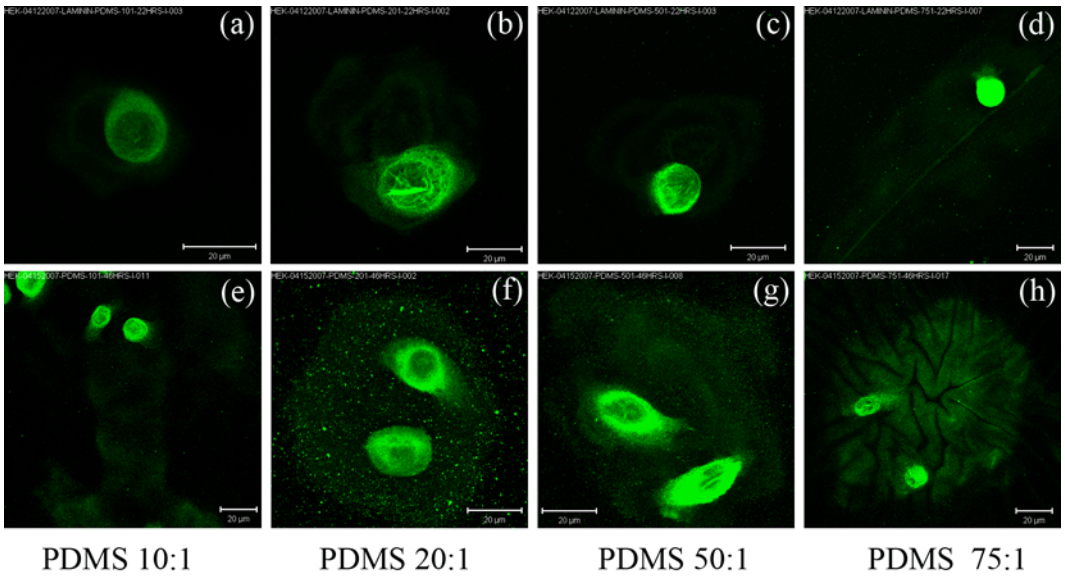

Figure 4-3: Laminin-332 secreted by HEK on PDMS substrates with different stiffness: (a-d) 24 hours and (e-h) 46 hours after seeding cell. Young's modulus of substrates: (a, e) 744 kPa, (b, f) 244 kPa, (c, g) 14.3 kPa, and (d, h) 1.2 kPa. Scale bars = 20 μm

It should also be noted here that for the first 24 hours of the culture, all of the cells, more or less, moved in a circular pattern with a very minimal net migration. However, on the second day, many cells on the stiffest substrate (PDMS 10:1) had some linear component in their migration where those cells on the softer substrates still maintain their circular motion with very little linear component to their migration. Although there seem to be no linear migration, these HEK expanded the surface area they cover during the circular migration. In fact, if the surface areas cover by the two cells on a 75:1 PDMS (softest) is approximately 80% larger than that cover by two cells on 20:1 PDMS (7900 μm^2 vs. 4400 μm^2). A careful examination of the cells revealed that cells on the 75:1 PDMS substrates are about half the size of those on the stiffer 20:1 PDMS substrates. These imply that cells on softer substrates have to move much more in order to secrete laminin to cover the same amount surface area as those on the stiff substrates. As noted,

the surface area of laminin secreted by cells on soft substrates are in fact much larger than those on stiff substrate, suggesting that the cells' motility on the soft substrate is much higher than those on the stiffer ones as reported by other researchers.

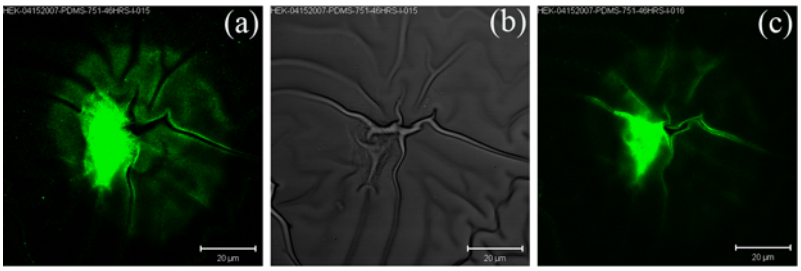

Figure 4-4: HEK secreted laminin-332 on all surfaces it contacts regardless of the topography of the surface (a) laminin staining and (b) phase image of primary surface of the substrate, and (c) laminin on top of the ridges (wrinkles on substrate with E ~ 1.2 kPa). Scale bar = 20 μm

Another interesting observation is that the cells seem to preferentially attach to sites where multiple topographical features converged. This was observed with most of the cells on the softest PDMS substrate (E~1.2 kPa) where wrinkles were formed during the oxygen plasma treatment. To check whether HEK, on substrates with topography, secrete laminin selectively or over all surfaces it contacts, the laminin staining was imaged at both the primary surface of the substrate and on top of the ridges (wrinkles). Figure 4-4 proved that HEK does secrete laminin on all surfaces, flat or curve, that it contact.

4.5.2. Focal adhesion and Hemidesmosme assembly on soft substrates with different Young's modulus

Similar to other cell types reported by other groups [1, 2], the focal adhesions matured faster on stiffer substrates as apparent from Figure 4-5. The numbers and size of FA complexes increased

as the substrate stiffness increased. This would allow the cells to anchor it self much stronger than on the softer substrates. This, in turn, will require much more force on the stiff substrate to detach the focal adhesion complex. This observation is in agreement with that of the increase in surface area covered by HEK secreted laminin on a softer substrate compared to a stiffer one. Since it takes less energy, in general, to detach the FAs on soft substrates, HEK can move much faster on it than on the stiff substrates. As for the hemidesmosome, it was generally observed to be better assembled on softer substrates. On substrates shown in Figure 4-7, HEK were seeded on compliant PDMS with two different substrates stiffness, E~744 kPa and E~14.3 kPa. These images clearly showed that the HD assemblies are more prominent on the softer substrates for both the 24 hours and 48 hours cultured cells.

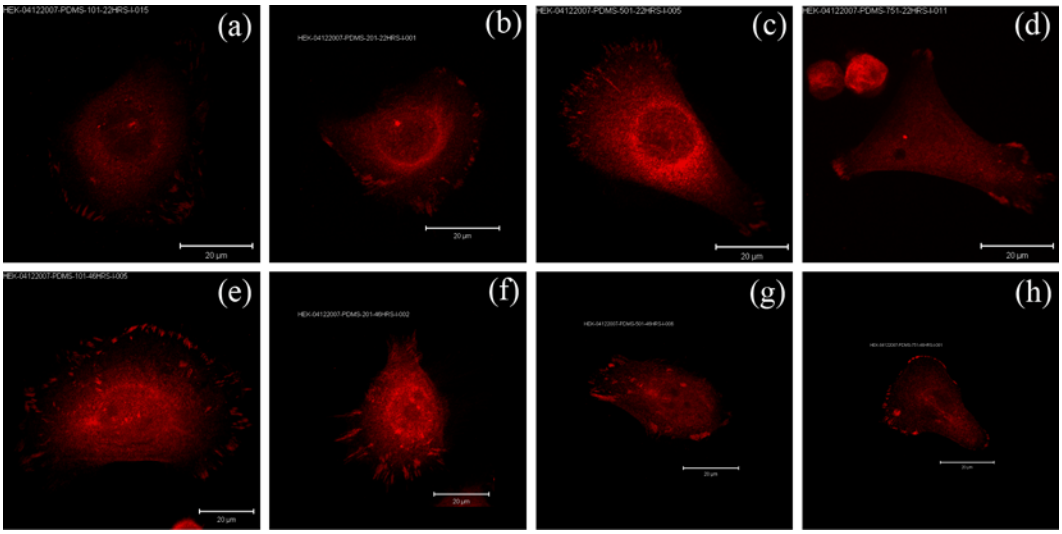

Figure 4-5: Focal adhesion assembly on PDMS substrates with different stiffness: (a-d) 24 hours and (e-h) 46 hours after seeding on PDMS with a mixing ratio of (a, e) 10:1, (b, f) 20:1, (c, g) 50:1 and (d, h) 75:1. HEK cultured for 22 Hours. Young's modulus of substrates: (a, e) 744 kPa, (b, f) 244 kPa, (c, g) 14.3 kPa, and (d, h) 1.2 kPa. Scale bar = 20 μm

In all experiments, the focal adhesion complexes and the hemidesmosomes were found to be distinctly localized [Figure 4-6, Figure 4-7, and Figure 4-8]. In some instances, the two complexes seem to co-localized but a careful analysis (zooming) indicated that they are in fact not co-localized. When the substrates is soft, the cells can generate wrinkles, a measure of the force they apply, on the substrate as shown in Figure 4-8c.

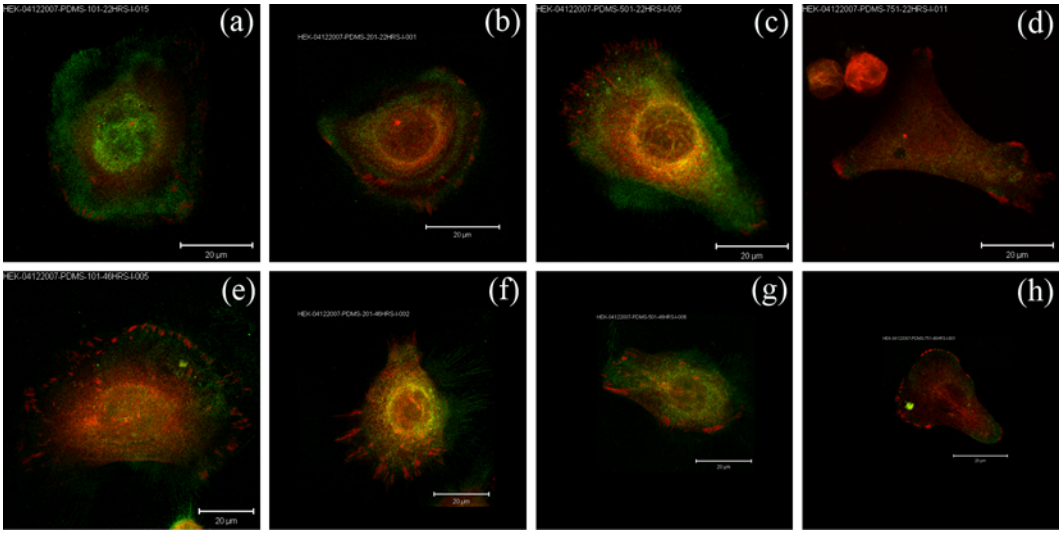

Figure 4-6: Merged images of staining of FA (RED) and HD (Green) assembly on various PDMS substrates (same cells from Figure 4.4). HEK cultured for 22 Hours. Young's modulus of substrates: (a, e) 744 kPa, (b, f) 244 kPa, (c, g) 14.3 kPa, and (d, h) 1.2 kPa. Typically, FA are located on the periphery of the cells while the HD are assembled in the center. Scale bar = 20 μm

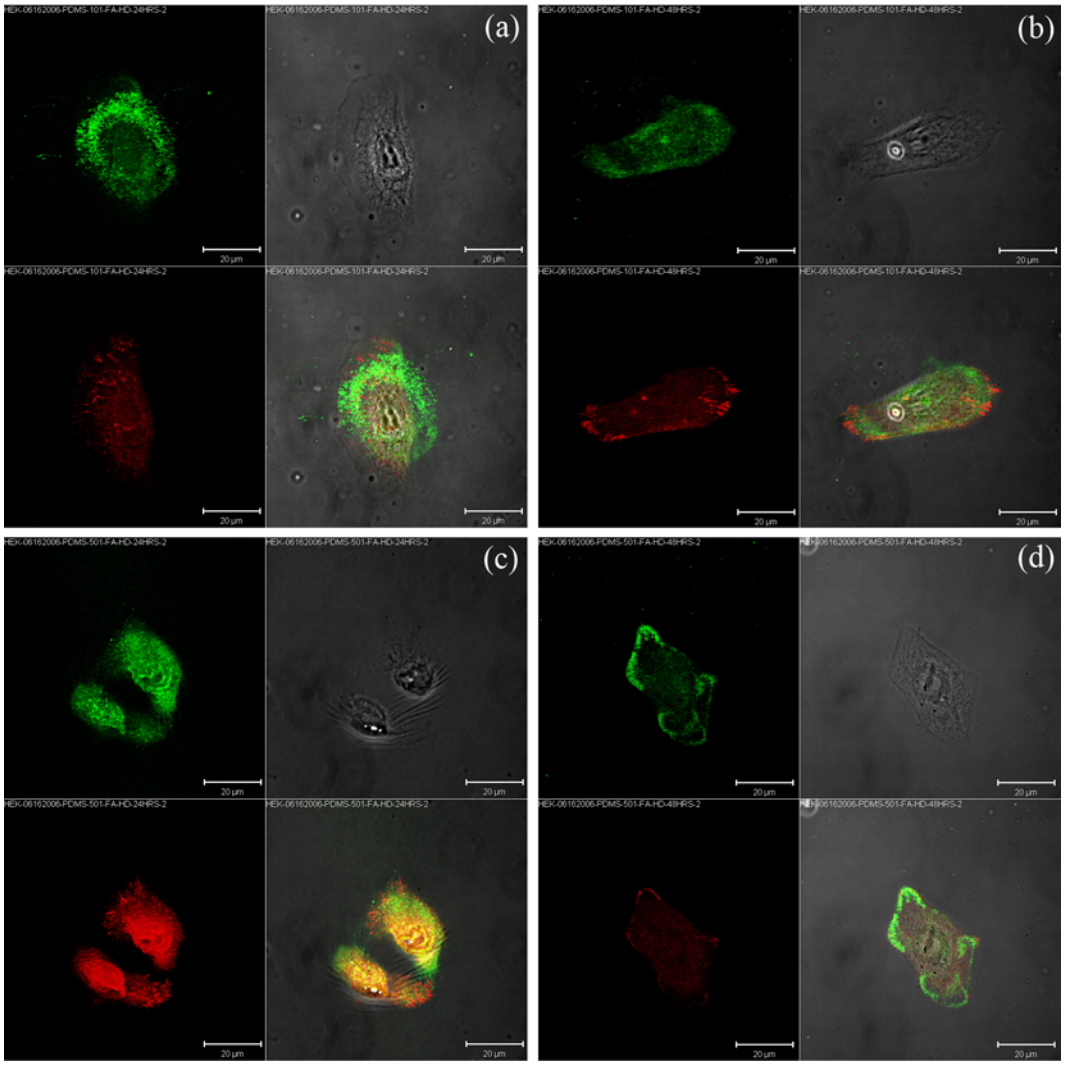

Figure 4-7: Focal adhesion (RED) and hemidesmosome (Green) assemblies on PDMS substrates: (a, b) E~744 kPa, (c,d) E ~14.3 kPa. Culture time: (a, c) 24 hours, (b, d) 48 hours. The FAs are more prominent on stiffer substrates while the HDs are be more developed on softer substrates. In both cases the FA and HD localized separately. Scale bar = 20 μm

4.5.2.1. Hemidesmosomes form anchor-like assembly on soft substrates

Individual cells typically migrate in a random path on uniform substrates. When a small colony of cells is formed, the cells tend to move around a centroid of the group. This is likely due partly to the hemidesmosomes that assembled strongly in the center of the colony. These anchoring hemidesmosmes are formed by a few numbers of cells in the middle of the colony. Cells from the outer edge of the colony are still capable of migrating but due to the cell-to-cell interaction, which seems to be dominantly strong, they typically move in circular pattern around the anchor. In order for the colony to have a net migration, the hemidesomosme complexes will have to be broken. These anchor-like assemblies of HD were observed in both very small (2 to 3 cells), and a little larger (> 10 cells) groups of cells (see Figure 4.7).

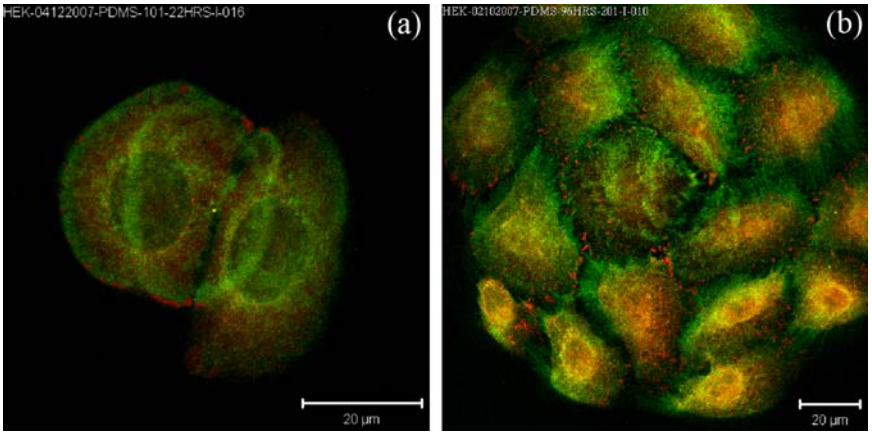

Figure 4-8: Merged images of focal adhesion (Red) and hemidesmosome (Green) on small groups of cells. (a) Two HEK cells and (b) a larger number of cells with staining for FA and HD. In both cases HD assembly formed ring-like structure in the middle of the group. Young's modulus of substrates: (a) 744 kPa, (b) 14.3 kPa. Scale bars = 20 µm

4.5.3. Effects of topographical features on HEK

As part of the substrate's preparation for seeding cells, the PDMS substrates are exposed to oxygen plasma as mentioned in previous section. In this process, the ions bombarded the surfaces and when the surface is extremely soft the ion bombardment can cause topographical features to form on the surface. Some times, very shallows ridges formed while wrinkles, raised features, were more easily formed. Typically, the features are a few microns wide and the vertical dimension, depth or height, is usually smaller than the height of the cells themselves. These features are typically formed on the least rigid substrate used in the experiments, PDMS with 75:1 base to curing mixing ratio. The Young's modulus of these substrates is 1.2 kPa.

4.5.3.1. HEK migrate along shallow trench features

When the HEK are cultured on a surface with shallow trenches, they tend to attach preferentially to the trenches. Once the matrix proteins are secreted, the cells migrate along the trench. This is evident from the images of laminin secreted on the surfaces as shown in Figure 4.2d. This happens only when there is an isolated trench. The reason for these cells migrating along the trench is probably due to contact guidance [38, 151, 152]. In some instances, this feature may be exploited to actively direct cell migration in such processes as wound healing.

4.5.3.2. HEK moves parallel to raised features

Contrary to the shallow trenches, the raised features have the opposite effects. Typically the HEK cells were found to be oriented in the direction perpendicular to the ridges. Similar to the

trenches, cells seem to preferentially attach to these features when they are randomly seeded on the substrate [Figure 4-9].

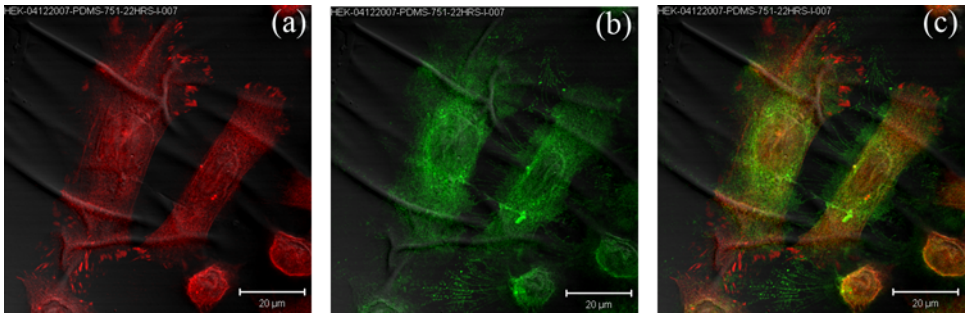

Figure 4-9: HEK on PDMS substrate with wrinkles with staining for (a) Focal adhesion, (b) hemidesmosomes, and (c) merged images of the (a) and (b). Note that all FAs are formed on the flat portion of the substrate, not on the ridges where the surfaces are curved. E ~ 1.2 kPa.

In one particular experiment, it was observed that two cells that are migrating in the same general direction generated wrinkles that span the space between them and two other cells were migrating perpendicular to the wrinkle features, in the same direction as the other two [Figure 4-10]. The two inner cells in this case were using the wrinkles as physical cues to determine the direction of migration. Interestingly, the focal adhesion complexes of the cells in such situations are always observed to form just before or beyond the wrinkle features, but never directly on the wrinkles [Figure 4-9]. Note again here that the wrinkles are features that protrude above the flat base surface and have curve surfaces. This observation seems to support the assertion that cells cannot form focal adhesion complexes on a curved surface [151, 152]. Dunn and Heath [151] previously reported that chick heart fibroblasts align themselves along the axis of a cylindrical substrate.

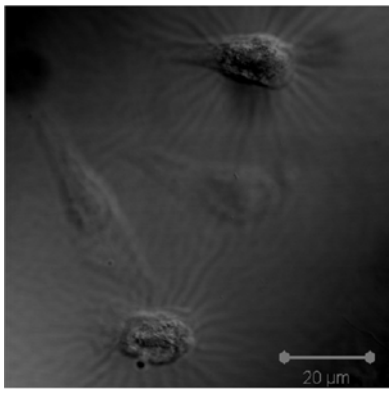

Figure 4-10: Two HEK (outer) generating wrinkles while two other (inner) used that as cues for migration direction

4.5.4. Wound healing experiment on compliant PDMS substrates

Wound healing experiments were carried out on PDMS substrates to study the effects of the substrate's stiffness. The wound was induced by scratching the confluent HEK cells with the tip of a plastic pipette. The culture media was replaced prior to the time-lapse imaging. Though the experiment was not ideal, the wound healing process was observed to be faster on the softer substrates in general. The relative migration velocities of the cells on different PDMS substrates are shown in Figure 4.11. HEK migration speed on the softest substrate (75:1 PDMS) is almost twice that on the stiff (10:1 or 20:1). This is in agreement with the area coverage mentioned for laminin-332 secretion.

An important step that should be carefully done for wound healing assay on compliant substrate is the wounding process. With the current technique, the substrates can be physically modified (generate tears and wrinkles) as were observed with the 75:1 PDMS substrate. One way to correct this issue is by placing a strip of blocking material, glass or PDMS, on the surface of the

substrate before seeding the cells. Once the cells are confluent, the blocking strip can be removed. This will generate a very sharp edge with minimal disturbance to the system.

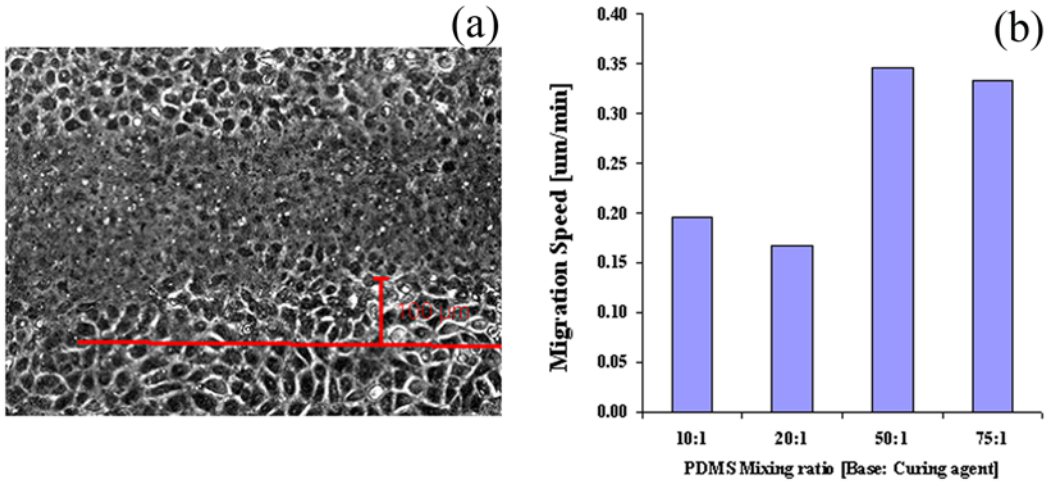

Figure 4-11: Wound healing assay on various PDMS substrates. HEK migrate faster on the softer substrates (Only one assay each for the four different substrates). Young's modulus of substrates: (10:1) 744 kPa, (20:1) 244 kPa, (50:1) 14.3 kPa, and (75:1) 1.2 kPa. Horizontal line (red) in (a) represent initial wound edge and the vertical line (red) indicates 100 µm, the distance traveled by leading cells for the duration of experiment.

4.6. Cell-substrate interaction: HEK on freely suspended PDMS with spatially varying stiffness

4.6.1. Cell accumulation trend

The fabrication of PDMS membrane with spatially varying stiffness was described in Chapter 3. As mentioned, the patterned membrane can be divided into three different regions based on the gradient of stiffness. The first region encompasses the portions where the micropatterns density is high, approximately the first 33% of the patterned membrane. The second region is located in the middle of the patterned area while the third region encompasses approximately the last 20%

of the patterned membrane. The stiffness gradient is the steepest in the first region, followed by the third region. In the second region, there is very minimal change in stiffness across the length of the region.

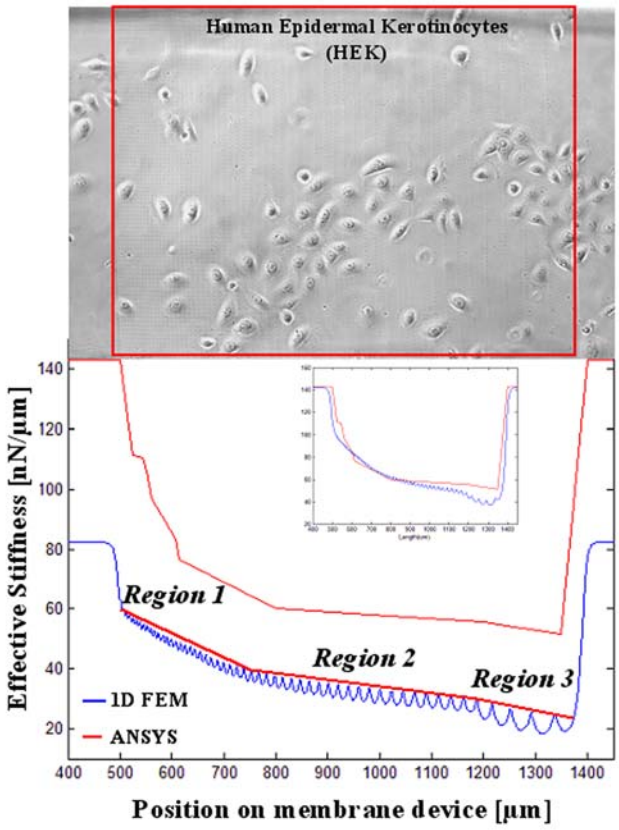

Figure 4-12: Membrane stiffness profile with an example of HEK accumulation

In the first region of the patterned portion of the membrane, HEK cells were found to be very mobile and migrated toward the stiffest site (left) where the membrane is not patterned. This is similar to what others have observed [2, 6]. These mobile cells, however, were also able to migrate in the opposite direction within the first region. There are a few possible explaination. (1) HEK secretes laminin-332 track as they migrate. It is also known that HEK follow the

existing laminin track [154]. Thus, these mobile cells may be migrating back and forth on the same track. (2) Unlike the system used by others where the change in stiffness is abrupt, the gradient in the current membrane device was gradual, and it is possible that HEK can move back and forth on such stiffness gradient.

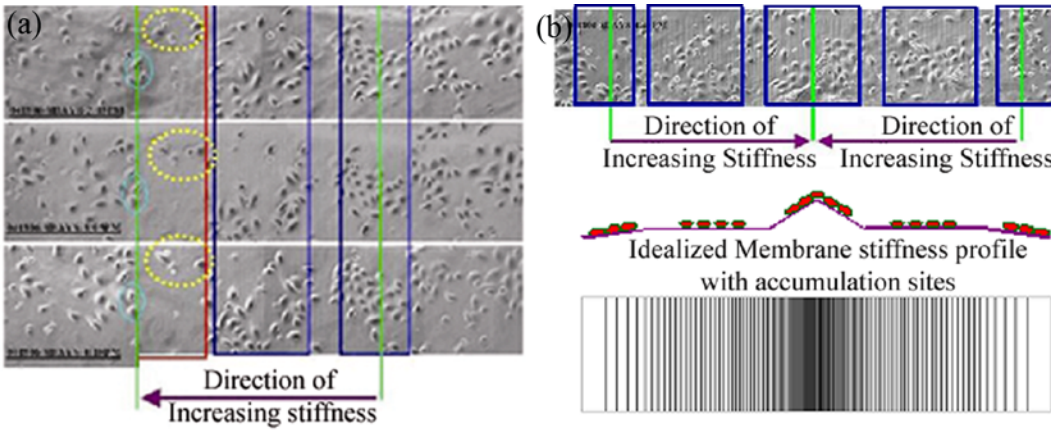

Figure 4-13: HEK accumulation on (a) PDMS membrane with stiffness variation in one direction and (b) on a PDMS membrane with two converging stiffness gradient. The direction of increasing stiffness of the system is shown with arrows in the images.

Interestingly, cells accumulated in the second and third regions, Figure 4-13. While cell accumulation in the second region centered on the middle of the region, in the third region it centered at the intersection of the patterned membrane and the un-patterned regions. In the second region of the patterned membrane, it's likely that the minimal change in stiffness is one of the major mechanisms, if not the only one, that cause the cells to aggregate in the middle of the membrane. It appeared that the gradient was not large enough to cause the cells to migrate in any particular direction. The patterned portion, active region, of the membrane is bounded by two green lines and the accumulation regions are indicated by blue boxes in the Figure 4-13. When HEKs were seeded on a membrane that has two similar stiffness gradient converging in

the middle, cells accumulated on the convergence region where the stiffness peaks (Figure 4-13b).

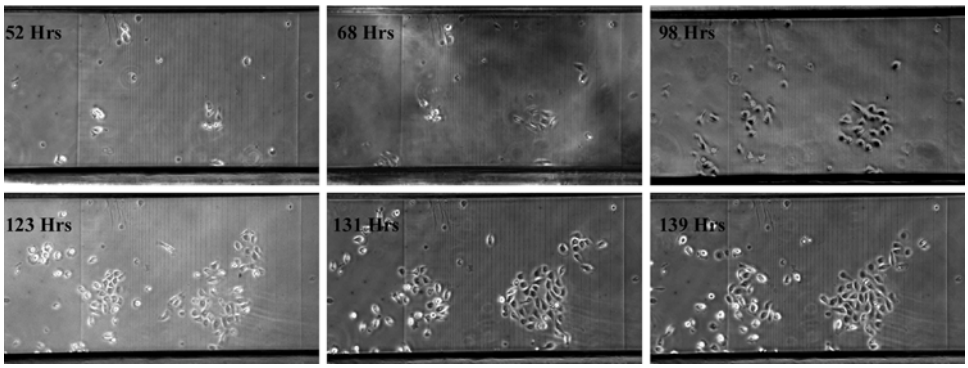

Figure 4-14: Time history of HEK cells on suspended PDMS membrane

Unlike other regions within the patterned membrane, cells in the third region that adhere to the transition region are exposed to two different gradients in opposite directions. To the right, the stiffness gradient is high; in fact it is abrupt since the thickness of the film increases at least by two times. In the opposite direction, the gradient of the membrane stiffness increases gradually as the density of the micropatterns increases. It is speculated that the cells sense the edge created by the two different thicknesses of the film and approach it from both directions. If cells in general do prefer a stiffer region within a substrate as reported, the accumulation of HEK cells on the thicker membrane side of this transition region should be expected as the membrane is stiffer in that region. For the present situation, however, the cells seem to be pulled in both directions and unable to overcome either one of the gradients, suggesting that there is a threshold value of stiffness gradient that the cells need to experience before they can decide how to reorganize themselves to migrate in a particular direction. In this case, both gradients are above the threshold value and the cells are trapped in the middle.

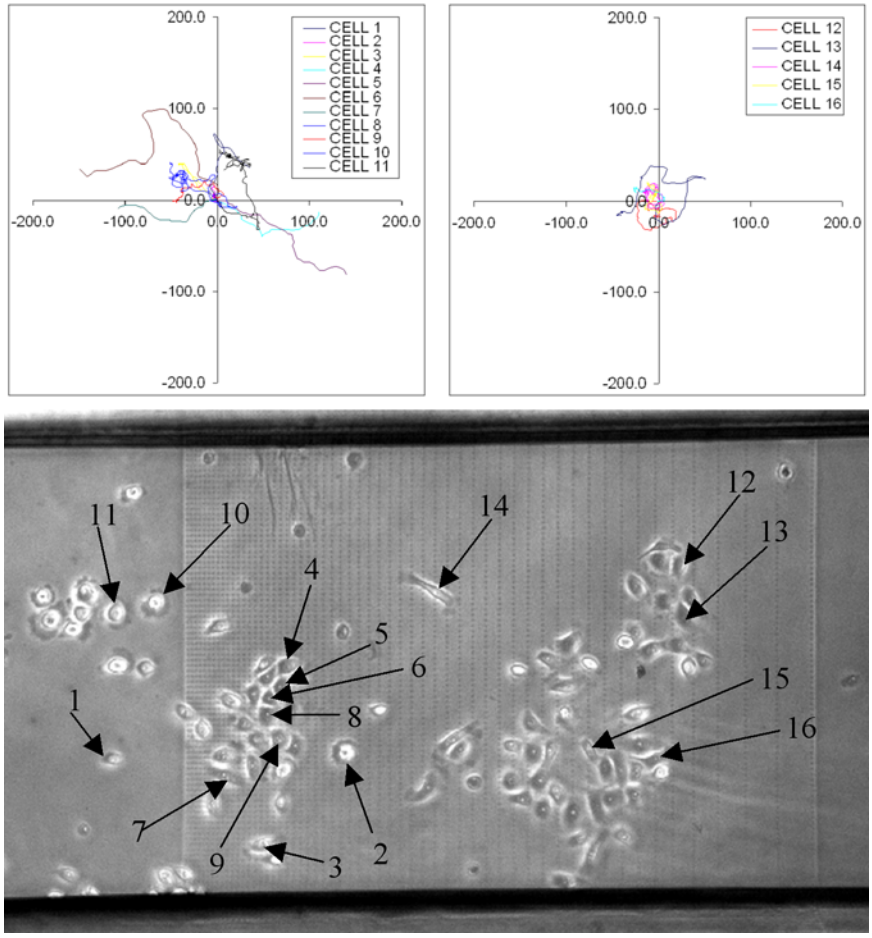

Figure 4-15: Migration trajectories of some cells from (a) region 1 and (b) region 2 and (c) a phase image of the cells on the membrane.

While it is believed that the primary reason for cell accumulation in the regions observed are due to the different gradients of stiffness, the possibility that the spacing of the micropatterns may also be a contributing factor has to be considered. However, when the spacing of the integrated micropatterns is comparable to the size of the HEK cells, two or three of these features are spanned by the cells as can be seen in the middle or tail end of the patterned area of the membrane [Figure 4-12, Figure 4-14]. When these cells migrate in any direction, they encounter a very similar stiffness in all direction. Many of these cells in the accumulation regions moved in

circular patterns while those in the steep gradient region moved back and forth along the length of the membrane (Figure 4.14). Thus, it is reasonable to say that the spacing between the micropatterns was not the reason for accumulation.

4.6.2. Laminin-332 secretion on PDMS membrane with spatially varying stiffness

Laminin-332 secretion was monitored on PDMS membrane with a spatially varying stiffness in a manner similar to that on the PDMS substrates. See Figure 4.16. Similar to the observation on thick PDMS substrates, laminin secretion increased as the substrates' rigidity decreased. In these membrane devices, cells on region 3 secreted the most laminin. A set of images showing the phase images of cells with the corresponding laminin stains are shown in Figure 4-16 and Figure 4.16, respectively. In these images, membrane stiffness gradually decreases from (b) to (k). Figure 4-16 (a, l) and Figure 4.16(a, l) are images on the thick membrane that bounded the active region of the membrane and are the stiffest parts of the membrane (flat, outer regions of stiffness curve – Figure 4-12.)

It should be noted from these images that HEKs initially migrated in a linear fashion on the stiffer region while they moved in circle on the softer region. More importantly, the cells on Figure 4-16 (b, c, d, e) migrated toward the stiffer region, to the left, from their original position. These observations are consistent with those in the migration assay discussed above: HEK migrated along the length of the membrane. While the trajectories shown in Figure 4-15 were mostly for cells that are in contact with other cells, the lamin-332 track left behind by the HEK

indicates that the individual cells does seems to sense the gradient in stiffness and initially migrate preferentially toward the stiffer region. It should also be pointed out that HEK typically follow the laminin protein secreted by other cells (153). Thus it is reasonable to assume that the HEK migrating back and forth as shown in Figure 4-15 is likely due to those cells migrating along the laminin track left behind by the original cells that migrate due to the stiffness gradient.

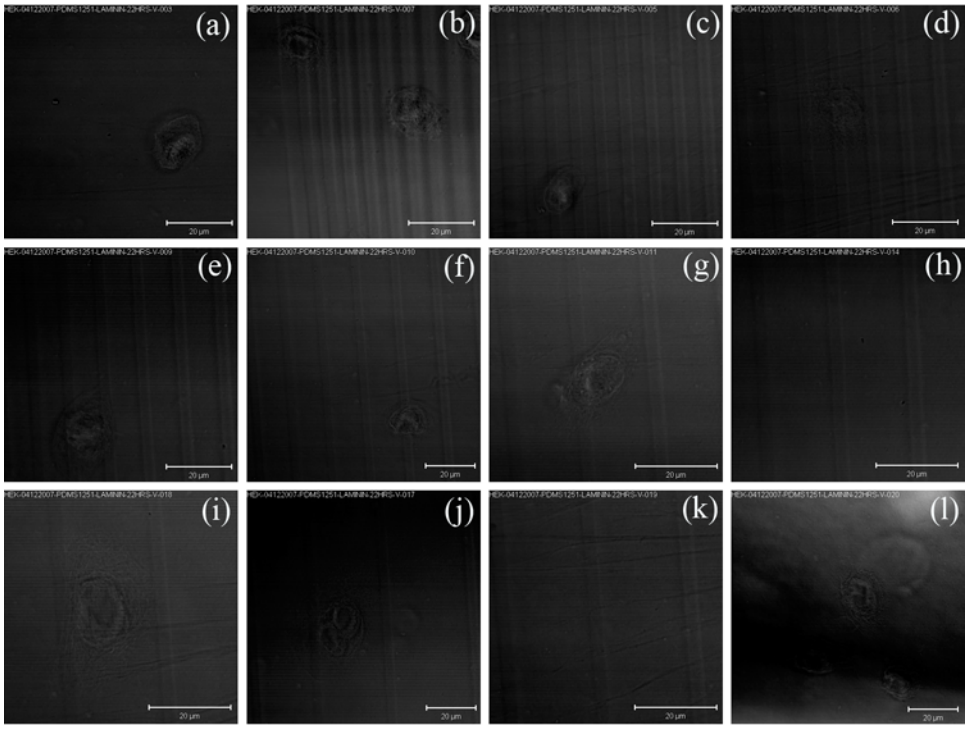

Figure 4-16: Phase images showing the positions of cells on suspended PDMS membrane. Substrate stiffness decreases from (b) to (k). HEK cultured for 22 hours. Scale bars = 20 μm

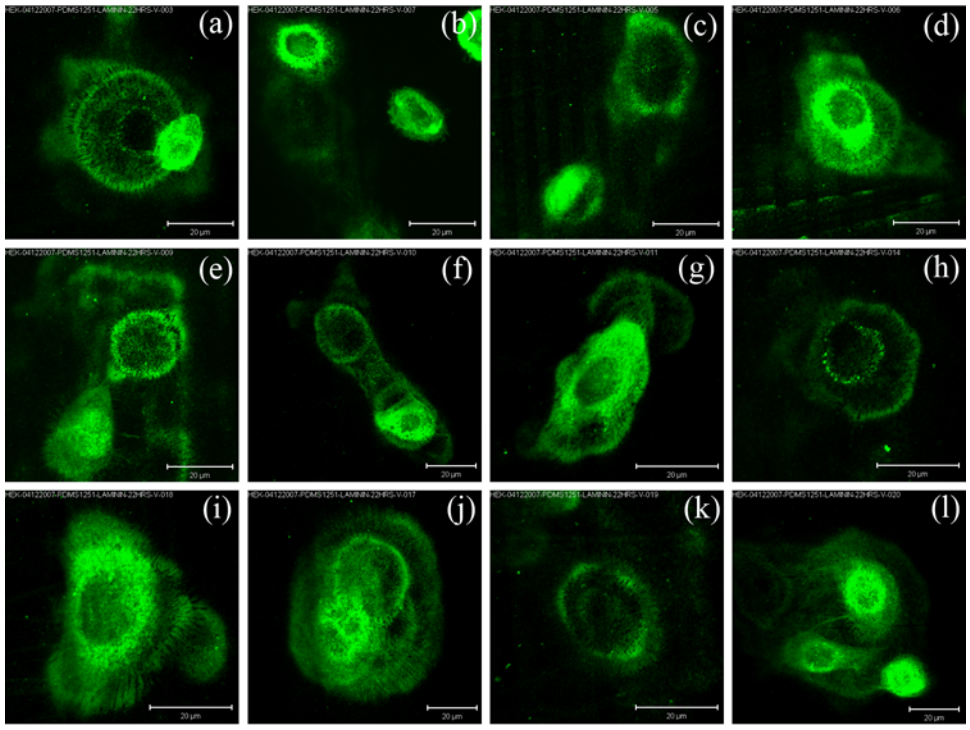

Figure 4-17: Laminin-332 deposition increase as substrates gets softer.

Substrate stiffness decreases from (b) – (k). See Figure 4.16 for phase image. HEK cultured for 22 hours.

Scale bars = 20 μm

4.6.3. Focal adhesion and hemidesmosome assembly on PDMS membrane with spatially varying stiffness

Figure 4-18 shows phase images of a few cells on different regions within the active area of the PDMS membrane with spatially varying stiffness. The corresponding FA and HD stained images are shown in Figure 4-19. Similar to the compliant PDMS substrates, the focal adhesion complexes were better established on the stiffer regions of the freely suspended PDMS membrane. As apparent from this and previous images, HEK take almost 24 hours to establish

attachment to the current PDMS substrates through the focal adhesion complexes. Hemidesmosome, on the other hand, were already well established by the same time.

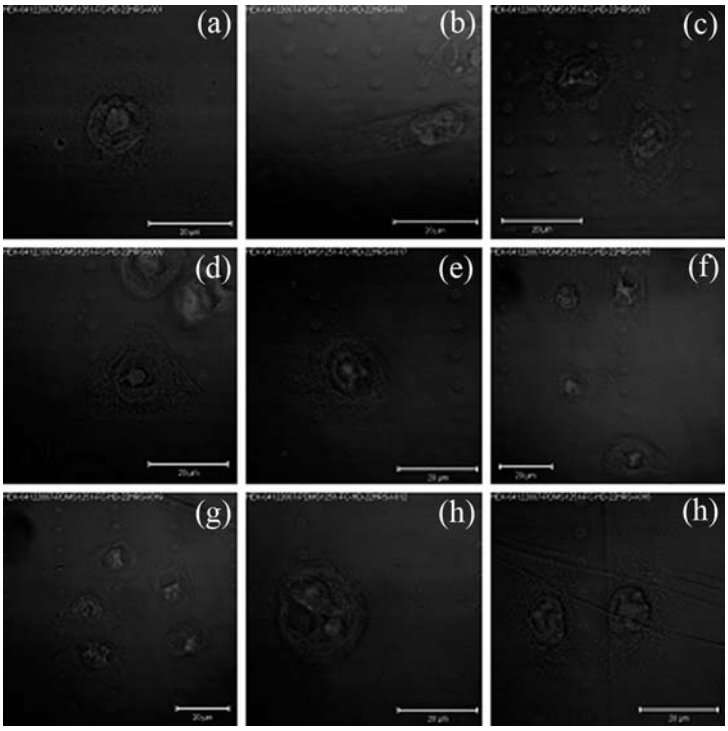

Figure 4-18: Phase images showing cells on suspended PDMS membrane. Substrate stiffness decreases from (b) to (k). HEK cultured for 22 hours. Scale bars = 20 μm

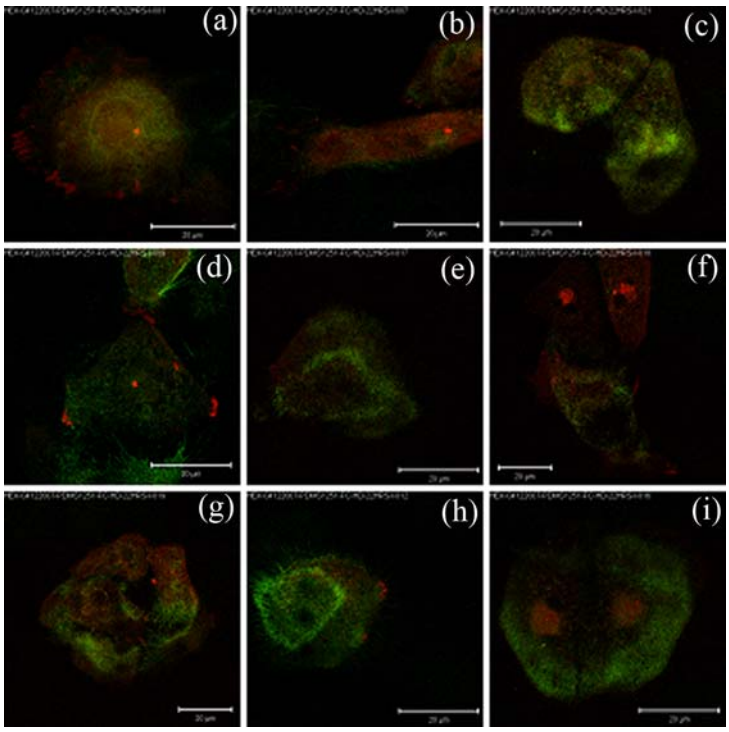

Figure 4-19: The focal adhesion and hemidesmosomes assemblies of cells shown in Figure 4.18. Substrate stiffness decreases from (b) to (k). More developed FA can be observed on stiff region while HD is more prominent on soft region. HEK cultured for 22 hours. Scale bars = 20 μm

4.7. Conclusion

In this section, the qualitative results indicating cells' response to the substrate depending on the mechanical properties of the substrates were presented. Experiments with both simple compliant PDMS substrates on glass coverslips with multiple stiffness level and freely suspended PDMS membrane with spatially varying stiffness suggest that human epidermal karatinocytes tend to deposit more laminin as indicated by the increased in fluorescent intensity. When comparing the intensity of fluorescent stained for lamin on simple compliant PDMS and freely suspended

membrane devices, HEK tends to secrete more laminin on the freely suspended PDMS membrane compare to the simple compliant PDMS substrates as shown in Figure 4-20.

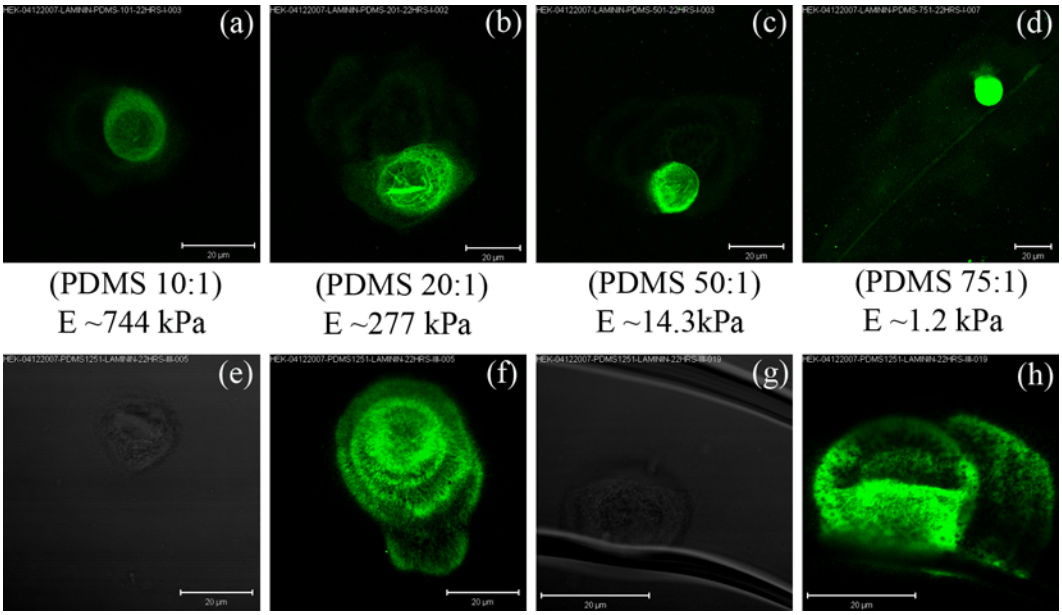

Figure 4-20: Comparing laminin secretion on compliant PDMS substrates (Top) to Suspended PDMS membrane. HEK cultured for 22 hours in both cases. Scale bars = 20 μm

It should be noted that the Young's modulus values of the simple compliant PDMS substrates were much lower than that of the suspended PDMS membrane. Recall that the compliant PDMS substrates in the current work have Young's modulus ranging from 1.2 – 744 kPa while it was experimentally determined to be 7.75 MPa for the suspended PDMS membrane. The fact that more laminin was secreted on the suspended membrane in this comparison indicates that the Young's modulus of materials in cell's microenvironment is important but the way the tissue scaffold is constructed (which will affect the overall stiffness - spring constant) seems to have more effect on the behavior of the cells.

Current experiments also shows that the focal adhesions are more mature, larger size and larger in numbers, on stiffer substrates/region. On the other hand, hemidesmosme assemblies were found to be better defined and prominent on the softer substrates/region. At this point, it is not exactly clear if the smaller stiffness is the reason why hemidesmosomes are better assembled on softer substrates since hemidesomosomes assembly is also known to be promoted and maintained by laminin proteins [144]. Since, more laminin-332 was secreted on softer substrates by HEK, it is plausible that amount of secreted protein regulate how well the hemidesmosome can be assembled by the cells. Thus, it is necessary to carry out experiments in the future that would isolate the two possible promoters (mechanical property, and density of laminin on substrate) from each other.

The suspended membrane devices, which incorporated a spatially varying stiffness, also provide a mean to study the preferential cell migration on the region with a gradient in stiffness and the peculiar accumulation of cells in a region where there was very minimal change in stiffness.

Chapter 5 : Conclusion

In this work, micro/nano fabrication technologies were developed, and they were applied to develop substrates to study cell interaction with its mechanical environments. Two systems of elastic substrates were used: (1) elastic PDMS substrates that are formed on coverslips, and (2) freely suspended microfabricated PDMS membrane. In both cases cells were exposed to variation in the stiffness of the substrates. The variation in the stiffness of the substrates in the first system was accomplished by varying the mixing ratio of the PDMS perpolymer to the curing agent from 10:1 to 75:1. On the second system, the variation in stiffness was generated on the membrane by strategically incorporating micropatterns on one side of the membrane. These micropatterns were placed in the middle of the rectangular membrane, thus forming an active region of the membrane bounded on either side by thicker membrane. Within this active region, the micropattern density gradually increases from one end to the other (in the direction along the length of the membrane), which generated a gradually changing stiffness.

Human epidermal keratinocytes were used as the cell model system. In general, HEK secretes more laminin-332, its primary adhesive protein, on softer substrates/region, which may be an indication of a cellular mechanism by which the cells modulate their microenvironment. Similar to other cell types, HEK form better focal adhesion complexes on stiffer substrates/region. The hemidesmosome, on the other hand, seem to be more prominent on the softer region. It was also observed that when two or more of these HEK cells form a group, the HD tends to form a ring-like structure in the center of the local colony. With the observation of small groups of cell moving on substrates in a circle, it is speculated that the HDs in the center of the colony is likely

anchoring the group, causing cells on the outer periphery to move in a circular pattern. With the suspended membrane device, cell migration was very dynamic in region with high stiffness gradient, where as they are generally static and accumulate in regions with very little stiffness change. More laminin-332 secretion was also observed on the suspended membrane devices.

In the process of developing the fabrication technique for freely suspended ultra-thin PDMS membrane substrates, two non-traditional nano/microfabrication techniques were developed. First, using 1.1μm polystyrene spheres (nanospheres lithography), many different nano/micropatterns were fabricated in conjunction with traditional microfabrication technology. Secondly, a novel lithography technique, Bond-Detach lithography, was developed based on the bonding and detaching a PDMS stamp to PDMS membrane. While the NSL technique provides limited features assembly and shape, it allows one to fabricate a large array of these nanofeatures relatively easily and, sometimes more importantly, very cheaply. The Bond-Detach lithography, on the other hand, allows the fabrication of nano, micro or a mixture of these features with ease. Though there is no theoretical limitation to what features can be patterned with BDL, there are practical limitations such as how far or close the features can be. It should also be noted that BDL relies on a master mold fabricated by traditional nano/microfabrication technology, and it is a tool to easily replicate those features without using other expensive tools.

Chapter 6 : Future Work

A solid engineering groundwork was laid for studying cell-substrate interaction using simple PDMS substrates having different Young's modulus and also with a suspended PDMS membrane with varying gradient of stiffness. The developed membrane device in particular is suitable for studying many other topics. Two important features of the membrane device that will be exploited in the future are (1) the extreme flexibility of the membrane, and (2) the channel that is formed under the suspended membrane during the experiment.

6.1. PDMS membrane based cell stretching device

As demonstrated during the characterization described in Chapter 3, the PDMS membrane are extremely flexible and they exhibit very little hysteresis during repeated loading, unloading cycles. This membrane can be outfitted with a computer controlled pressure pump such as a syringe pump. Other actuation mechanism utilizing electromagnetic or piezoactuators can also be incorporated. The device with an active membrane that is a few hundred micrometers to a few millimeters can be configured to fit within any microscope stage. Such system will allow studying cells in a dynamic environment, enabling to induce cyclic loading on cellular system and at the same time perform a live observation using the microscope. Cells from the lung, heart or other dynamic organs will be ideal candidate for study using this system.

6.2. The effects of substrate's mechanical properties and fluid flow on cellular processes

In the current experimental set up using PDMS membrane, the membrane is suspended over two PDMS spacers for imaging purposes. The two spacers form a channel underneath the membrane. With a properly designed channel and integrated fluidic system, the device will be used to study the effect of multiple environmental cues, such as mechanical properties and fluid flow.

6.3. Interaction between different cells types cultured on opposite sides of membrane

Another simple yet interesting experiment is to culture one cell type on one side of the membrane and another type on the opposite side. In such experiment, the interaction between the two different cell types would be mediated through the elastic membrane separating them. Another variation to this experiment would be, to use a porous membrane where the direct cell types interaction will be limited/confined to the holes on the membrane.

Figure 6-1: Sample experiment setup for studying interaction between different cell types separated by elastic membrane

REFERENCES

1. R. J. Pelham, Y. L. Wang, "Cell locomotion and focal adhesions are regulated by substrate flexibility," PNAS, 1997. 94(25): p. 13661-13665.
2. C. M. Lo, H. B. Wang, M. Dembo, and Y. L. Wang, "Cell Movement Is Guided by the Rigidity of the Substrate," Biophysical Journal, 2000. 79: p. 144-152.
3. H. B. Wang, M. Dembo, Y. L. Wang, "Substrate flexibility regulates growth and apoptosis of normal but not transformed cells," American Journal of Physiology-Cell Physiology, 2000. 279(5): p. C1345-C1350.
4. A. Brock, E. Chang, C. C. Ho, P. LeDuc, X. Jiang, G. M. Whitesides, D. E. Ingber, "Geometric determinants of directional cell motility revealed using microcontact printing," Langmuir, 2003. 19(5): p. 1611-1617.
5. J. Y. Wong, A. Velasco, P. Rajagopalan, and Q. Pham, "Directed Movement of Vascular Smooth Muscle Cells on Gradient-Compliant Hydrogels," Langmuir, 2003. 19: p. 1908-1913.
6. D. S. Gray, J.Tien, C. S. Chen, "Repositioning of cells by mechanotaxis on surfaces with micropatterned Young's modulus," Journal of Biomedical materials research Part A, 2003. 66A(3): p. 605-614.
7. A. J. Engler, M. A. Griffin, S. Sen, C. G. Bönnemann, H. Lee Sweeney, and D. E. Discher, "Myotubes differentiate optimally on substrates with tissue-like stiffness: pathological implications for soft or stiff microenvironments," Journal of Cell Biology, 2004. 166(6): p. 877-887.

8. E. J. Semler, P. A. Lancin, A. Dasgupta, P.V. Moghe, “Engineering hepatocellular morphogenesis and function via ligand-presenting hydrogels with graded mechanical compliance,” Biotechnology and Bioengineering, 2004. 89(3): p. 296-307.

9. S. R. Peyton, A.J.Putnam, “Extracellular matrix rigidity governs smooth muscle cell motility in a biphasic fashion,” Journal of cellular Physiology, 2005. 204(1): p. 198-209.

10. A. Saez, A. Buguin , P. Silberzan, and B. Ladoux, “Is the mechanical activity of epithelial cells controlled by deformations or forces?,” Biophysical Journal, 2005. 89: p. L52-L54.

11. T. M. Freyman, I. V., Yannas, R., Yokoo R., and L. J. Gibson, “Fibroblast contractile force is independent of the stiffness which resists the contraction,” Exp. Cell Res. 272:153-162., 2002. 272: p. 153-162.

12. D. E. Discher, P. Janmey, Y-L Wang, “Tissue cells feel and respond to the stiffness of their substrate,” Science, 2005. 310: p. 1139-1143.

13. M. M. Stevens, J. H. George, “Exploring and engineering the cell surface interface,” Science, 2005. 310: p. 1135-1138.

14. T. Yeung, P. C. Georges, L. A. Flanagan, B. Marg, M. Ortiz, M. Funaki, N. Zahir, W. Ming, V. Weaver, P. A. Janmey, “Effects of Substrate Stiffness on Cell Morphology,Cytoskeletal Structure, and Adhesion,” Cell Motility and the Cytoskeleton, 2005. 60: p. 24-34.

15. A. Engler, L. Bacakova, C. Newman, A. Hategan, M. Griffin, and D. Dischery, “Substrate compliance versus ligand density in cell on gel responses,” Biophysical Journal, 2004. 86(1): p. 617-628.

16. J. Y. Wong, J. B. Leach, X. Q. Brown, "Balance of chemistry, topography, and mechanics at the cell-biomaterial interface: Issues and challenges for assessing the role of substrate mechanics on cell response," Surface Science, 2004. 570(1-2): p. 119-133.

17. S. Hsu, R. Thakar, D. Liepmann, S. Li, "Effects of shear stress on endothelial cell haptotaxis on micropatterned surfaces," Biochemical and Biophysical Research Communications, 2005. 337(1): p. 401-409.

18. S. K. W. Dertinger, D. T. Chiu, N. Li Jeon, and G. M. Whitesides, "Generation of Gradients Having Complex Shapes Using Microfluidic Networks," Analytical Chemistry, 2001. 73(6): p. 1240-1246.

19. N. L. Jeon, H. Baskaran, S. K. W. Dertinger, G. M. Whitesides, L. Van De Water and M. Toner, "Neutrophil chemotaxis in linear and complex gradient of interleukin-8 formed in a microfabricated device," Nature Biotechnology, 2002. 20: p. 826-830.

20. M. R. Tomlinson, J.Genzer, "Formation of surface-grafted copolymer brushes with continuous composition gradients," Chemical Communication, 2003. 12: p. 1350-1351.

21. J. T. Smith, J.K.Tomfohr, M. C. Wells, T. P. Beebe, Jr., T. B. Kepler, and W. Monty Reichert, "Measurement of cell migration on surface-bound fibronectin gradients," Langmuir, 2004. 20(8279-8286).

22. B. Liedberg, P.Tengvall, "Molecular gradients of w-substituted alkanethiols on gold: Preparation and characterization," Langmuir, 1995. 11: p. 3821-3827.

23. T. Ueda-Yukoshi, T.Matsuda, "Cellular Responses on a Wettability Gradient Surface with Continuous Variations in Surface Compositions of Carbonate and Hydroxyl Groups," Langmuir, 1995. 11: p. 4135-4140.

24. J. Monahan, A.A.Gewirth, and R. G. Nuzzo, "A Method for Filling Complex Polymeric Microfluidic Devices and Arrays," Anal. Chemistry, 2001. 73: p. 3193-3197.

25. I. Caelen, A.Bbernard, D. Juncker, B. Michel, H. Heinzelmann, and E. Delamarche, "Formation of Gradients of Proteins on Surfaces with Microfluidic Networks," Langmuir, 2000. 16: p. 9125-9130.

26. E. Delamarche, A.Bbernard, H. Schmid, B. Michel, H. Biebuyck, "Patterned delivery of immunoglobulins to surfaces using microfluidic networks," Science, 1997. 276: p. 779-781.

27. K. Fosser, R.G.Nuzzo, "Fabrication of patterned multicomponent protein gradients and gradient arrays using microfluidic depletion," Anal. Chemistry, 2003. 75: p. 5775-5782.

28. W. S. Dillmore, M.N.Yousaf, and M. Mrksich, "A Photochemical Method for Patterning the Immobilization of Ligands and Cells to Self-Assembled Monolayers," Langmuir, 2004. 20: p. 7223-7231.

29. Y. Ito, M.Nogawa, "Preparation of a protein micro-array using a photo-reactive polymer for a cell-adhesion assay," Biomaterials, 2003. 24: p. 3021-3026.

30. R. R. Bhat, B. N. Chaney, J. Rowley, A. Liebmann-Vinson, and J. Genze, "Tailoring cell adhesion using surface-grafted polymer gradient assemblies," Advanced Materials, 2005. 17: p. 2802-2807.

31. A. Andersson, F.Backhed, A. von Euler, A. Richter-Dahlfors, D. Sutherland, B. Kasemo, "Nanoscale features influence epithelial cell morphology and cytokine production," Biomaterials, 2003. 24: p. 3427 -3436.

32. A. Curtis, “Tutorial on the biology of nanotopography,” IEEE Transactions on Nanobioscience, 2004. 3(4): p. 293-295.

33. M. E. Manwaring, J.F.Walsh, P. A. Tresco, Contact guidance induced organization of extracellular matrix. Biomaterials, 2004. 25(17): p. 3631-3638.

34. A. I. Teixeira, G.A.Abrams, C. J. Murphy, P. F. Nealey, “Cell behavior on lithographically defined nanostructured substrates,” JVST B, 2003. 21(2): p. 683-687.

35. A. I. Teixeira, P.F.Nealey, C. J. Murphy, “Responses of human keratocytes to micro- and nanostructured substrates,” Journal of Biomedical Materails Research Part A, 2004. 71A(3): p. 369-376.

36. N. W. Karuri, S.Lilensiek, A. I. Teixeira, G. Abrams, S. Campbell, P. F. Nealey and C. J. Murphy, “Biological length scale topography enhances cell-substratum adhesion of human corneal epithelial cells,” Journal of Cell Science, 2004. 117(15): p. 3153-3164.

37. J. H. Fitton, B.A.Dalton, G. Beumer, G. Johnson, H. J. Griesser, J. G. Steele, “Surface topography can interfere with epithelial tissue migration,” Journal of Biomedical Materails Research, 2004. 42(2): p. 245-257.

38. A. I. Teixeira, G.Abrams, P. J. Bertics, C. J. Murphy and P. F. Nealey, “Epithelial contact guidance on well-defined micro- and nanostructured substrates,” Journal of Cell Science, 2003. 116(10): p. 1881-1892.

39. B. Baharloo, M.Textor, D. M. Brunette DM, “Substratum roughness alters the growth, area, and focal adhesions of epithelial cells, and their proximity to titanium surfaces," Journal of Biomedical Materails Research Part A 74A (1): 12-22. Journal of Biomedical Materails Research Part A 74A (1): 12-22, 2005.

40. H. G. Craighead, C.D.James, A. M. P. Turner, "Chemical and topographical patterning for directed cell attachment," Current Opinion in Solid State & Materials Science 5 (2-3): 177-184, 2001.

41. X. Q. Brown, K.O., J. Y. Wong, "Evaluation of polydimethylsiloxane scaffolds with physiologically- relevant elastic moduli:interplay of substrate mechanics and surface chemistry effects on vascular smooth muscle cell response," Biomaterials, 2005. 26: p. 3123 -3129.

42. A. K. Harris, P.Wild, and D. Stopak, "Silicone Rubber Substrata: A New Wrinkle in the Study of Cell Locomotion," Science, 1980. 208: p. 177-179.

43. L. L. Hench, J. M. Polak, "Third-Generation Biomedical Materials," Science, 2002. 295: p. 1014-1017.

44. K. D. Mossman, G. Campi, J. T. Groves, M. L. Dustin, "Altered TCR Signaling from Geometrically Repatterned Immunological Synapses," Science, 2005. 310: p. 1191-1193.

45. T. Veikkola, M. Lohela, K. Ikenerg, T. Makinen, T. Korff, A. Saaristo, T. Petrova, M. Jeltsch, H. G. Augustin, and K. Alitalo, "Intrinsic versus microenvironmental regulation of lymphatic endothelial cell phenotype and function," FASEB, 2003. 17(14): p. 2006-2013.

46. J. Genzer, K. Efimenko,"Creating Long-Lived Superhydrophobic Polymer Surfaces Through Mechanically Assembled Monolayer," Science, 2000. 290: p. 2130-2133.

47. J. Genzer, D. A. Fischer, and K. Efimenko, "Fabricating two-dimentional molecular gradients via asymmetric deformation of uniformly-coated elastomer sheets," Advanced Materials, 2003. 15: p. 1545-1547.

48. C. M. Waters, M. R. Glucksberg, E. P. Lautenschlager, C. Lee, R. M. Van Matre, R. J. Warp, U. Savla, K. E. Healy, B. Moran, D. G. Castner, and J. P. Bearinger, "A system to impose prescribed homogenous strains on cultured cells," J. Appl Physiology, 2001. 91(1600-1610).

49. H. Sato, N. Kataoka, F. Kajiya, M. Katano, T. Takigawa, T. Masudad, "Kinetic study on the elastic change of vascular endothelial cells on collagen matrices by atomic force microscopy," Colloids and Surfaces B: Biointerfaces, 2004. 34: p. 141-146.

50. J. Qi, A. M. Fox, L. G. Alexopoulos, L. Chi, D. Bynum, F. Guilak, and A. J. Banes, "IL-1beta decreases the elastic modulus of human tenocytes," J. Appl Physiology, 2006. 101: p. 189-195.

51. Z. Balint, I. A. Krizbai, I. Wilhelm, A. E. Farkas, A. Parducz, Z. Szegletes, G. Varo, "Changes induced by hyperosmotic mannitol in cerebral endothelial cells: an atomic force microscopic study," European Biophysical Journal. 2007, 36,113-20, 2007. 36: p. 113-120.

52. I. Dulinska, M. Targosz, W. Strojny, M. Lekka, P. Czuba, W. Balwierz and M. Szymonski, "Stiffness of normal and pathological erythrocytes studied by means of atomic force microscopy," Journal of Biochemical and Biophysical Methods, 2006. 66: p. 1-11.

53. F. Rico, P. Roca-Cusachs, N. Gavara, R. Farré, M. Rotger, and D. Navajas, "Probing mechanical properties of living cells by atomic force microscopy with blunted pyramidal cantilever tips," Phys. Rev. E, 2005. 72: p. 021914.

54. T. K Berdyyeva, C. D Woodworth and I. Sokolov, “Human epithelial cells increase their rigidity with ageing in vitro: direct measurements,” Phys. Med. Biol., 2005. 50: p. 81-92.

55. M. Lekka, P. Laidler, D. Gil, J. Lekki, Z. Stachura, A.Z. Hrynkiewicz, “Elasticity of normal and cancerous human bladder cells tudied by scanning force microscopy,” Eur Biophysical Journal, 1999. 28: p. 312-316.

56. P. D. Gasson, R. J. Lapeer, “In vitro skin-tissue experiment for increased realism in open surgery simulations,” Stud Health Technol Inform., 2007. 125: p. 143-145.

57. T. R. Tilleman, M. M. Tilleman, M. H. Neumann, “The elastic properties of cancerous skin: Poisson's ratio and Young's modulus,” The Israel Medical Association Journal, 2004. 6: p. 753-755.

58. A. Samani, J. Bishop, C. Luginbuhl and D. B Plewes, “Measuring the elastic modulus of ex vivo small tissue Samples,” Phys. Med. Biol., 2003. 48: p. 2183-2198.

59. R. D. Kamm, “Airway wall mechanics,” Annual Review of Biomedical Engineering, 1999. 1: p. 47-72.

60. D. Calvet, P. Boutouyrie, E. Touze, B. Laloux, J. Mas, S. Laurent, “Increased Stiffness of the Carotid Wall Material in Patients With Spontaneous Cervical Artery Dissection,” Stroke, 2004, 35, 2078-2082, 2004.

61. L. A. Flanagan, Y. E. Ju, B. Marg, M. Osterfield, P. A. Janmey, “Neurite branching on deformable substrates,” Neuroreport, 2002. 13: p. 2411-2415.

62. H. Ai, Y. M. Lvov, D. K. Mills, M. Jennings, J. S. Alexander; S. A. Jones, “Coating and selective deposition of nanofilm on silicone rubber for cell adhesion and growth,” Cell Biochemistry and Biophysics, 2003. 38(2): p. 103-114.

63. C.-J. Kim, J.Kim, “Nanostructured surfaces for dramatic reduction of flow resistance in droplet-based microfluidics.” Proc. IEEE Int. Conf. MEMS, Las Vegas, NV, Jan. 2002. 2002. Las Vegas, NV.

64. M. K. Chaudhury, G.M.Whitesides, “How to make water run uphill,” Science, 1992. 256: p. 1539-1541.

65. S. Daniel, M.K.Chaudhury, J. C. Chen, “Fast drop movements resulting from the phase change on a gradient surface,” Science, 2001. 291: p. 633-636.

66. H. Suda, S. Yamada, “Force Measurements for the Movement of a Water Drop on a Surface with a Surface Tension Gradient,” Langmuir, 2003. 19: p. 529-531.

67. J. Y. Pan, P. Lin, F. Maseeh, S. D. Senturia, “Verification of FEM analysis of load-deflection methods for measuring mechanical properties of thin films,” Technical Digest, 1990 Solid-State Sensor and Actuator Workshop. 1990.

68. K. Autar, “Mechanics of Composite Materials,” 1997: CRP.

69. D. Armani, C. Liu, and N. Aluru, “Re-configurable fluid circuits by PDMS elastomer micromachining,” 12th Int. Conf. on MEMS (MEMS '99) (Orlando, FL) pp 222-227. 1999. Orlando, FL.

70. S. Y. Chou, P. R. Krauss, and P. J. Renstrom, “Nanoimprint Lithography,” J. Vac. Sci. Technol. B, 1996. 14(6): p. 4129-4133.

71. R. D. Piner, J. Zhu, F. Xu, S. Hong, C.A. Mirkin, “Dip-Pen Nanolithography,” Science, 283:661-63, 1999. 283: p. 661-663.

72. C. L. Haynes, R.P.Van Duyne, Nanosphere Lithography: A Versatile Nanofabrication, "Tool for Studies of Size-Dependent Nanoparticle Optics," J. Phys. Chemistry B, 2001. 105: p. 05, 5599-5611.

73. C. L. Haynes, R.P.Van Duyne, "Angle-Resolved Nanosphere Litohgraphy: Manipulation of Nanoparticle Size, Shape, and Interparticle Spacing. J. Phys. Chemistry B, 2002. 106: p. 1898-1902.

74. R. P. Van Duyne, Personal communication. .

75. S. Henry, D. V. McAllister, M. G. Allen, M. R. Prausnitz, "Microfabricated microneedles: A novel approach to transdermal drug delivery," Journal of Pharmaceutical Sciences, 1998. 87(8): p. 922-925.

76. K. R. Williams, K.Gupta, and M. Wasilik, "Etch Rates for Micromachining Processing-Part II," J. Microelectormechanical Systems, 2003. 12: p. 761-778.

77. M. Winzer, M. Kleiber, N. Dix, and R. Wiesendanger, "Fabrication of nano-dot and nano-ring-arrays by nanosphere lithography," Applied Physics A, 1996. 63: p. 617-619.

78. W. Frey, C. K. Woods, A. Chilkoti, "Ultraflat Nanosphere Lithography: A New Method to Fabricate Flat Nanostructures," Advanced Materials, 2000. 12(20): p. 1515-1519.

79. G.J. Dolan, "Offset mask for lift-off photoprocessing," Applied Physic Letter, 1977. 31: p. 337-339.

80. T. R. Jensen, M. D. Malinsky, C. L. Haynes, and R. P. Van Duyne, "Nanosphere Lithography: Tunable Localized Surface Plasmon Resonance Spectra of Silver Nanoparticles," J. Phys. Chemistry B, 2000. 104: p. 10549-10556.

81. J. C. Riboh, A. J. Haes, A. D. McFarland, C. R. Yonzon, and R. P. Van Duyne, "A Nanoscale Optical Biosensor: Real-Time Immunoassay in Physiological Buffer Enabled by Improved Nanoparticle Adhesion," J. Phys. Chemistry B, 2002. 107: p. 1772-1780.

82. W. Barthlott, C. Neinhuis, "Purity of the sacred lotus, or escape from contamination in biological surfaces," Planta, 1997. 202(1-8).

83. R. Wenzel, " Resistance of solid surfaces to wetting by water," Ind. Eng. Chem, 1936. 28: p. 988.

84. A. B. D. Cassie, S. Baxter, "Wettability of porous surfaces," S., Trans. Faraday Soc., 1944. 3: p. 16.

85. J. Bico, C. Marzolin, and D. Quere, "Pearl drops," Europhys. Lett.ers, 1999. 47(2): p. 220-226.

86. T. Onda, S. Shibuichi, N. Satoh, and K. Tsujii, "Super-Water Repellent Fractal Surfaces," Langmuir, 1996. 12(9): p. 2125-2127.

87. J. Bico, C. TOrdeux, and D. Quere, "Rough Wetting," Europhys. Lett.ers, 2001. 55(2): p. 214-220.

88. N. Patankar, "On the Modeling of Hydrophobic Contact Angles on Rough Surfaces," Langmuir, 2003. 19: p. 1249-1254.

89. N. Patankar, "Mimicking the Lotus Effect: Influence of Double Roughness Structures and Slender Pillars," Langmuir, 2004. 20: p. 8209-8213.

90. B. He, N. Patankar, and J. Lee, "Multiple Equilibrium Droplet Shapes and Design Criterion for Rough Hydrophobic Surfaces," Langmuir, 2003. 19: p. 4999-5003.

91. J. Lee, B. He and N. Patankar, "A roughness-based wettability switching membrane device for hydrophobic surfaces," J. Micromech. Microengineering, 2005. 15: p. 591-600.

92. B. Jo, L. Van Lerberghe, K. M. Motsegood, D. J. Beebe, "Three-Dimensional Micro-Channel Fabrication in Polydimethylsiloxane (PDMS) Elastomer," J. Microelectromechanical Systems, 2000. 9: p. 76-81.

93. T. Sulchek, R. Hsieh, J. D. Adams, S. C. Minne, C. F. Quate, D. M. Adderton, "High-speed atomic force microscopy in liquid," Rev. of Scientific Inst., 2000. 71: p. 2097-2099.

94. A. Kumar, H. Biebuyck, G. M. Whitesides, "Patterning Self -Assembled Monolayers: Applications in Materials Science," Langmuir, 1994. 10: p. 1498-1511.

95. Y. Xia, G.M.Whitesides, "Soft Lithography," Annu. Rev. Mater. Sci., 1998. 28: p. 153-184.

96. Y. Xia, G.M.Whitesides, "Extending Microcontact Printing as a Microlithographic Technique," Langmuir, 1997. 13: p. 2059-2067.

97. H. Schmid, B. Michel, "Siloxane Polymers for High-Resolution, High-Accuracy Soft Lithography," Macromolecules, 2000. 33: p. 3042-3049.

98. B. Michel, A. Bernard, A. Bietsch, E. Delamarche, M. Geissler, D. Juncker, H. Kind, J.-P. Renault, H. Rothuizen, H. Schmid, P. Schmidt-Winkel, R. Stutz, H. Wolf, "Printing meets lithography: Soft approaches to high-resolution patterning," IBM J. Res. & Dev., 2001. 45: p. 697-719.

99. Y. S. Kim, K. Y. Suh, H. Lee, “Fabrication of three-dimensional microstructures by soft molding,” Appl. Phys. Lett., 2001. 79: p. 2285-2287.

100. Y. S. Kim, K. Y. Suh, H. Lee, “Three-dimensional pattern transfer and nanolithography: modified soft molding,” Appl. Phys. Lett., 2002. 81: p. 1011-1013.

101. R. J. Jackman, J.Wilbur, G. M. Whitesides, “Fabrication of submicrometer features on curved surbstrates by microcontact printing. Science, 1995. 269: p. 664-666.

102. Y. Xia, D. Qin, G. M. Whitesides, “Microcontact Printing with a Cylindrical Rolling Stamp: A Practical Step Toward Automatic Manufacturing of Patterns with Submicrometer. Sized Features,” Advanced Materials, 1996. 8: p. 1015-1017.

103. C. Kim, P. E. Burrows, S. R. Forrest, “Micropatterning of organic electronic devices by cold-welding,” Science, 2000. 288: p. 831-833.

104. J-H. Choi, D. Kim, P. J. Yoo, H. Lee, “Simple Detachment Patterning of Organic Layers and Its Application to Organic Light-Emitting Diodes,” Advanced Materials, 2005. 17: p. 166-171.

105. N. Stutzmann, T. A. Tervoort, K. Bastiaansen, P. Smith, “Patterning of polymer supported metal film by microcutting,” Nature, 2000. 407: p. 613-616.

106. T. Granlund, T. Nyberg, L. S. Roman, M.Svensson, and O. Inganäs, “Patterning of polymer light-emitting diodes with soft lithography,” Advanced Materials, 2000. 12: p. 269-273.

107. Z. Wang, J. Zhang, R. Xing, J. Yuan, D. Yan, and Y. Han, “Micropatterning of Organic Semiconductor Microcrystalline Materials and OFET Fabrication by "Hot Lift Off",” JACS, 2003. 125: p. 15278-15279.

108. F. Hua, Y. Sun, A. Gaur, M. A. Meitl, L. Bilhaut, L. Rotkina, J. Wang, P. Geil, M. Shim, and J. A. Rogers, "Polymer imprint lithography with molecular-scale resolution," Nano Letters, 2004. 4: p. 2467-3471.

109. H. Ahn, K. J. Lee, A. Shim, J. A. Rogers, and R. G. Nuzzo, "Additive soft-lithographic patterning of submicrometer- and nanometer-scale large-area resists on electronic materials," Nano Letters, 2005. 5: p. 2533-2537.

110. S. L. Peterson, A. McDonald, P. L. Gourley, D. Y. Sasaki, "Poly(dimethylsiloxane) thin films as biocompatible coatings for microfluidic devices: Cell culture and flow studies with glial cells," J. Biomed. Mat. Res. Part A, 2005. 72: p. 10 - 18.

111. E. Ostuni, R. Kane, C. S. Chen, D. E. Ingber, G. M. Whitesides, "Patterning Mammalian Cells Using Elastomeric Membranes," Langmuir, 2000. 16: p. 7811-7819.

112. K. S. Ryu, X. Wang, K. Shaikh, C. Liu, "A Method for Precision Patterning of Silicone Elastomer and Its Applications," J. Microelectromechanical Systems, 2004. 13: p. 568-575.

113. A. Pawlowski, A. Sayah, M. Gijs, "Precision Poly-(Dimethyl Siloxane) MaskingTechnology for High-Resolution Powder Blasting," J. Microelectromechamical Systems, 2005. 14: p. 619-624.

114. J. Garra, T. Long, J. Currie, T. Schneider, R. White, M. Paranjape, "Dry etching of polydimethylsiloxane for microfluidic systems," J. Vac. Sci. Technol. A, 2002. 20: p. 975-982.

115. W. R. Childs, R. G. Nuzzo, "Decal transfer microlithography: A new soft-lithographic patterning method," J. Am Chem. Society, 2002. 124: p. 13583-13596.

116. W. R. Childs, R.G.Nuzzo, “Patterning of thin-film microstructures on non-planar substrate surfaces using decal transfer lithography,” Advanced Materials, 2004. 16(1323-1327).

117. W. R. Childs, R.G.Nuzzo, “Large-area patterning of coinage-metal thin films using Decal Transfer Lithography,” Langmuir, 2005. 21: p. 195-202.

118. D. J. Sirbuly, G. M. Lowman, B. Scott, G. D. Stucky, S. K. Buratto, “Patterned microstructures of porous silicon by dry-removal soft lithography,” Advanced Materials, 2003. 15: p. 149-152.

119. P. R. Krauss, S. Y. Chou, “Nano-compact disks with 400 Gbit/in 2 storage density fabricated using nanoimprint lithography and read with proximal probe,” Appl. Phys. Lett., 1997. 71: p. 3174-3176.

120. X. Liang, W. Zhang, M. Li, Q. Xia, W. Wu, H. Ge, X. Huang, and S. Y. Chou, “Electrostatic force-assisted nanoimprint lithography (EFAN),” Nano Letters, 2005. 5: p. 527-530.

121. B. Faircloth, H. Rohrs, R. Tiberio, R. Ruoff, R. Krchnavek, “Bilayer, nanoimprint lithography,” J. Vac. Sci. Technol. B, 2000. 18: p. 1866-1873.

122. K. J. Hsia, Y. Huang, E. Menard, J-U Park, W. Zhou, J. Rogers, J. M. Fulton, “Collapse of stamps for soft lithography due to interfacial adhesion,” Appl. Phys. Lett., 2005. 86: p. 154106.

123. T. W Odom, J. C. Love, D. B. Wolfe, K. E. Paul, and G. M. Whitesides, “Improved pattern transfer in soft lithography using composite stamps,” Langmuir, 2002. 12: p. 5314-5320.

124. Dynasolve-220, (Technical Data Sheet), , Dynaloy Inc, USA.

125. K. Burton, D. Lansing Taylor, “Traction forces of cytokinesis measured with optically modified elastic substrata,” Nature, 1997: p. 450-454.

126. N. Q. Balaban, U. S. Schwarz, D. Riveline, P. Goichberg, G.Tzur, I. Sabanay, D. Mahalu, S. Safran, A. Bershadsky, L. Addadi and B. Geiger, “Force and focal adhesion assembly: a close relationship studied using elastic micropatterned substrates," Nature Cell Biology. Nature Cell Biology, 2001. 3: p. 466-472.

127. M. N. De Silva, R. Desai, and D. J. Odde, “Micro-patterning of animal cells on PDMS substrates in the presence of serum without use of adhesion inhibitors,” Biomedical Devices, 2004. 6(3): p. 219-222.

128. J. L. Tan, J. Tien, D. M. Pirone, D. S. Gray, K. Bhadriraju, and C. S. Chen, “Cells lying on a bed of microneedles: An approach to isolate mechanical force,” PNAS, 2003. 100(4): p. 1484-1489.

129. O. du Roure, A. Saez, A. Buguin, R. H. Austin, P.Chavrier, P. Siberzan, and B. Ladoux, “Force mapping in epithelial cell migration,” PNAS, 2005. 102(2): p. 2390-2395.

130. H-B. Wang, M. Dembo, S. K. Hanks, and Y. Wang, “Focal adhesion kinase is involved in mechanosensing during fibroblast migration,” PNAS, 2001. 98(20): p. 11295-11300.

131. B. Bischofs, U. S. Schwarz, “Cell organization in soft media due to active mechanosensing,” PNAS, 2003. 100(16): p. 9274-9279.

132. B. Bischofs, S. A. Safran, and U. S. Schwarz, “Elastic interactions of active cells with soft materials,” Physical Review E, 2004. 69: p. 021911.

133. D-Y. Khang, H. H. Lee, "Sub-100 nm Patterning with an Amorphous Fluoropolymer Mold," Langmuir, 2004. 20: p. 2445-2448.

134. J. C. Lotters y , W. Olthuis, P. H. Veltink and P. Bergveld, "The mechanical properties of the rubber elastic polymer polydimethylsiloxane for sensor applications," J. Micromech. Microengineering, 1997. 7: p. 145-147.

135. R. Singhvi, A. Kumar, G. P. Lopez, G. N. Stephanopoulos, D. I. Wang, G. M. Whitesides, D. E. Ingber, "Engineering Cells Shape and Function," Science, 1994. 264: p. 696-698.

136. N. Wang, E. Ostuni, G. M. Whitesides, and D. E. Ingber, "Micropatterning Tractional Forces in Living Cells," Cell Motility and the Cytoskeleton, 2002. 52: p. 97-106.

137. Y. Zhao, X. Zhang, "A Novel Pressure Indicator for Continuous Flow PCR Chip Using Micro Molded PDMS Pillar Arrays," Mater. Res. Soc. Symp. Proc. 2005.

138. S. Timoshenko, S. Woinowsky-Krieger, "Theory of plates and shells," 1959: McGraw-Hill Book Company, Inc., New York, NY.

139. J. Y. Pan, Pi. Lin, F. Maseeh, and S. D. Senturia, "Verification of FEM analysis of load-deflection methods for measuring mechanical properties of thin film," 1990.

140. C. Jiang, S. Markutsya, Y.Pikus and V. V. Tsukruk, "Freely suspended nanocomposite membranes as highly sensitive sensors," Nature Materials, 2004. 2004(3): p. 721-728.

141. D. T. Eddington, W. C. Crone, and D. J. Beebe, "Development of process protocols to fine tune PDMS material properties," 7th International Conference on Miniaturized Chemical and Biochemical Analysts Systems. 2003. Squaw Valley, California USA.

142. S. G. Charati, S. A. Stern, “Diffusion of gases in silicone polymer: molecular dynamics simulations,” Macromolecules, 1998. 31: p. 5529-5535.

143. S. E. Baker, S. B. Hopkinson, M. Fitchmun, G. L. Andreason, F. Frasier, G. Plopper, V. Quaranta and J. C. R. Jones, “Laminin-5 and hemidesmosomes: role of the a3 chain subunit in hemidesmosome stability and assembly,” Journal of Cell Science, 1996. 109: p. 2509-2520.

144. K. M. Haas, A. Berndt, K. J. Stiller, P. Hyckel, and H. Kosmeh, “A Comparative Quantitative Analysis of Laminin-5 in the Basement Membrane of Normal, Hyperplastic, and Malignant Oral Mucosa by Confocal Immunofluorescence Imaging,” The Journal of Histochemistry & Cytochemistry, 2001. 49: p. 1261-1268.

145. S. Stahl, S. Weitzman and J. C. R. Jones, “The role of laminin-5 and its receptors in mammary epithelial cell branching morphogenesis,” Journal of Cell Science, 1997. 110: p. 55-63.

146. D. E. Frank, W. G. Carter, “Laminin 5 deposition regulates keratinocyte polarization and persistent migration,” Journal of Cell Science, 2003. 117: p. 1351-1363.

147. P. H. Michelson, M. Tigue, and J. C.R. Jones, “Human Bronchial Epithelial Cells Secrete Laminin 5, Express Hemidesmosomal Proteins, and Assemble Hemidesmosomes,” The Journal of Histochemistry & Cytochemistry, 2000. 48: p. 535-544.

148. R. Q.J. Schaapveld, L. Borradori, D. Geerts, M. R. van Leusden, I. Kuikman, M. G. Nievers, C. M. Niessen, R. D.M. Steenbergen, P. J.F. Snijders, and A. Sonnenberg, “Hemidesmosome Formation Is Initiated by the b4 Integrin Subunit, Requires Complex

Formation of b4 and HD1/Plectin, and Involves a Direct Interaction between b4 and the Bullous Pemphigoid tigen 180," The Journal of Cell Biology, 1998. 142: p. 271-284.

149. L. Borradori, A. Sonnenberg, "Hemidesmosomes: roles in adhesion, signaling and Human diseases," Current Opinion in Cell Biology, 1996. 8: p. 647-656.

150. K. J. Green, J. C. R. Jones, "Desmosomes and hemidesmosomes: structure and function of molecular components," FASEBJ, 1996. 10: p. 871-881.

151. G. A. Dunn, J.P. Heath, "A new hypothesis of contact guidance in tissue cells," Experimental Cell Research, 1976. 101: p. 1-14.

152. G. A. Dunn, T. Ebendal, "Contact guidance on oriented collagen gels," Experimental cell research, 1978. 111(2): p. 475-479.

153. B. U. Sehgal, P. J. D., S. Matzno, T-L Chew, J. N. Claiborne, S. B. Hopkinson, A. Russell, M. P. Marinkovich, and J. C. R. Jones, "Integrin β4 Regulates Migratory Behavior of Keratinocytes by Determining Laminin-332 Organization," The journal of biological chemistry, 2006. 281(46): p. 35487-35498.

154. M. Langhofer, S. B. Hopkinson, J. C. Jones, "The matrix secreted by 804G cells contains laminin-related components that participate in hemidesmosome assembly in vitro," Journal of Cell Science, 1993, 105. p753-764.

155. M. P. Marinkovich, "Laminin 332 in squamous-cell carcinoma," Nature Review (2007), 7, p. 370-380.

156. G. Meneguzzi, M. P. Marinkovich, D. Aberdam, A. Pisani, R. Burgeson, J. P. Ortonne, "Kalinin is abnormally expressed in epithelial basement membranes of Herlitz's junctional epidermolysis bullosa patients," Exp Dermatol. (1992), 1(5), p. 221-229.

157. L. Pulkkinen, A. M. Christiano, D. R. Gerecke, D. W. Wagman, R. E. Burgeson, M. R. Pittelkow, J. Uitto, "A homozygous nonsense mutation in the 3 chain gene of laminin 5 (LAMB3) in Herlitz junctional epidermolysis bullosa," Genomics (1994) 24, p. 357–360.

158. D. Aberdam, M-F Galliano, J. Vailly, L. Pulkkinen, J. Bonifas, A. M. Christiano, K. Tryggvason, J. Uitto, E. H. Epstein Jr, J-P Ortonne & G. Meneguzzi, "Herlitz's junctional epidermolysis bullosa is linked to mutations in the gene (LAMC2) for the 2 subunit of nicein/kalinin (LAMININ−5)," Nature Genetics (1994), **6**, p. 299 – 304.

159. S. K. Sastry, and K. Burridge, "Focal Adhesions: A nexus for intercellular signaling and cytoskeletal dynamics," Experimental Cell Research (2000), 261, p. 25-36.

160. http://cellix.imolbio.oeaw.ac.at/

161. K. J. Green and J. C. Jones, **"**Desmosomes and hemidesmosomes: structure and function of molecular components," The FASEB Journal, 1996, 10, p. 871-881.

162. D. Tsuruta, S. B. Hopkinson, and J. C. R. Jones, "Hemidesmosome protein dynamics in live epithelial cells," Cell motility and the Cytoskeleton (2003), 54, p. 122-134.

163. F. Mainiero, A. Pepe, K. K. Wary, L. Spinardi, M. Mohammadi, J. Schlessinger, and F. G. Giancotti, "Signal transduction by the α6β4 integrin: distinct β4 subunit sites mediate recruitment of Shc/Grb2 and hemidesmosomes," EMBO (1995), 14(18), p. 4470-448.

Appendix

A.1. Detail Drawing for PDMS membrane devices with precisely controlled spatially varying stiffness

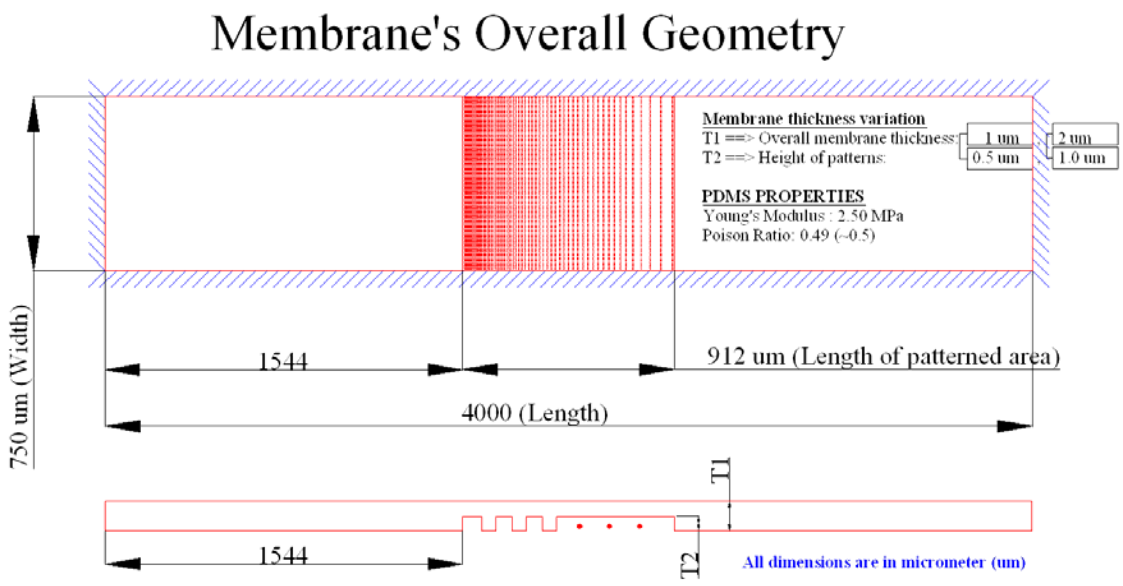

Figure A.1 : The overall geometry of PDMS membrane device

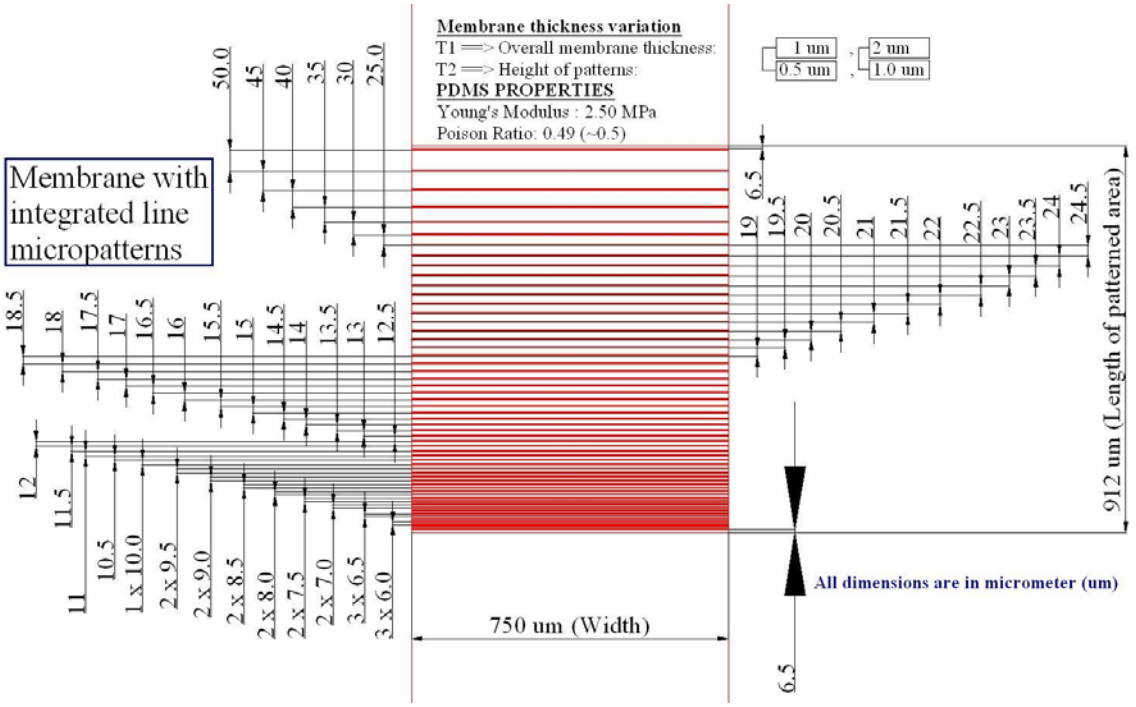

Figure A.2: Detail dimensions for line micropatterns integrated PDMS membrane

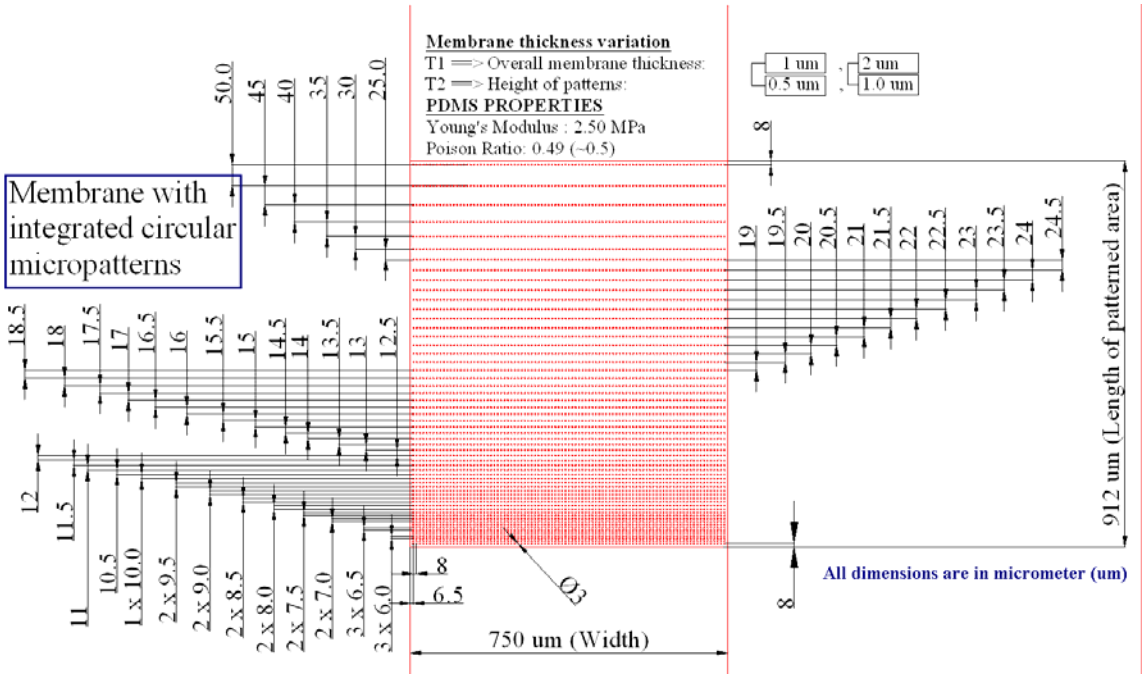

Figure A.3: Detail dimensions for dot micropatterns integrated PDMS membrane

A.2. Detail information of antibodies used

Paxilin : Paxillin (N-term) Rabbit Antibody [Epitomics Inc., #1500-1]

β4 : Purified Mouse Anti-Human Monoclonal Antibody (CD 104) [BD Biosciences, #555752]

J18: Rabbit antiserum against rat laminin-332 (Langhofer et al, 1993)

GAM-F: Fluorescence (FITC) conjucated Affini Pure Goat-Anti mouse, IgG [Jackson Immunology Research #115-095-166]

GARb-F Fluorescence (FITC) Affini Pure Fab Fragment Goat Anti-Rabbit IgG (H+L) [Jackson Immunology Research #111-097-003]

GARb-Rh Rhodamine Red-X-AffiniPure Fab Fragment Goat Anti-Rabbit IgG (H+L) [Jackson Immunology Research #111-297-003]

A.3. Materials Used

Silicon wafer: (100) P-Type [Polishing Corporation of America]

SU8-2100: Thick negative resist [MicroChem, # Y111075 0500L1GL]

Photoresist: Shipley S1805 positive resist [MicroChem, #41201]

Photoresist: Shipley S1818 positive resist [MicroChem Corp.]

Resist developer: Microposit 351 for Shipley 1800 series resist [MicroChem Corp.]

Resist developer: SU8 developer [MicroChem Corp.]

PDMS: Slygard 184 [Corning Corporation]

Hexane: ACS grade [Fisher Scientifics, #H292-4]

Teflon AF®: Teflon AF® resin [DuPont, #601S1-100-6]

Coverslips:	Squares No. 1 - 0.13 to 0.17mm thick; Size: 22mm [Fisher Scientifics, #12-542B]
Microscope slide:	Fisherbrand Superfrost Excell Microscope Slides, 144 pk [Fisher Scientifics, #22-034-985
Cell culture dish:	Glass bottom Dish, 20mm well, #0 Glass, [MatTek Corporation, #P35G-0-20-C]
Cell culture dish:	100mm sterile Corning Petri Dish [Sigma Aldrich, # CLS3262]
HEK Media:	500ml Defined Keratinocyte-SFM (1X), liquid [Invitrogen Corp, #10744-019]
Serum:	Fetal Bovine Serum [Invitrogen Corp, #16000-044]
Pen/Strap:	Penicillin-Streptomycin-Glutamine (100X), liquid [Invitrogen Corp, #10378-016]
Trypsin:	Trypsin-EDTA (0.05% Trypsin 0.53 mM EDTAx4Na) (1X) liquid [Invitrogen Corp, #25300054]